$MgCl_2$.nROH: New Molecular Adducts for the Preparation of $TiCl_x/MgCl_2$ Catalyst for Olefin Polymerization (R = isopropyl, isobutyl, 2-butyl, tertiary butyl)

Thesis Submitted to AcSIR for the Award of
the Degree of
DOCTOR OF PHILOSOPHY
In Chemistry

By
K. S. Thushara
Registration Number: 10CC11J26104

Under the guidance of
Dr. Chinnakonda S. Gopinath

CSIR – National Chemical Laboratory
Pune – 411 008, India

DECLARATION BY RESEARCH SCHOLAR

I hereby declare that the thesis "**$MgCl_2$.nROH: New Molecular Adducts for the Preparation of $TiCl_x/MgCl_2$ Catalyst for Olefin Polymerization (R= isopropyl, isobutyl, 2-butyl, tertiary butyl)**" submitted for the degree of Doctor of Philosophy to the AcSIR has been carried out by me at the Catalysis and Inorganic Chemistry Division, National Chemical Laboratory, Pune – 411 008, India, under the supervision of Dr. Chinnakonda S. Gopinath. Such material as has been obtained by other sources has been duly acknowledged in this thesis. I declare that the present work or any part thereof has not been submitted to any other University for the award of any other degree or diploma.

Date: 07/05/13 **K. S. THUSHARA**

Catalysis Division,
CSIR - National Chemical Laboratory,
Dr. Homi Bhabha Road, Pune-411 008
Maharashtra, India

हीरक जयन्ती वर्ष 2009-10

राष्ट्रीय रासायनिक प्रयोगशाला
(वैज्ञानिक तथा औद्योगिक अनुसंधान परिषद)
डॉ. होमी भाभा मार्ग, पुणे - 411 008. भारत
NATIONAL CHEMICAL LABORATORY
(Council of Scientific & Industrial Research)
Dr. Homi Bhabha Road, Pune - 411 008. India.

CERTIFICATE BY RESEARCH GUIDE

This is to certify that the work incorporated in the thesis entitled, "**$MgCl_2$.nROH: New Molecular Adducts for the Preparation of $TiCl_x/MgCl_2$ Catalyst for Olefin Polymerization (R= isopropyl, isobutyl, 2-butyl, tertiary butyl)**" submitted by **K.S. Thushara**, for the Degree of **Doctor of Philosophy,** was carried out by the candidate under my supervision in the Catalysis Division, National Chemical Laboratory, Pune – 411 008, India. Such material as has been obtained from other sources has been duly acknowledged in the thesis. To the best of my knowledge, the present work or any part thereof has not been submitted to any other University for the award of any other degree or diploma.

Date: 07/05/13
Catalysis Division,
CSIR - National Chemical Laboratory,
Dr. Homi Bhabha Road, Pune - 411 008
Maharashtra, India

Dr. C. S. Gopinath
(Research Supervisor)

डॉ. सी. एस. गोपीनाथ
Dr. Chinnakonda S. Gopinath
वैज्ञानिक, उत्प्रेरक प्रभाग
Scientist, Catalysis Division
राष्ट्रीय रासायनिक प्रयोगशाला
NATIONAL CHEMICAL LABORATORY
पुणे/PUNE - 411 008.

Communication Channels

☎
NCL Level DID : 2590
NCL Board No. : +91-20-25902000
EPABX : +91-20-25893300
+91-20-25893400

FAX
Director's Office : +91-20-25902601
COA's Office : +91-20-25902660
COS&P's Office : +91-20-25902664

WEBSITE
www.ncl-india.org


Dedicated to
Achan, Amma,
Sudhi & Raj

Acknowledgement

It gives me immense pleasure to extend my cordial gratitude to all those who helped me in pursuing my work presented in this thesis. I take this opportunity to express my deepest sense of gratitude and reverence towards my research supervisor, Dr. C. S. Gopinath for guiding me throughout the course of this work. I feel deeply indebted to his immense contribution in developing this thesis.

I am grateful to Dr. S. Sivaram, and Dr. Sourav Pal, erstwhile and current Directors, NCL, for allowing me to carry out the research work in a prestigious and well-equipped laboratory. I would like to thank the present and past heads of the catalysis division, for providing me all the divisional facilities required for my research work. CSIR, New Delhi is gratefully acknowledged for the senior research fellowship.

I would like to acknowledge our collaborators, Dr.P.R.Rajamohanan, Dr.T.G.Ajithkumar and Dr. Sumit Bhaduri for their thoughtful comments, provocative ideas and encouraging suggestions towards improvement of the thesis and framing it in right direction.

A special note of thanks to Drs. A. P. Singh, D. Srinivas, , C. V. V. Satyanarayana, Nandini Devi, Subhangi Umbarkar, C. P. Vinod, T. Raja, S. D. Prasad, Ms. Violet Samuel, Mr. R. K. Jha for their help and support in scientific and technical matters. Staff members of Catalysis Division and administrative section, NCL are also acknowledged for alleviating all the official jobs.

It gives me great pleasure to thank my seniors Drs. Vijayaraj, Thirunavakarasu, Maitri, Nagarajan (Raj) and labmates Dhanashree, Anjani, Kanak, Edwin, Jino, Sanjay, Ashwin, Naveen, Deva, Khiru, Geethu, Cimi, Mothi, Maneesh, Pradnya, Raja Ambal, Sivarajani, Ruchi, Meenu, Akrati, Amit, Madhulekha, Apurba Ranjan Sahoo, Anwesha and Mamta, for their constant help, encouragement and the nice time I had with them.

I am grateful to my dear friends Leenamma, Bindhu, Jobychan, Unnichan, Remya, Girish, Sreejith and Kuttan for their constant encouragement and for being always with me in my difficult times. I would like to thank my M.Sc. Classmates, CUSAT friends (Rahul, Renny, Reji and Aani), Geethu, Praji, Swati, Poonam, Soumya, Jijil, Yogita , Ketaki, Anuj, Bhogesh, Nilofer, Rajesh, Mehejabeen, Vinisha, Nisha mol, Nisha Kumari, Sangeeta, Hari, Anu, Saadi, Shoy, Aneesh, Javix, Vijay anna, Kannan, Sridhar, Srikant, Snehal, Vysakh, Sunil, Ashok, Sreedhala, Anju, Remya, Sumathi, Trupti, other NCL friends, divisional friends, tamil friends and all malayali friends in NCL for their co-operation, invaluable help and moral support.

Words are not enough to express my love and gratitude to my family members, Achan & Amma, Appa & Amma, Sudhi and Ramu. It gives me great pleasure to thank them for their love, unfailing support, tremendous patience, trust and encouragement that they have shown to me. I wouldn't have overcome all the hurdles to achieve any goal without their blessings, care and love. All the knowledge that I have acquired today is the result of their upbringing.

I find this an excellent opportunity to appreciate and acknowledge the immense support of my husband, Raj, for his unparallel belief and affection in me that has driven me to excel even under difficult situations. I could not have reached my goals without his help and support at all times. His presence made me feel special even when times were tough for me. He has been my pillar of strength through all my ups and downs.

Above all, I thank my God, Lord Krishna for his blessings, for forgiving my mistakes, for leading me in the right path, for giving me the opportunity to fulfil my wishes and for being there whenever I needed.

Date: 07/05/13 *Thushara*

ABBREVIATIONS

AFM	Atomic Force Microscopy
BC	Benzoyl chloride
BET	Brunauer-Emmett-Teller
BJH	Barrett-Joyner-Halenda
2-BuOH	2-Butanol
CP-MAS	Cross Polarization-Magic Angle Spinning
DTA	Differential Thermal Analysis
DD MAS	Dipolar Decoupled Magic Angle Spinning
EED	External Electron Donor
EtOH	Ethanol
HDPE	High Density Polyethylene
HRTEM	High Resolution Transmission Electron Microscopy
IED	Internal Electron Donor
i-BuOH	Isobutanol
II	Isotactic Index
IR	Infrared
iPrOH	Isopropanol
LDPE	Low Density Polyethylene
LLDPE	Linear Low Density Polyethylene
NMR	Nuclear Magnetic Resonance
PE	Polyethylene
PP	Polypropylene
SEM	Scanning Electron Microscopy
SLF	Separated Local Field
tBuOH	Tertiary Butanol
THF	Tetrahydrofuran
TG	Thermo Gravimetry
UHMWPE	Ultrahigh Molecular Weight Polyethylene
VTNMR	Variable Temperature Nuclear Magnetic Resonance
XRD	X-ray Diffraction

XPS	X-ray Photoelectron Spectroscopy
Z-N	Ziegler-Natta
MgEtOH	$MgCl_2$.6 EtOH
MgiPrOH	$MgCl_2$.4 iPrOH
Mg-*i*-BuOH	$MgCl_2$.4(*i*-BuOH)
Mg2-BuOH	$MgCl_2$.4 (2-BuOH)
MgtBuOH	$MgCl_2$.2(tBuOH)
Ti/MgEtOH	Titanated MgEtOH
Ti/MgiPrOH	Titanated MgiPrOH
Ti/Mg-*i*-BuOH	Titanated Mg-*i*-BuOH
Ti/Mg2-BuOH	Titanated Mg2-BuOH
Ti/MgtBuOH	Titanated MgtBuOH
Est-ME	Esterified MgEtOH
Est-MiP	Esterified MgiPrOH
Est-MiB	Esterified Mg-*i*-BuOH
Est-M2B	Esterified Mg2-BuOH
Ti/Est-ME	Titanated Esterified MgEtOH
Ti/Est-MiP	Titanated Esterified MgiPrOH

Table of Content

Chapter 1: Introduction

Chapter 2: Experimental Methods

Chapter 6: Conclusion & future scope of the work

Chapter 1

1. Introduction

1.1. General background

In 1836, Berzelius, a Swedish chemist, introduced the term 'catalysis' to identify a substance capable of promoting the occurrence of a chemical reaction by a catalytic contact [1]. According to him, catalyst is a substance that is added to enhance the rate of the reaction without being consumed or altered during the process. It's a Greek words *kata*, which stands for down, and *lusein*, which means to split or break. Later on William Ostwald had given the definition of a catalyst:

"A catalyst is a substance that changes the rate of a chemical reaction without itself appearing in the products".

It is important to note that a catalyst does not influence the thermodynamic equilibrium of reactants and products during the reaction [2]. In eighteenth century itself, industry started to use mixture of nitric oxide as a catalyst for the production of sulphuric acid (Lead Chamber process). During 20^{th} century, catalysis plays a major role in industrial process. Today, almost 95 % of all chemicals that are produced have been in contact with a catalyst somewhere in their synthesis process. This number highlights the importance of the role of catalysis in the chemical industry. Without a catalyst, processes are less clean and sometimes impossible to perform. Presence of catalysts opens a new reaction pathway with lower activation energy which results high reaction rates under comparable reaction conditions by Arrhenius Law [3].

$$k = Ae^{-\Delta E_a/RT} \tag{1.1}$$

where A is the Arrhenius constant, R is the universal gas constant (8.32 $Jmol^{-1}K^{-1}$), T is reaction temperature (K), and ΔE_a is the activation energy (J/mol).

Based on whether a catalyst exists in the same phase as the substrate, catalysts can be divided into heterogeneous or homogeneous. In homogeneous catalysis, both the reactant and catalyst exist in the same phase and in other words the catalyst is codissolved in a solvent with the reactants. In heterogeneous catalysis, catalyst and reactants exist in different phase. Most of the heterogeneous catalysts are usually in a solid form and the reaction occurs either in the liquid or gaseous phase. Haber process and Fischer-Tropsch processes, **Ziegler-Natta olefin polymerization** are examples. The major advantage of heterogeneous catalyst over homogeneous is the easy separation and recyclability of catalyst. Due to its definite technical advantages, like production process, competitiveness and economy, heterogeneous catalysts gained lot of importance to the world's economy, to convert the inexpensive raw materials into value added fine chemicals and fuel in an economic, environmental efficient manner and also in the production of pharmaceuticals. Table 1.1 below describes the major advantages/ disadvantages of heterogeneous vs. Homogeneous catalyst [4].

Table 1.1: Comparison of main advantages / disadvantages of Homogeneous vs Heterogeneous catalysts.

Property	**Homogeneous**	**Heterogeneous**
Catalyst recovery	Difficult and expensive	Easy and cheap
Thermal stability	Poor	Good
Selectivity	Excellent/ good, single active site	Good/poor, multiple active site

1.2. Olefin Polymerization

Polymerization is a process of reacting monomer molecules together in a chemical reaction to form polymer chains or three-dimensional networks.

The general polymerization reaction can be represented as:

(1.2)

where R and R' can represent hydrogen atoms, halogen atoms, alkyl or other carbon-containing side chains.

In 1935, Perrin, at the ICL laboratory produced semi crystalline solid from ethylene by applying higher pressure (600 till 3500 bar) and high temperature (200 till 350°C). This discovery led to the commercialization of low-density polyethylene in 1938. This radical polymerization leads to a highly branched polyethylene [5].

In 1950 Hogan and Banks, researchers from the Phillips Petroleum Company, produced highly crystalline polyethylene using CrO_2 supported on silica. Moderate temperature (70 till 100°C) and pressure (30 till 40 bar) was sufficient to carry out the polymerization [6].

In 1953, Ziegler, at the University of Mülheim, discovered that highly crystalline polyethylene could be synthesized under very mild conditions, atmospheric pressure and temperatures between 50 and 100 °C. A combination of titanium chloride and alkylaluminum was used as catalyst for the reaction. This single catalyst is used effectively for preparing variety of polyethylene such as high density polyethylene (HDPE), low density polyethylene (LDPE), linear low density polyethylene (LLDPE). The classification of PE is based on their density or degree of crystallization. Density of a polymer can be controlled by varying the polymerization conditions, temperature, pressure, catalyst amount, monomer concentration etc. Natta used the same catalyst for the preparation of highly stereo specific polypropylene [7-11].

Metallocene catalysts were already known since the 1950's, but the breakthrough came after Reichert and Meyer (1973) added small amounts of water to titanocene/alkyl aluminium chloride systems. This resulted finally in methylaluminoxane (MAO), which proved to be a good co-catalyst for metallocene catalysts. In 1976 Kaminsky and Sinn obtained a highly active catalyst with a metallocene complex and MAO [12]. Despite

intensive experimental [13-16], theoretical [17, 18], and combined [19, 20] studies, MAO has remained a "black box". Proposed structures of alkylaluminoxanes are shown in Figure 1.1. The polymers produced with metallocene catalysts have narrower molecular weight distributions and more uniform incorporation of co-monomers than polymers produced with Ziegler catalysts [12, 21-25]. The main disadvantage of this metallocene-based polymerization technology lays in the lack of morphology control of the polymer particle and requirement of large amounts of MAO. Therefore, several technical problems have been solved before metallocene catalysts started to be present in the industrial plants.

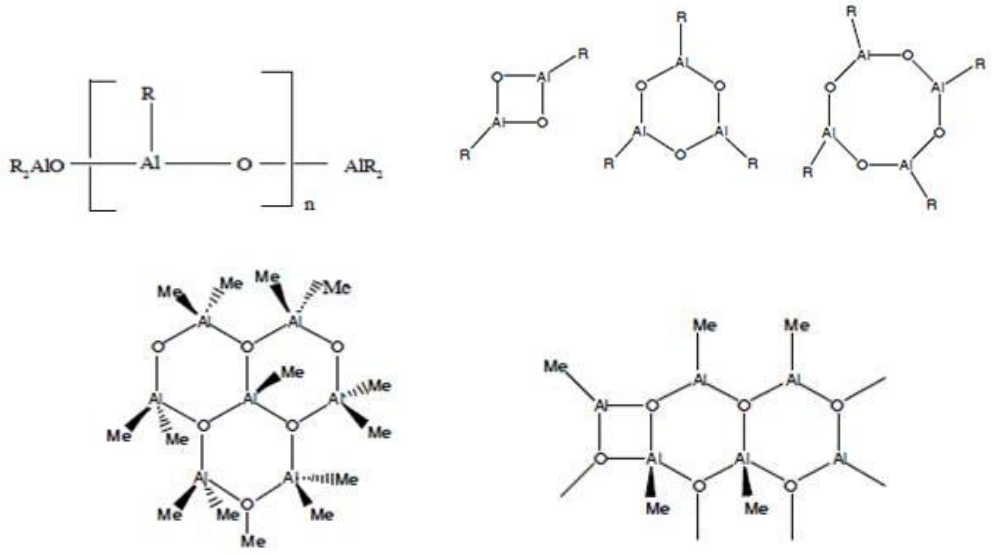

Figure 1.1: Proposed structures of alkylaluminoxanes

Nowadays polyolefin such as polyethylene (PE) and polypropylene (PP) are the major plastic produced in the polymer industry. According to survey, the production of polyolefin exceeds to 140 million ton in 2010. In commercial olefin polymerisation processes Ziegler-Natta catalysts (Z-N), Phillips-type catalysts and single-site catalysts (Metallocene) are used, with Z-N catalysts being the most common. Tens of millions tons of PE are being produced by Z-N catalysts each year [26] (Figure 1.2). Z-N catalysts have advantages of producing product with high molecular weight, high melting point and controllable morphology. Heterogeneous Z-N consists of $TiCl_4$ as an active catalyst, $MgCl_2$ as support, trialkyl

aluminium as co-catalyst and optionally Lewis base as electron donor.

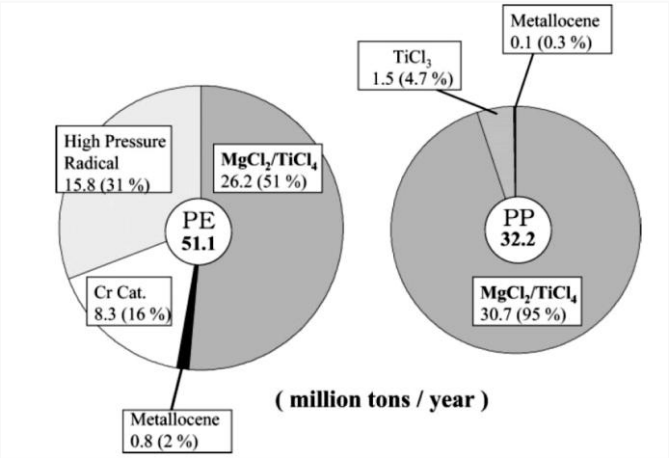

Figure 1.2: Catalysts for global PE and PP production

PP is a thermoplastic polymer made by polymerisation of propylene. It is used in a wide variety of applications including food packaging, ropes, textiles, plastic parts and reusable containers of various types, laboratory equipment, loudspeakers automotive components and polymer banknotes. These polymer banknotes are developed by Reserve Bank of Australia using polymer biaxially-oriented polypropylene in order to improve the durability of the banknotes. Depending on the position of the methyl groups relative to the polymer back bone, PP can be classified into isotactic, syndiotactic and atactic polypropylene. Properties of the PP vary with stereospecificity. In isotactic PP, all methyl groups are located on the same side of the macromolecular backbone. The methyl groups are arranged in alternate positions along the chain in syndiotactic PP and for actactic PP, the methyl groups are placed randomly along the chain (Figure 1.3).

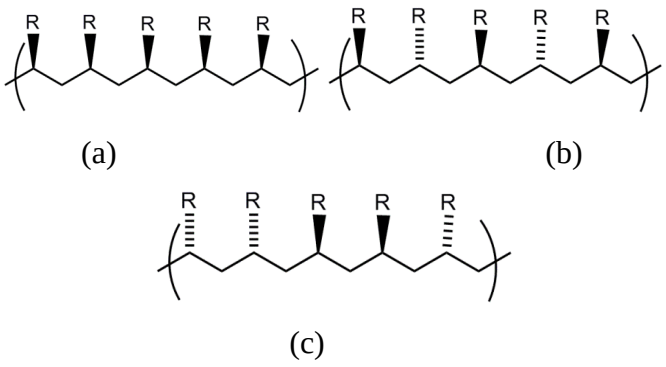

Figure 1.3: Schematic representation of (a) isotactic (b) syndiotactic and (c) actactic PP.

PE is a thermoplastic polymer made by polymerisation of ethylene. It is used in a wide variety of applications where blow molding, injection molding or extrusion coating can be applied. PE is the most common polymer and is produced on a multi-million tonne scale annually. The major differences between different types of Polyethylene are the following:

HDPE has a low degree of branching and thus low intermolecular forces and tensile strength. It can be produced by chromium/silica catalysts, Ziegler-Natta catalysts or metallocene catalysts.

LDPE has a high degree of short and long chain branching, therefore, it possess less strong intermolecular forces. LDPE is created by Free radical polymerization is used for LDPE production.

LLDPE is a substantially linear polymer with significant numbers of short branches, commonly made by copolymerization of ethylene with short-chain alpha-olefins. It has higher tensile strength than LDPE, it exhibits higher impact and puncture resistance than LDPE.

UHMWPE is polyethylene with a molecular weight numbering in the millions, usually between 3.1 and 5.67 million which makes it a very tough material. Table 1.2 shows the different types of PE, property and their commercial application.

1.2.1. Different Catalyst Used for Olefin Polymerization

1.2.1.1. Ziegler-Natta Catalysts

Z-N catalyst is mainly based on Ti as an active centre, magnesium alkoxide or magnesium halides are used as support and alkylaluminum compounds as co-catalyst. Different alkyl aluminium compound such as Et_3Al, Et_2AlCl, $EtAlCl_2$ etc were used as co-catalyst. Out of these aluminium alkyls, Et_3Al is the most widely used co-catalyst for ethylene and propylene polymerization. However, for propylene polymerization, though Et_2AlCl was used as a co-catalyst in the earlier generations, use of Et_3Al as co-catalyst gained precedence and

was also more effective and economical since the subsequent generations of the PP catalyst were having suitable internal electron donors like esters, ethers etc.

Table 1. 2: Commercial classification, property and application of PE.

Acronym	**Designation**	**Density (kg/m^3)**	**Application**
HDPE	High density polyethylene	>940	Blow molding (milk bottles, drums, containers), films and sheets, extruded pipe, injection molding.
UHMWPE	Ultrahigh molecular weight polyethylene	930-935	Specialty applications
LLDPE	Linear low-density polyethylene	915-925	Film applications, injection molding, wire and cable sheathing
LDPE	Low-density polyethylene	910-940	Thin films, extrusion coating, injection molding, wire and cable sheathing.

As compared to Et_2AlCl, Et_3Al is a high reducing agent; it will reduce the Ti^{4+} to Ti^{3+} and Ti^{2+}. The Ti^{3+} and Ti^{2+} are active species for ethylene polymerization but Ti^{3+} only active for propylene polymerization. In chemical routes, Mg and Ti precursors are treated with Lewis bases in solvents. Toluene, chlorobenzene, hexane, heptanes etc are examples of solvents used in olefin polymerization [7-11, 26-30].

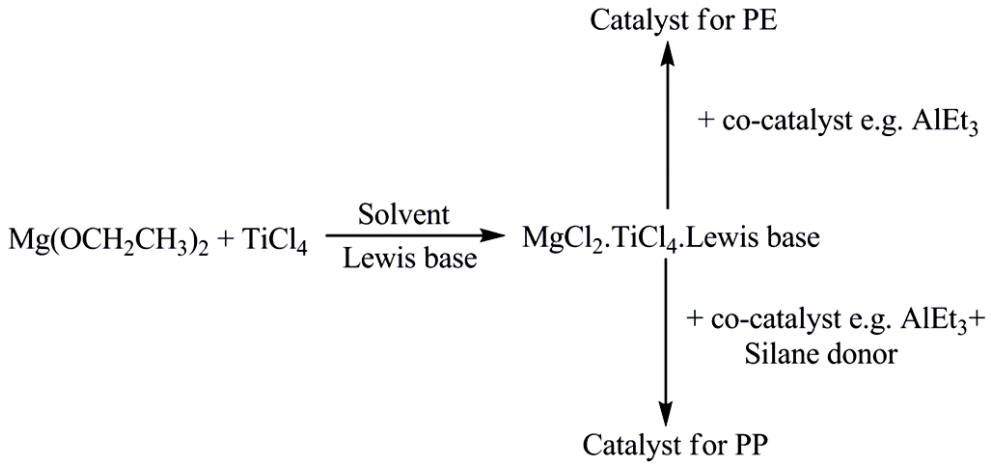

1.2.1.2. Phillips type catalyst

Phillips-type catalysts, which are composed of a chromium oxide supported on an amorphous material such as silica (e.g. Cr/SiO_2). The catalyst is prepared by impregnation of a chromium oxide on wide pore silica [31-33]. CrO_3, *Bis*(triphenyl silyl) chromate, chromocene etc were used as chromium source. The impregnated material is subsequently heated in air at high temperature, cooled down, flushed with nitrogen, and stored under dry nitrogen until loaded in the polymerization reactor. Chromium-based catalysts are able to polymerize olefins which have no branching closer than the 4- position to the double bond and which contain no more than about eight carbon atoms. Thus, propylene, 1- butene, 1-pentene, and 1-hexene are polymerized to branched, high molecular weight polymers ranging from solids to viscous liquids. Phillips catalysts are able to make more than 50 different types of polyethylene, and a whole battery of chromium-based catalysts are developed, each of which are able to produce a different type of HDPE or LLDPE [34].

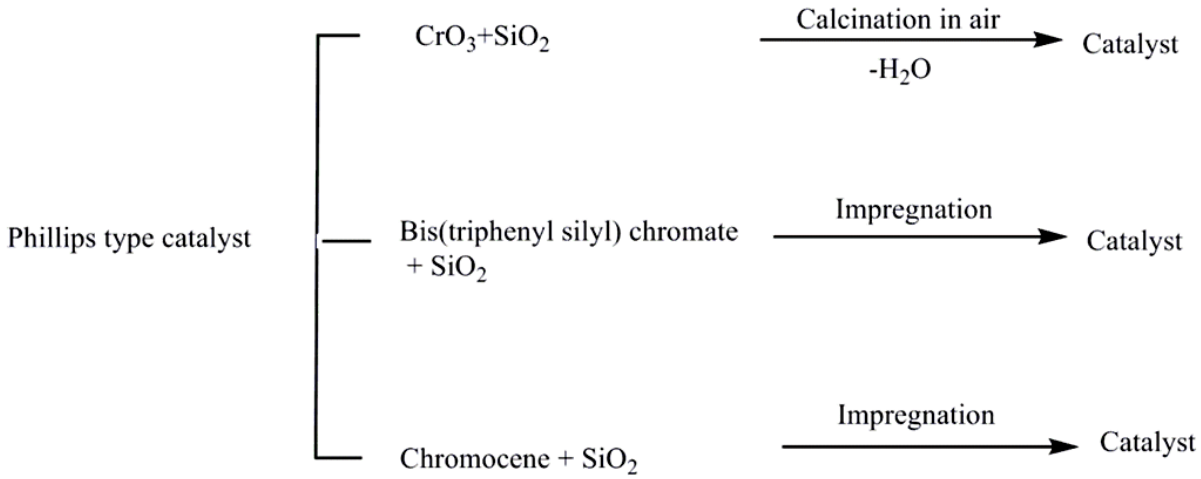

1.2.1.3. Single-site catalyst

Metallocene compounds are discrete molecules that have two cyclic ligands bonded to a metal center. Single site metallocene catalysts consist of *bis*-cyclopentadienyl derivatives of either Zr, Hf or Ti, in combination with methylaluminoxane (e.g. Cp_2ZrCl_2+ [MeAlO]n). PE produced with metallocene catalysts have narrower MWD than the polymers produced with

the other two catalyst systems [12].

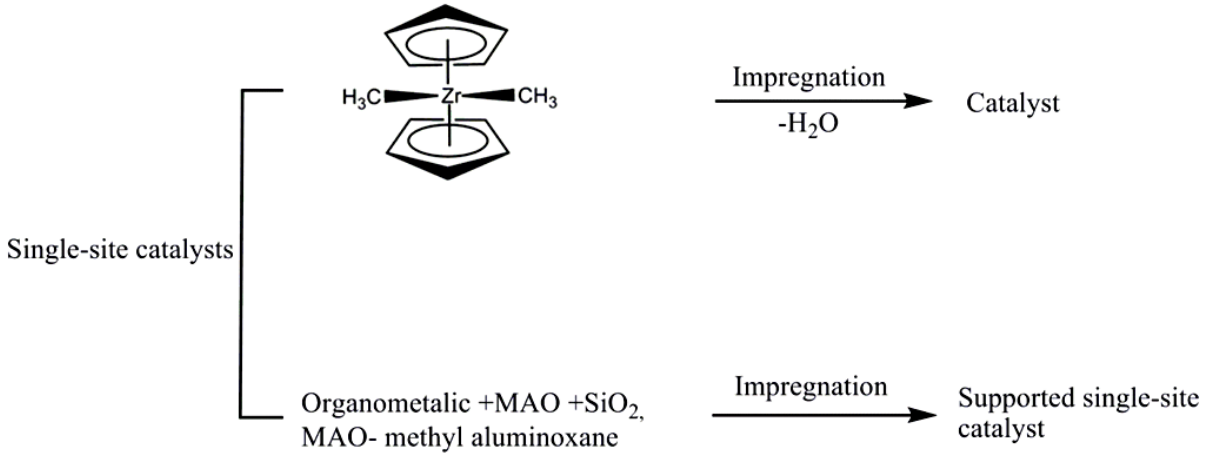

1.3. Discovery of Ziegler-Natta (Z-N) Catalyst

The origin of the highly efficient olefin polymerization catalyst was discovered by Karl Ziegler in 1950's while trying to synthesise olefin using his newly synthesized triethylaluminium. The final product is exclusively 1-butene instead of oligomeric product. This is due to the Nickel effect which was caused by nickel contaminant. Further they studied different catalyst with Et_3Al and wide range of transition metal. Out of these transition metal salt (group IV to VI), the most active metal salt is $TiCl_4$ and this catalyst ($TiCl_4$ +$AlEt_3$) was used for the manufacture of high density polyethylene (HDPE). In 1954, Natta, at the Polytechnic of Milan apply the same methodology for propylene polymerization. He succeeded in isolating crystalline polypropylene using Ziegler's $TiCl_4$ +$AlEt_3$ catalyst. These discoveries led to a breakthrough in polymer industry and they shared the Nobel Prize in 1963 [7-11].

1.4. Discovery of $MgCl_2$ supported Ziegler-Natta catalyst

The first generation of Z-N catalyst is $TiCl_3$. $0.33AlCl_3$ produced by the reduction of $TiCl_4$ with $AlEt_3$ [35]. Eventhough the discovery of Z-N catalyst open a new era for olefin polymerization, the catalyst has its own disadvantages. The demerits of the first generation Z-N catalyst was (i) less number of active Ti species (ii) difficulty of catalyst removal from the

final product (deashing), (iii) less stereospecificity in the case of propylene polymerization (iv) less control of growing polymer branching due to multiple metal sites of transition metal and (v) encapsulation effect of polymer chains [36]. The method to increase the activity of the Z-N catalyst is to disperse the catalyst on a support. The function of the support is to disperse the active Ti species for high activity for olefin polyolefin polymerization. A variety of metal halides and oxides such as Mg(OH)Cl, hydroxylated MgO or $MgSO_4$ have been reported as suitable supports for the catalysts [27-29]. The most significant result was obtained in 1960's by the discovery of $MgCl_2$ as an efficient support for Z-N catalyst by Kashiwa [26]. This discovery led to the generation of second generation catalyst. The best support is $MgCl_2$ due to the fact that Mg and Ti have similar atomic size and shape. The ionic radii of Mg^{2+} (0.66 Å) and Ti^{4+} (0.68 Å) are having same value and the highly disordered δ-$MgCl_2$ and the active δ-$TiCl_3$ belongs to same cubic close packed structure. Table 1.3 shows the comparison between the crystallographic parameters of different form of $MgCl_2$ and $TiCl_4$ crystal modifications. The atomic distance between the Mg-Cl and Ti-Cl is 2.57 and 2.51 Å [28, 29].

To improve the interaction of $MgCl_2$ and $TiCl_4$ and increase the surface area of the $MgCl_2$ support, different synthetic procedure such as ball milling, recrystallization and the chemical reaction methods etc were employed [30]. The recrystallization method consists of a chemical activation by reaction of crystalline $MgCl_2$ with alcohol. In chemical method, active catalyst formed by the reaction between $TiCl_4$ and magnesium alkoxides such as $Mg(OEt)_2$ which shows a very high activity for the polymerization of ethylene. Details about the different experimental methods are discussed later. The highly crystalline nature of the $MgCl_2$ makes it difficult to incorporate $TiCl_4$ on the lateral cuts of $MgCl_2$.

Kashiwa used n-butanol as a Lewis base to reduce the crystallanity of $MgCl_2$. Reaction of $MgCl_2$ with n-butanol leads to the formation of molecular adduct with a formula

of $MgCl_2$.2 (n- Butanol). The main advantages of introducing Lewis base in the lattice of $MgCl_2$ are reduction in the crystallanity of $MgCl_2$ and increase in the surface area of the support material [26].

Table 1.3: Comparison between the crystallographic parameters of $MgCl_2$ and $TiCl_4$ crystal modifications.

Product	**α - $MgCl_2$**	**γ -$TiCl_4$**	**β - $MgCl_2$**	**α - $TiCl_4$**
Structure	Cubic close packed layer structure		Hexagonal close packed layer structure	
Lattice parameters (Å)	a = b = 3.63 c = 17.79	a´ = b´ = 3.54 a´ = a/√3 c = 17.58	a = b = 3.64 c = 5.93	a´ = b´ = 3 a´ = a/√3 c = 5.87 c´ = c/3
Crystalline form	Rhombohedral		Rhombohedral	
Cation coordination	Octahedral		Octahedral	
Atomic distances (Å)	Mg – Cl = 2.56	Ti – Cl = 2.51	Mg – Cl = 2.51	Ti – Cl = 2

Table 1.4 shows the changes in the specific surface area by reaction of $MgCl_2$-2(n-Butanol) with $TiCl_4$. Surface area of the bare $MgCl_2$ is < 1 m^2/g, after the adduct formation the value increases to ~ 2 m^2/g. The surface area of the final Z-N catalyst shows 292 m^2/g by dispersing on the active $MgCl_2$ support. Moreover, the catalyst synthesis procedure seems to be the most important factor for determining the catalyst performance since they give the final polymer with different properties. Ethanol is the most widely used Lewis base in $MgCl_2$ supported Z-N catalyst. Other than $MgCl_2$, SiO_2 [37], intercalated silicates [38], zeolites [39] etc are the examples of support used for heterogeneous Z-N catalyst. After the discovery of the $MgCl_2$ supported Z-N catalyst, lot of modification has been carried out to improve the yield of polymer and the production of highly stereospecific polypropylene. This

modification leads to the different generation of Z-N catalyst. Before going to discuss about it, let's discuss about the structure of the $TiCl_3$ catalyst and about the property of $MgCl_2$.

Table 1.4: Changes of Specific Surface Area by the Reaction of $MgCl_2$-2(*n*-Butanol) with $TiCl_4$ [26].

Solid	**Specific Surface Area (m^2/g)**
$MgCl_2$	0.75
$MgCl_2$-2(n-butanol)	1.49
Product of the reaction between $MgCl_2$-2(n-butanol) and 12 equiv $TiCl_4$	292

1.4.1. Structure of $TiCl_3$ catalysts

$TiCl_3$ can be prepared from $TiCl_4$ by many different routes including reduction with hydrogen, irradiation, and the commercially preferred reduction with aluminium alkyls [35], e.g.

$$TiCl_4 + 0.33\ AlEt_3 \longrightarrow TiCl_3.\ 0.33\ AlCl_3 + 0.5\ C_2H_6 + 0.5\ C_2H_4 \qquad (1.3)$$

$$TiCl_4 + 0.5\ AlEt_2Cl \longrightarrow TiCl_3.\ 0.5\ AlCl_3 + 0.5\ C_2H_6 + 0.5\ C_2H_4 \qquad (1.4)$$

Natta found these catalysts to exist in four different structural modifications, depending on the reduction procedure used, and designated them α,β, γ and δ modifications. Theα,β, γ, and δ forms are deep purple in colour and have a layer lattice structure (Figure 1.4), whereas β- $TiCl_3$ is brown and has a chainlike structure (Figure 1.5) [40].

In each individual $TiCl_3$ layer, titanium ions fill two-thirds of the octahedral holes between two chloride layers. In α- $TiCl_3$ the individual layers are stacked to give a hexagonal close packing of the chloride ions; γ- $TiCl_3$ has a cubic packing arrangement, while the δ-form, an intermediate between α and γ is more disordered [35,40].

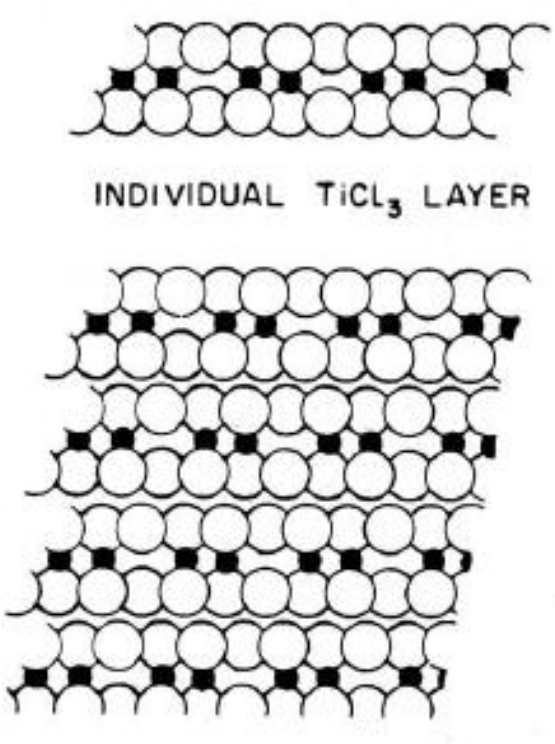

Figure 1.4: α- $TiCl_3$ layer lattice structure

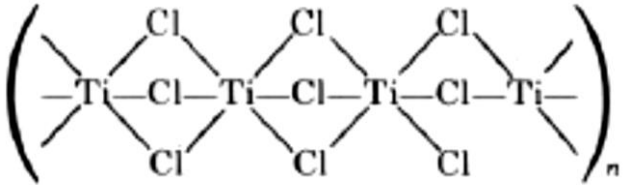

Figure 1.5: β- $TiCl_3$ chain like structure.

Natta and co-workers demonstrated that the $TiCl_3$ catalyst lattice structures determined the stereoselectivity of the catalyst and hence polymer isotacticity; brown β-$TiCl_3$ gave low isotacticity, while purple (α,γ, δ)- $TiCl_3$ gave high isotacticity. The elegant work of Cossee and Arlman presented a rational and still widely accepted explanation of these facts [41, 42]. Arlman and Cossee proposed that the catalytically active centers are Ti ions which possess vacant octahedral site and are bounded to five chlorine atoms. Out of five chlorine atoms, one chlorine atom protrudes from the surface; the other four are bridged to further Ti atoms. By reaction with the co-catalyst the chlorine atom protrudes from the surface is replaced by an alkyl group from co-catalyst to form active Ti-C bond. Figure 1.6 shows the

mechanism of olefin polymerization known as Cossee- Arlman mechanism. This mechanism consists of two steps in which the transition state is assumed to be four- membered ring:

i. Coordination of the monomer at the vacant octahedral coordination.

ii. Chain migratory insertion of the coordinated monomer with migration of the growing chain to the position previously occupied by the coordinated monomer [41, 42].

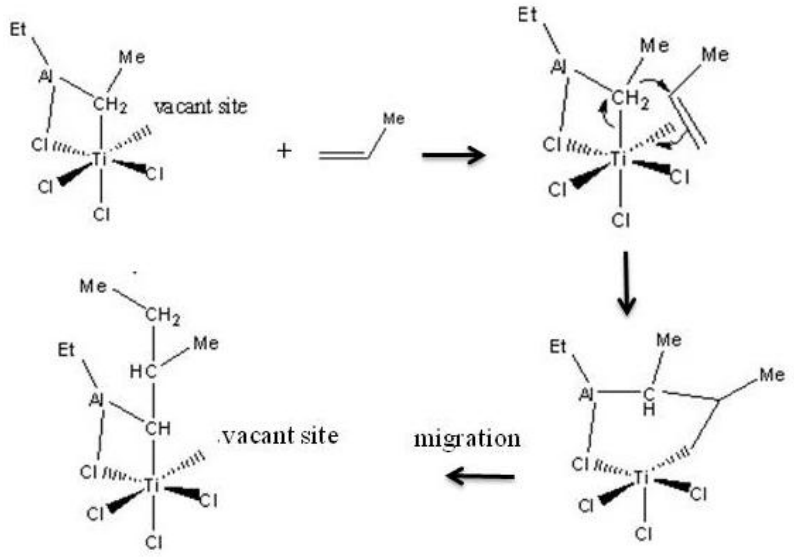

Figure 1.6: The Cossee- Arlman polymerization mechanism.

1.4.2. Structure of $MgCl_2$

Magnesium Chloride is an inorganic salt, which has the chemical formula of $MgCl_2$ and molecular weight 95.210 g/mol. $MgCl_2$ crystallites exhibits cadmium chloride structure with Mg atom in octahedral coordination (Figure 1.7). $MgCl_2$ exist in different crystalline forms - α, β and δ- $MgCl_2$. α and β-$MgCl_2$ exhibit cubic close packed and hexagonal close packed structure, respectively. δ- $MgCl_2$ shows a disordered structure.

Table 1.5 exhibits the structural similarities between δ- $MgCl_2$ and δ- $TiCl_3$. The schematic presentation of the interaction of $TiCl_4$ with $MgCl_2$ was shown in Figure 1.8 which leads to the formation of active species [26]. This precatalyst is treated with trialkyl aluminium (Et_3Al), as co-catalyst to reduce the Ti^{4+} to Ti^{3+} by alkylation process.

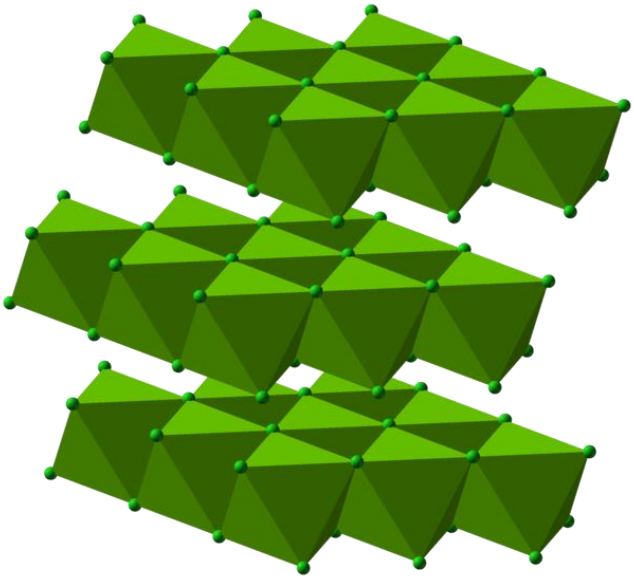

Figure 1.7: Structure of $MgCl_2$

Table 1.5: Comparison between the crystallographic parameters of the active forms of $MgCl_2$ and $TiCl_4$.

Product	**δ – $MgCl_2$**	**δ – $TiCl_3$**
Structure	Closed packed layer structure with stacking defects	
Lattice parameters (Å)	a = b = 3.63; c = 5.93	a = b = 3.54;c = 5.86
Specific gravity (g/cm^3)	2.33	2.71
Cation coordination	Octahedral	
Atomic distances (Å)	Mg – Cl = 2.57	Ti – Cl = 2.51

Table 1.6 shows that from the 3rd generation onwards researchers started to introduce electron donor such as benzoate with heterogeneous Z-N catalyst [43]. As compared to the previous generation catalyst, 3rd one results in high activity and PP with high isotactic index (II, i.e., the fraction of isotactic polymer). Instead of benzoate, much modification has been done on Z-N catalyst with phthalate as internal donor and silane as external donor. Studies shows that diether will be the suitable internal electron donor (IED) because of the O-O bond distance matches with Mg-Cl bond which form a strong chelating effect. By using diether as

IED, there is no need to use any external donor during polymerization.

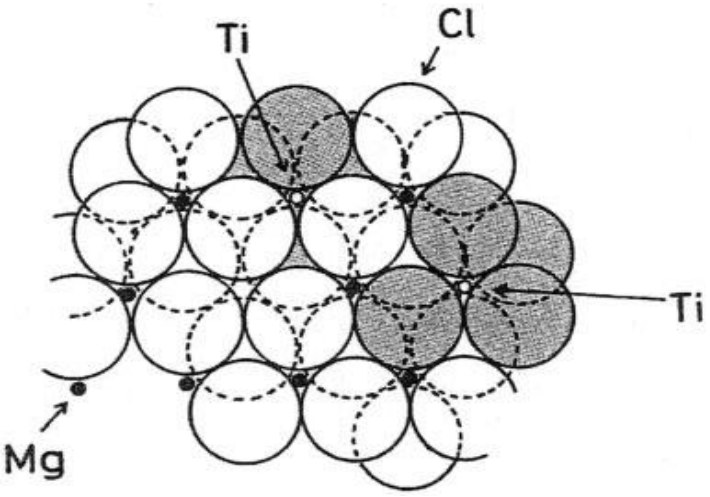

Figure 1.8: Interaction of $TiCl_4$ with $MgCl_2$.

Table 1.6: Different Generation of Ziegler-Natta Catalyst and its activity for propylene polymerization.

Generation (year)	Catalyst composition	Productivity (kg_{pp}/g_{cata})	II (%)
First (1954)	$\delta - TiCl_3/ 0.33AlCl_3 + AlEt_2Cl$	2-4	90-94
Second (1970) (1986)	$\delta - TiCl_3 + AlEt_2Cl$ $MgCl_2/TiCl_4 + AlR_3$	10-15 15	94-97 40
Third (1971)	$MgCl_2/TiCl_4$/benzoate + AlR_3/benzoate	15-30	95-97
Fouth (1980)	$MgCl_2/TiCl_4$/phthalate + AlR_3/silane	40-70	95-99
Fifth (1988)	$MgCl_2/TiCl_4$/diether + AlR_3 $MgCl_2/TiCl_4$/diether + AlR_3/silane	100-130 70-100	95-98 98-99
(1999)	$MgCl_2/TiCl_4$/succinate + AlR_3/silane	40-70	95-99

1.5. Role of Electron Donors

Electron donors (Lewis bases) play a major role in controlling the stereospecificity of PP. However, in the case of PE, presence of electron donor enhances the activity. Electron donor (ED) can be internal and external electron donor. Internal electron donors (IED) are added during the catalyst preparation process while external electron donors (EED) are added during polymerization. Ethanol, ether, amine, ester, phthalate etc are examples for IED and alkoxysilane is an example for EED [44-54]. Figure 1.9 shows the ball and stick models of ED's.

Mainly there are three types of uncoordinated Mg^{2+} ions are present on the surface of a poly crystalline $MgCl_2$. They are the following: $\mathbf{Q^5}$ sites, five-coordinated Mg ions at the (1 0 0) face; $\mathbf{Q^4}$, four-coordinated Mg ions at the (1 1 0) face, and $\mathbf{Q^3}$, three-coordinated Mg ions at the edges and corners of $MgCl_2$ crystals (Figure 1.10) [52, 55]. These low-coordinated Mg ions demonstrate pronounced Lewis acidic properties and are capable of strong coordination of ester molecules. The equilibrium crystal shape calculations show that the five-coordinated Mg cations are the dominant adsorption sites since the surface area of the (104) $MgCl_2$ plane is greater by several times than that of the (110) $MgCl_2$ plane [56].

The function of the IED at least twofold:

i. stabilization of the crystallites of $MgCl_2$.

ii. control of the distribution of $TiCl_4$ on the possible $MgCl_2$ cuts.

On the other hand, it has recently been observed that the nature of the IED also has a considerable impact on the size of the $MgCl_2$ crystallites and thus on the working surface and the productivity of the resulting catalyst. For stereospecific polymerisation, the function of IED are : (i) IED blocks the (110) $MgCl_2$ surface on which aspecific active sites are likely to form [52], (ii) IED shifts the equilibrium between aspecific mononuclear Ti species and stereospecific dinuclear Ti species on the (104) $MgCl_2$ surface toward the latter species [52],

(iii) IED turns aspecific Ti species into stereospecific Ti species due to coordination with Ti [57], (iv) IED turns aspecific Ti species into stereospecific Ti species due to coordination with the $MgCl_2$ surface not far from the Ti species [58, 59]. Ethyl benzoate (EB) and diisobutyl phthalate are the two Lewis bases well studied by different groups.

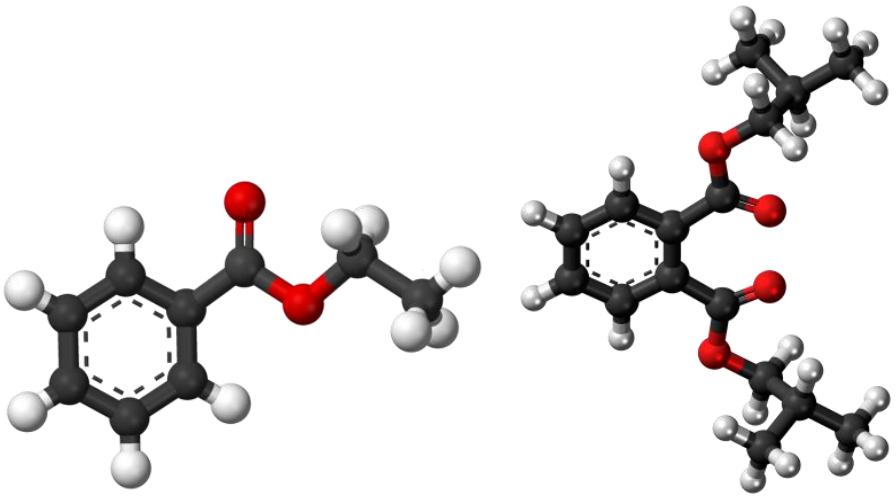

(a) (b)

Figure 1.9: Electron donors (a) Ethyl Benzoate and (b) Diisobutyl phthalate.

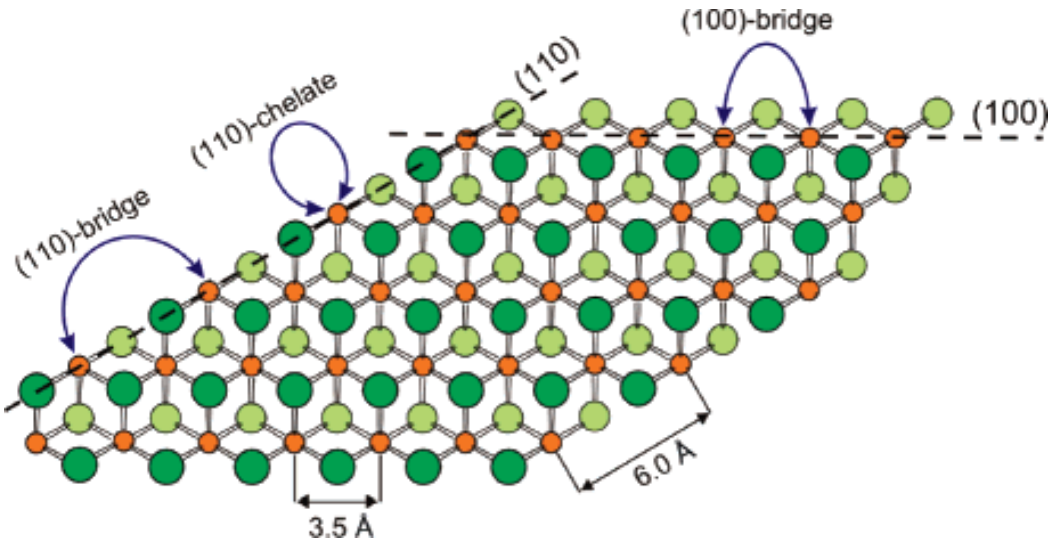

Figure 1.10: Schematic representation of an $MgCl_2$ monolayer. The Mg atoms are colored in orange. The Cl atoms above the Mg plane are dark green colored, whereas the Cl atoms below the Mg plane are light green colored. The (100) and (110) lateral cuts with 5- and 4-coordinated Mg atoms are indicated.

1.6. Preparation of Ziegler-Natta catalyst

The synthetic procedures for the catalyst preparation can be divided into three main classes: Mechanical Routes, chemical routes and mixed mechanical-chemical routes.

1.6.1. Mechanical Routes

This approach is directly derived from the methods used for the activation of the early $TiCl_3$- based catalysts, it consists of a step in which the catalyst components ($MgCl_2$, $TiCl_4$ and optionally, the Lewis base) are milled together for several hours [60-62]. A ball mill is usually employed. $MgCl_2$ can be also generated during the milling process by reacting a magnesium compounds with a chlorinating agent (e.g., $SiCl_4$).

1.6.2. Mechanical plus chemical routes

There are two different approaches belonging to this type of catalyst synthesis.

i) Co-milling of $MgCl_2$ or a $MgCl_2$-precursor and optionally, a Lewis base or internal donor. The resulting solid is then separately treated with an excess of $TiCl_4$ at a temperature usually higher than 80 °C, and washed with hydrocarbons to remove all the unreacted $TiCl_4$ [63-66]. The treatment with $TiCl_4$ has a double role: (i) binding itself to the $MgCl_2$ surface and, in particular to the vacant Mg coordination sites, displacing part of the internal donor, if present; and (ii) removal of all the undesired by-products formed during the reaction from the catalyst surface. In some cases, $TiCl_4$ can be diluted in aromatic or halogenated compounds that are good solvents for the by-products.

ii) Co-milling of all the catalyst components, as described in the pure mechanical approach, followed by one or more washing with halogenated or aromatic solvents. This type of post treatment of the solid increases the activity and stereospecificity of the final catalyst [67, 68].

1.6.3. Chemical Routes

In this class of preparation methods, both the formation of the active form of $MgCl_2$

and the incorporation of the other components are carried out by means of a chemical reaction. The most common synthetic procedures can be divided into four families, according to the both types of reagents and of the reaction(s) involved.

i) A complex of $MgCl_2$ with a Lewis base (e.g., an alcohol) is treated with excess $TiCl_4$ in the presence of an internal donor at 80 °C or higher temperature. The solid is then carefully washed with hydrocarbon solvents [69-73]. Minor modifications of this approach are either the use of aromatic or halogenated solvents to dilute $TiCl_4$ or a separate treatment with $TiCl_4$ and the Lewis base. The $MgCl_2$-Lewis base complex can be transformed into the active form of $MgCl_2$ before the treatment with $TiCl_4$ and the internal donor, by removing the Lewis base via either a chemical reaction or via thermal decomposition.

ii) $MgCl_2$ is obtained in situ from the reaction of a precursor and $TiCl_4$ in the presence of the internal donor and an aromatic or halogenated solvent. Typical precursors can be $Mg(OR)_2$ and Mg(OR)Cl and the titanium alkoxides formed are removed during the treatment or in the final washings [73-76].

iii) Active $MgCl_2$ is obtained from the reactions of MgR_2 or MgRCl and a chlorinating agent. In order to get morphology control, the magnesium compound can be dispersed on a support, e.g., silica, alumina, or other inorganic carriers, before the reaction. The final step is the usual treatment with $TiCl_4$ and when desired, the internal donor. In some cases, the active $MgCl_2$ is pre-treated with some amounts of a Lewis base, e.g., an alcohol [77-79].

iv) Either $MgCl_2$ or a precursor (e.g., $Mg(OR)_2$, $Mg(OCOR)_2$, MgR_2) is dissolved in a solvent (ROH, trialkyl-phosphate, titanium alkoxides, etc). The solution is treated with a chlorinating agent to precipitate the active $MgCl_2$. This can be reacted directly with $TiCl_4$ and the internal donor or treated according to the conditions described above [80-84].

To improve the catalyst performance, some parameters are necessary to be controlled. In the case of catalyst obtained from mechanical and mixed routes, the main factors affecting

the catalyst performances are the time and the efficiency of milling and the ratio between the components. In the case of chemical routes, the purity of the reagents, their ratio, the order of mixing, the reaction time, and the treatment temperature are the main key parameters to be optimized inorder to obtain high-performance catalyst.

Active $MgCl_2$ obtained through ball milling (mechanical routes) results in a support with no morphology control in terms of shape, size and size distribution. However, chemical routes results in catalyst to control shape, especially spherical. Nowadays, chemical route is the most attractive procedure to prepare the highly efficient catalyst for the industrial production of polyolefin.

To obtain supports and catalysts having finely controlled morphology, different approaches have been developed. They are the following

i) Controlled precipitation of the solid support.

ii) Spray-drying or cooling of either dissolved or molten magnesium derivatives.

iii) Use of silica or other solid carriers having controlled shape to support $MgCl_2$ or $MgCl_2$ precursors.

iv) Fast cooling of an emulsion, e.g., in paraffin oil, of $MgCl_2$.nROH complexes.

The latter procedure results in perfect spherical particles with narrow size distribution, and a very fine control of the size of the catalysts particles in the range of 10-100 μm. It is possible to improve the morphological stability and tune the porosity of the resulting catalyst in the range of 0.3-0.6cm^3/g.

1.7. Objective of the Thesis

A survey of literature reports since past few decades reveals that Z-N catalyst supported on $MgCl_2$ with ethanol as Lewis base is the most widely used catalyst for olefin polymerization. Even though homogeneous metallocene catalyst is more active than heterogeneous Z-N catalyst, many polymer industries are working based on heterogeneous Z-

N catalyst. Literature studies are based on the characterization of polymer, and then based on the property of the polymer, researchers were correlating the structure and property with that of the catalyst. Direct investigation of the active species on the catalyst is an extremely complex problem even if other difficulties such as complexity of the composition, low content of the active sites in the catalyst, high sensitivity to oxygen and moisture in the ambient conditions are ignored. As we know that in heterogeneous catalysis, supports play a major role in the final catalytic activity. In the case of Z-N catalyst, the fundamental molecular level understanding of the $MgCl_2$ support is not explored sufficiently. Hence, the main objective of the thesis is to understand the molecular level properties of $MgCl_2$ based molecular adduct with different alcohols and correlate structure activity relationship with olefin polymerization activity. Several patents and papers discussed about the preparation of active $MgCl_2$ with different Lewis bases like aromatic esters, ethanol, ether etc. Among alcohols, ethanol is the most studied and used by researchers. There is no report about the molecular adduct formation with other aliphatic alcohols such as isopropanol, isobutanol, 2-butanol and tertiary butanol [85, 86]. Different alcohols were chosen based on their size and nature. Lewis basicity of the alcohol vary from ethanol to isopropanol to isobutanol to 2-butanol to tertiary butanol. We also explored how the textural properties of the molecular adduct support vary with the nature of alcohols. When Lewis base like ethyl benzoate (EB) is introduced into the system, there is a chance of interaction between EB with $MgCl_2$, $TiCl_4$, Et_3Al and solvent etc. In order to avoid that situation, we prepared ester via in-situ esterification of alcoholic adduct with benzoyl chloride (BC). Here benzoyl chloride is used as a chlorinating agent. In $MgCl_2$.nROH adduct (where n = 6 or 4), we are esterifying only one alcohol molecule.

1.8. Outline of the Thesis

This thesis mainly deals with the synthesis procedure of different $MgCl_2$.nROH adduct

(R= -CH_2CH_3, -$CH_2CH(CH_3)_2$, -$CH(CH_3)_2$, CH_3 (-CH)CH_2CH_3 and –$C(CH_3)_3$ by chemical routes (Azeotropic distillation method) and detailed characterization of prepared materials and their catalytic activity by ethylene polymerization after transforming them into Z-N catalysts through reaction with $TiCl_4$. An attempt has been taken to synthesize alcoholic adduct with $MgCl_2$ by using primary, secondary and tertiary alcohols and esterification of few alcoholic adduct with benzoyl chloride. These esterified adducts where treated with $TiCl_4$ to generate potential Z-N catalysts for olefin polymerization.

Three types of system have been discussed in this thesis,

(i) $MgCl_2$ molecular adduct with linear and branched primary alcohols, eg. CH_3CH_2OH, $(CH_3)_2$ $CHCH_2OH$.

(ii) $MgCl_2$ molecular adduct with linear and branched secondary and tertiary alcohols, e.g. $(CH_3)_2$ $CHOH$, $CH_3CH_2CH(OH)CH_3$ and $(CH_3)_3COH$.

(iii) Esterification of $MgCl_2$- alcoholic adduct with benzoyl chloride.

The following is the chapter-wise outline of the present thesis work.

Chapter 1 presents the general introduction to heterogeneous catalysts with a suitable emphasis on heterogeneous Z-N catalyst. It gives a brief description to olefin polymerization, different generation of Z-N catalyst and details of different synthetic procedure used for making active Z-N catalyst. At the end of this chapter the scope of the thesis is presented.

Chapter 2 mainly deals with the experimental methods involved in the preparation of $MgCl_2$.nROH. It includes general introduction to the physico-chemical characterization techniques. The theory and experimental procedures involved to characterize the prepared materials are discussed.

Chapter 3 is divided into two parts - **Part A** and **Part B**. **Part A** describes detailed characterization of ethanol and isobutanol adduct ($MgCl_2$.6 (CH_3CH_2OH) and $MgCl_2$.4

($(CH_3)_2CHCH_2OH$.Through various physico-chemical, spectroscopic and microscopic methods the effect of linear and branched alcohol in tuning the final catalytic activity was explored. Catalytic activity of the catalyst is tested for ethylene polymerization.

Part B brings out the effect of temperature and set to reflux time on the isobutanol adduct.

Chapter 4 describes the characterization and activity testing of isopropanol, 2-butanol and tertiary butanol adduct and their titanated catalyst. Catalytic activity of the catalyst is tested for ethylene polymerization.

Chapter 5 brings out the role of internal electron donor in the polymerization reaction by preparing esterified adduct with BC. Molecular adduct with IED in it has been characterized thoroughly and some of them are evaluated for PE synthesize after titanation to transfer them into Z-N catalysts.

Chapter 6 summarizes the conclusions derived based on the observation and results obtained from the entire study. At the end scope of further research work in the area of the present study have been discussed.

1.9. References:

1 G.C. Bond in: *Heterogeneous Catalysis: Principles and Applications*, Clarendon Press, Oxford, 1987.

2 B.C. Gates in: *Catalytic Chemistry*, John Wiley & Sons Inc., New York, 1992.

3 G. Ertl. *Angew. Chem. Int. Ed*. **47** (2008) 3524.

4 E. Farnetti, R. D. Monte, J. Kašpar, *Inorganic and Bio- Inorganic Chemistry- Vol II- Homogeneous and Heterogeneous Catalysis.*

5 R. B. Seymour, T. Cheng (Hrsg.), *History of Polyolefins,* D. Riedel Publ. Co., Dordrecht, **1986**.

6 J.P. Hogan, R.L. Banks, Belg. Pat. 530 617 (1955).

7 K. Ziegler, H. G. Gellert, K. Zosel, W. Lehmkuhl, W. Pfohl, *Angew. Chemie.* **67** (1955)

424.

8 K. Ziegler, E. Holzkamp, H. Breil, H. Martin, DE Patent 973626 (1953).

9 K. Ziegler, *Angew. Chem.* **76** (1964) 545.

10 G. Natta, *Angew. Chem.* **68** (1956) 393.

11 G. Natta, P. Pino, P. Corradini, F. Danusso, E. Mantica, G. Mazzanti, G.Moraglio, *J. Am. Chem. Soc.* **77** (1955) 1708.

12 W. Kaminsky, *J. Chem. Soc., Dalton Trans.* **9** (1998) 1413.

13 C.J. Harlan, S.G. Bott, A.R. Barron, *J. Am. Chem. Soc.* **117** (1995) 6465.

14 I. Tritto, M.C. Sacchi, P. Locatelli, *Macromol. Chem. Phys.* **197** (1996) 1537.

15 I. Tritto, R. Donetti, M.C. Sacchi, P. Locatelli, G. Zannoni, *Macromol.* **30** (1997)1247.

16 W. Kaminsky, *Macromol. Chem. Phys.* **197** (1996) 3907.

17 I.I. Zakharov, V.A. Zakharov, A.G. Potapov, G.M. Zhidomirov, *Macromol. Theory Simul.* **8** (1999) 272.

18 T.N.P. Luhtanen, M. Linnolahti, T.A. Pakkanen, *J. Organometallic Chem.* **648** (2002) 49.

19 M. Ystenes, J.L. Eilertsen, J.K. Liu, M. Ott, E. Rytter, J.A. Stovneng, *J. Polym. Sci. Pol. Chem.* **38** (2000) 3106.

20 P.L. Bryant, C.R. Harwell, A.A. Mrse, E.F. Emery, Z. Gan, T. Caldwell, A.P. Reyes, P. Kuhns, D.W. Hoyt, L.S. Simeral, R.W. Hall, Butler, L.G. *J. Am. Chem. Soc.* **123** (2001) 12009.

21 H. Sinn, *Macromol. Symp.* **97** (1995) 27.

22 W. Kaminsky, *J. Polym. Sci., Part A: Polym. Chem.* **42** (2004) 3911.

23 G.W. Coates, *Chem. Rev.* **100** (2000) 1223.

24 *Metallocene Based Polyolefins,* ed. J. Scheirs and W. Kaminsky, Wiley & Sons, Chichester 2000, vol. I & II.

25 W. Kaminsky, A. Frunk, H. Hähnsen, *Dalton Trans.* **41** (2009) 8803.

26 N. Kashiwa, *J. Polym. Sci.: Part A: Polym. Chem.* **42** (2004) 1.

27 D-H. Lee, Y-T. Jeong, K. Soga, and T. Shiono, *J. Appl. Polym. Sci.* **47** (1993) 1461.

28 G. H. Zohuri, F. Azimfar, R. Jamjah, and S. Ahmadjo, *J. Appl. Polym. Sci.* **89 (**2003) 1177.

29 X. Cheng, *"The use of functionalized zirconocenes as precursors to silica-supported zirconocene olefin polymerization catalysts."* Faculty of the Virginia Polytechnic Institute and State University, Blacksburg, Virginia: VT Electronic Thesis and Dissertation Archive (United States), pp. 14-22, 2001.

30 A. Parada, T. Rajmankina, and J. Chirinos, *Polym. Bull.* **43** (1999) 231.

31 M.P. McDaniel, *Adv. Catal.* **33** (1985) 47.

32 A. Clark, *Catal. Rev.* **3** (1969) 145.

33 B. M. Weckhuysen, R. A. Schoonheydt, *Catal. Today* **51** (1999) 215.

34 M.P. McDaniel, *Ind. Eng. Chem. Res.* **27** (1988) 1559.

35 B. L. Goodall, *J. Chem. Educ.***63** (1986) 191.

36 P. Kaewarsa, *"Polymerization of ethylene over the supported Ziegler-Natta and metallocene catalysts on magnesium hydroxide and magnesiuum hydroxychloriede,"* in *Thesis in Chemistry Science, Graduate School*: Khonkaen University,2005.

37 F. Alobaidi, Z. Ye, S. Zhu, *Macromol Chem Phys* **204** (2003)1653.

38 Q. Wang, L. Peng, *J Polym Sci.: Part A: Polym Chem* **43** (2005) 5506.

39 S. Chen, C. Guo, L. Liu, H. Xu, J. Dong, Y. Hu, *Polymer* **46** (2005) 11093.

40 G. Natta, P. Corradini, G. Allegra, *J. Polym. Sci.* **51**(1961) 399.

41 P. Cossee, *Tetrahedron Lett.* **17** (1960) 12.

42 P. Arlman, *J.Catal*. **3** (1964) 99.

43 N. Pasquini, Ed. *Polypropylene handbook*, Hanser Gardner Publications Inc. 2005

44 L. Luciani, N. Kashiwa, P. C. Barb, A. Toyota, Ger. 2643143, Montedison and Mitsui Petrochemical, invs. *Chem. Abstr.* 1977, 87, 68893v.

45 E. Albizzati, G. Cecchin, J. C. Chadwick, G. Collina, U. Giannini, G. Morini, L. Noristi, L. Resconi, *In Polypropylene handbook, 2nd ed.;* Pasquini, N., Ed.; Carl Hanser Verlag: Munich, 2005; Chapter 2.

46 J. C. Chadwick, *Macromol. Symp.* **173** (2001) 21.

47 G. Cecchin, G. Morini, A. Pelliconi, *Macromol. Symp.* **173** (2001) 195.

48 S. A. Sergeev, G. D. Bukatov, V. A. Zakharov, E. M. Moroz, *Makromol. Chem.* **184** (1983) 2421.

49 M. Terano, T. Kataoka, T. Keii, *In Catalytic polymerization of olefins*; Keii, T., Soga, K., Eds.; Kodansha-Elsevier: Amsterdam, 1986; p 407.

50 P. Sormunen, T. Hjertberg, E. Iiskola, *Makromol. Chem.* **191** (1990) 2663.

51 M. Terano, M. Saito, T. Kataoka, *Makromol. Chem. Rapid Commun.* **13** (1992) 103.

52 V. Busico, P. Corradini, L. D. Martino, A. Proto, V. Savino, E. Albizzati, *Makromol. Chem.* **186** (1985) 1279.

53 M. C. Sacchi, I. Tritto, C. Shan, R. Mendichi, L. Noristi, *Macromolecules*, **24** (1990) 6823.

54 D. Ribour, V. Monteil, R. Spitz, *J. Polym. Sci., Part A: Polym. Chem.* **46** (2008) 5461.

55 M.C. Sacchi, I. Tritto, C. Shan, R. Mendichi, L. Noristi, *Macromolecules* **24** (1990) 6823.

56 A.G. Potapov, G.D. Bukatov, V.A. Zakharov, *J. Mol. Cata. A: Chem.* **246** (2006) 248.

57 K. Soga, T. Shiono, Y. Doi, *Makromol. Chem.* **189** (1988) 1531.

58 B. Liu, T. Nitta, H. Nakatani, M. Terano, *Macromol. Chem. Phys.* **204** (2003) 395.

59 A. Correa, F. Piemontesi, G. Morini, L. Cavallo, *Macromolecules* **40** (2007) 9181.

60 U. Giannini, A. Cassata, P. Longi, R. Mazzocchi, U.S. Patent 4,336,360 (1982).

61 M. Miyoshi, Y. Tajima, K. Matsuura, N. Kuroda, M. Matsuno, U.S. Patent 4,288,579 (1981).

62 S. Tokunaga, A. Kato, T. Kimoto, K. Baba, U.S. Patent 4,415,713 (1983).

63 A. Sato, M. Tachibana, and K. Kikuta ,U.S. Patent 4,321,345 (1982).

64 B. L. Goodall, A. A. Van Der Nat, W. Sjardijn, U.S. Patent 4,329,253 (1982).

65 R. A. Epstein,R. I. Mink,U.S. Patent 4,325,836 (1982).

66 K. Kimura, H. Ohba, A. Murai, U.S. Patent 4,332,697 (1982).

67 B. L. Goodall, J. C. van der Sar, U.S. Patent 4,343,721 (1982).

68 H. Ueno, M. Imai, N. Inaba, M. Yoda, S. Wada, U.S. Patent 4,246,136 (1981).

69 G. Cecchin and E. Albizzati, U.S. Patent 4,294,721 (1981).

70 M. Ferraris and F. Rosati, U.S. Patent 4,469,648 (1984).

71 A. Toyota, K. Odawara, and N. Kashiwa, U.S. Patent 4,085,276 (1978).

72 M. Kioka and N. Kashiwa, U.S. Patent 4,742,139 (1988).

73 B. L. Goodall, A. A. van der Nat, W. Sjardijn, U.S. Patent 4,393,182 (1983).

74 B. L. Goodall, in R. P. Quirk, ed., *Transition Metal Catalyzed Polymerizations, Alkenes and Dienes, Part A*, Harwood Academic Publishers, New York, 1983, p. 355.

75 P. C. Barbé, L. Luciani,U. Scatá,U.S. Patent 4,220,554 (1980).

76 E. I. Band, U.S. Patent 4,472,521 (1984).

77 K. P. Wagner, U.S. Patent 4,186,107 (1980).

78 H. Ueno, T. Yano, T. Inoue, S. Ikai, Y. Kai, M. Shimizu, U.S. Patent 4,297,463 (1981).

79 A. Monte, L. Noristi, Eur. Patent 437,264 (1991).

80 M. Kioka, H. Kitani, N. Kashiwa, U.S. Patent 4,330,649 (1982).

81 N. Kashiwa, Y. Ushida, Eur. Patent 86,288 (1983).

82 G. G. Arzoumanidis, N. M. Karayannis, H. M. Khelghatian, S. S. Lee, B. V. Johnson,

U.S. Patent 4,866,022 (1989).

83 M. Matsuura, T. Fujita, U.S. Patent 4,703,026 (1987).

84 M. Harada, S. Miya, S. Yamada, M. Iijima, U.S. Patent 4,551,439 (1985).

85 D. D. Klendworth, K.W. Johnson, A.Winter, F. Langhauser, WO2009152268 A1 (2009).

86 F. Gundert, M. Schneider, WO 2011076692 A1 (2011).

Chapter 2

2. Experimental Methods

Preparation method of molecular adducts has an important role in controlling the morphology and properties of both Z-N catalyst and polymer. In the case of polyolefin's, polymer mimics the morphology of the catalyst. Among the different synthetic techniques, mechanical or mechanical plus chemical treatments were used in the early stage of the $MgCl_2$-supported catalysts development. Even though these methods are simple and low cost, control of morphology of the catalyst particles and particles size distribution (PSD) are almost impossible [1, 2]. The chemical routes have been preferred as the more suitable for the synthesis of the catalysts, and, thus, controlling morphology with controlled shape, size and PSD via replication phenomenon [1-6].

2.1. Materials

$MgCl_2$ powder (325 mesh contain < 5 % H_2O, from Sigma-Aldrich), ethanol, isobutanol, isopropanol, 2-butanol and tertiary butanol (≥ 99% and H_2O ≤ 1%, Merck) was used as received. Hexane and toluene (Merck, ≥ 99%) were used after dehydration. Benzoyl chloride (BC) from Merck was used as such. AR grade sulfuric acid, potassium titanium oxalate and ammonium sulphate were used as such. Ethylene (purity 99.9%) was taken from commercial plant and used without further purification. Titanium tetrachloride ($TiCl_4$, 99.9 %) and triethylaluminium (TEAL, 93%) (Both from Sigma- Aldrich) were used as such.

2.2. Molecular adduct preparation

Azeotropic distillation method is used to prepare $MgCl_2$ based molecular adducts with different alcohols. Molecular Adduct is extremely sensitive to moisture and a small amount of moisture can damage the entire system even in a highly inert atmosphere, hence molecular adduct preparation requires typical organometallic preparation requirements.

Azeotrope is a special kind of separation method which is done by adding an appropriate separation media to change the vapor liquid equilibrium between the separated

components. This method is mainly suitable for the mixtures that contain azeotropic composition and cannot be distilled directly. Usually, adding the entrainer such as toluene, benzene, hexane etc, forms lower azeotrope with one or more of the components. Then the separation medium is obtained from the top as one component of the azeotrope. The Dean-Stark apparatus is used for azeotropic distillation to collect water produced during set to reflux. Toluene is used as a solvent during the reactions that remove water in a reaction as an azeotrope. The condensed mixture of toluene and water collects in the burette and the denser water separates and falls to the bottom. The tap allows the water to be removed [7].

2.2.1. Preparation of $MgCl_2$.nROH (where ROH= ethanol, isopropanol, isobutanol, 2-butanol and tertiary butanol) adducts

0.95 gm of anhydrous $MgCl_2$ (Sigma- Aldrich, 0.01 M), 12 ml EtOH (0. 2 M), and 20 ml of toluene were refluxed in a 50 mL RB flask under continuous azeotropic distillation of toluene-water for three hours at 105 °C. The clear hot solution was cooled to 0°C for 2 h and the resultant crystalline white solid was washed at least 3- 4 times with dry n-hexane, dried and stored in a vacuum desiccator. Same procedure is used for all alcoholic adduct but the set to reflux temperature vary for each adducts. The molecular adducts are abbreviated as MgEtOH ($MgCl_2$.6EtOH), MgiPrOH ($MgCl_2$.4iPrOH), Mg-*i*-BuOH ($MgCl_2$.4(*i*-BuOH), Mg2-BuOH ($MgCl_2$.4(2-BuOH)) and MgtBuOH ($MgCl_2$.2(tBuOH)) for ethanol, isopropanol, isobutanol, 2-butanol and tertiary butanol adduct, respectively. For isopropanol, isobutanol and tertiary butanol adduct, a white emulsion is formed during the set to reflux, there was no cooling adopted for crystallization. Without any cooling to 0°C, the precipitate is washed 2-3 times with hexane and dried under vacuum. In the case of 2-butanol adduct there is no formation of emulsion while set to reflux, cooling to 0°C is needed to crystallize the adduct. In the case of tertiary butanol adduct, solubility of $MgCl_2$ in tertiary butanol is low, in order to make a homogeneous solution 1ml of methanol was added. The set to reflux temperature

for the $MgCl_2$.nROH is slightly different for each adduct. The temperature applied for the adducts are the following: 105 °C for MgiPrOH, MgtBuOH, 118 °C for Mg2-BuOH and 125 °C for Mg-*i*-BuOH [8, 11-13].

2.2.2. Preparation of Esterified $MgCl_2$.nROH (where ROH= ethanol, isopropanol, isobutanol and 2-butanol) adducts

Hydrated $MgCl_2$ (0.95 g with < 5 % H_2O), alcohol (12 ml) and toluene (20 ml) where heated at set to reflux temperature for 2-3 h under continuous azeotropic distillation of water. The liquid was concentrated to separate a white crystalline solid and then stirred with benzoyl chloride in toluene at 125-135 °C for 4 h to get solid esterified alcoholic adduct. The solid was filtered, washed with chlorobenzene and dried under vacuum. The known amount of benzoyl chloride was added to esterifying one alcohol molecule out of 'n' alcohols in $MgCl_2$.nROH. The esterified adduct are designated as Est-ME ($MgCl_2$.5(EtOH).$C_6H_5COOCH_2CH_3$), Est-MiP ($MgCl_2$.3(iPrOH).$C_6H_5COOCH(CH_3)_2$), Est-MiB ($MgCl_2$.3(iBuOH).$C_6H_5COOCH_2CH(CH_3)_2$) and Est-M2B ($MgCl_2$.3(2-BuOH).$C_6H_5COOCH(CH_3)CH_2CH_3$) for ethanol, isopropanol, isobutanol and 2-butanol, respectively [14].

2.3. Preparation of Ziegler –Natta catalyst (Ti/MgROH)

Z-N catalyst was prepared by a general procedure reported in several patents and papers [7-15]. Entire preparation of Z-N catalyst has been carried out in glove box and schlenk line under dry nitrogen atmosphere. A suspension of $MgCl_2$.nROH (~2.8 g) in chlorobenzene (22 mL) was stirred for 1 h at 110 ^oC under nitrogen atmosphere in a four necked 250 ml round bottom flask. $TiCl_4$ (22 ml, 0.2 mol) was added over the course of 10 min to the hot solution and refluxed for 1 h The supernatant liquid is removed by cannula or syringe and washed for 10 minutes each with two 10 mL portions of $TiCl_4$ at 110 ^oC. The supernatant liquid is filtered again followed by several washes with hexane at 60 ^oC to

remove surface adsorbed species. Washing continued till the supernatant liquid did not show detectable levels of titanium alkoxide. Then the catalyst was dried and stored in dry N_2 atmosphere. A similar approach was followed to prepare the Z-N catalysts from the product obtained after esterification of $MgCl_2$-alcoholic adduct with benzoyl chloride. Above Z-N catalysts were denoted as Ti/MgEtOH, Ti/Mg-*i*-BuOH, Ti/MgiPrOH, Ti/Mg2-BuOH, Ti/MgtBuOH, Ti/Est-ME and Ti/Est-MiP, throughout the thesis. Another important fact is that the alcohols used for adduct preparation washes away during the incorporation of $TiCl_4$ in $MgCl_2$ lattice. Even though these Lewis bases are not an integral part of the Z-N catalyst, changes in the nature of the alcohols very significantly affect the percent of titanium loading, textural properties of the catalyst and the activity.

2.3.1. Estimation of % Ti present in the Z-N catalyst

This method describes the process of quantitative determination of titanium in supported and unsupported Z-N catalyst. Potassium titanium oxalate (0.92 g) and ammonium sulphate (2 g) is taken in a 100 ml flask, 15 ml concentrated sulphuric acid is added to it. It is boiled for 10 minutes, cooled and poured in 100 ml of distilled water. The solution is made in 250 ml of standard measuring flask (SMF) (this solution contain 0.5 mg of titanium per ml of the solution). From the above solution four portions of 1, 2, 3, and 4 ml were withdrawn by a pipette and poured in 50 ml standard flak. 1 ml of 10 % H_2O_2 was added to each flask and solution is made up to the mark with distilled water. The optical densities of the yellow coloured solutions were recorded at 410 nm using 1 cm thick cell and H_2SO_4 containing water as reference liquid. The optical densities versus milligram of titanium are plotted to get a straight line.

0.5 g of sample is weighed and dissolved in 25 ml of 5% H_2SO_4 and poured in 100 ml SMF and made up to the mark with distilled water. By means of pipette 5 and 10 ml of aliquots were taken in 50 ml SMF and 1 ml of 10 % H_2O_2 was added to each flask and

solution is made up to the mark with distilled water. The optical densities versus milligram of titanium are plotted to get a straight line.

The amount of titanium is directly read from the calibration curve in mg.

$$\% \text{ titanium} = \text{weight of titanium} \times 100 / \text{wt of solid} \quad (2.1)$$

The tolerance of the procedure is ~ ± 0.1 %, and is sensitive for determination of titanium up to 50 ppm level.

2.4. Ethylene Polymerization

All the polymerization was carried out in a 1 L Buchi Glas Uster glass polyclave reactor fitted with a thermocouple, an automatic temperature control unit and at a stirring speed of ~ 500 rpm. After the addition of dry distilled n- hexane (500 mL), followed by addition of TEAL (9% solution in n-hexane) the solution was saturated with ethylene (5 bar). Finally the catalyst was added and polymerization was performed at a temperature of 75 ^{o}C. The addition of ethylene was continued for 1 hr. The polymerization was stopped by addition of sufficient amount of acidified methanol. The precipitated polymer was filtered, washed with methanol and dried under vacuum. The catalyst loading and Ti/ TEAL ratio were varied with the Z-N catalyst derived from different alcoholic adduct. The yield of polymer was calculated by using the formula:

$$\text{Yield} = (\text{gm of polymer} / \text{millmole of Ti}) / \text{hr} \quad (2.2)$$

2.5. Physicochemical Characterization

2.5.1. Introduction

Detailed physicochemical characterization is one of the crucial aspects to understand any material including catalyst. Spectroscopy, microscopy, diffraction and methods based on adsorption and desorption are the routine material characterization techniques. It gives information about crystallanity, surface structure, nature of active sites, particle size and morphology, and other characteristic features. Further, how activity and selectivity change

with structural and electronic properties of the catalyst is one of the major goals in catalysis research. The materials were characterized by adopting various physico-chemical methods such as X-ray diffraction analysis (XRD), thermo gravimetric - differential thermal analysis (TG-DTA), infrared spectroscopy (IR), Raman spectroscopy, surface area and pore volume measurements, nuclear magnetic resonance (NMR) spectroscopy, scanning electron microscopy (SEM) and optical microscopy. Information obtained from the above methods help us to understand the materials as well as catalyst better, so that materials can be improved or designed in better way, when required. The following part gives a brief account of the theory and principle of selected characterization techniques used for the current study. The procedure for each experimental technique is also described in this part.

2.5.2. Theory and Experimental Procedures

2.5.2.1. Thermo Gravimetric Analysis (TGA)

TGA is an analytical technique used to determine a material's thermal stability and its fraction of volatile components by monitoring the weight change that occurs as a specimen is heated. The measurement is normally carried out in air or in an inert atmosphere, such as helium, nitrogen or argon, and the weight is recorded as a function of increasing temperature. The variation in mass of a sample is measured when it undergoes a temperature scanning in a controlled atmosphere. Such analysis relies on a high degree of precision in three measurements: weight, temperature, and temperature change. As many weight loss curves look similar, the weight loss curve may require transformation before results may be interpreted. A derivative weight loss curve can be used to tell the point at which weight loss is most apparent.

Differential thermal analysis (DTA) is a technique measuring the difference in temperature between a sample and a reference (a thermally inert material) as a function of the time or the temperature, when they undergo temperature scanning in a controlled atmosphere.

The DTA method enables any transformation to be detected for all the categories of materials, providing information on exothermic and endothermic reactions taking place in the sample, which include phase transitions, dehydration, decomposition, redox, or solid-state reactions. In catalysis, these techniques are used to study the genesis of catalytic materials *via* solid-state reactions where alumina is used as a reference material [16].

In TGA experiment, test material is placed into a high alumina cup that is supported on, or suspended from an analytical balance located outside the furnace chamber. The balance is zeroed, and the sample cup is heated according to a predetermined thermal cycle. The balance sends the weight signal to the computer for storage, along with the sample temperature and the elapsed time. The TGA curve plots the TGA signal, converted to percent weight change on the Y-axis against the reference material temperature on the X-axis. Thermal analysis experiments were measured in Perkin-Elmer's Diamond TG/DTA at a rate of 10 ºC/min in air or N_2 atmosphere. Al_2O_3 was used as an internal standard.

2.5.2.2. Nujol Method

This is a simple sample pre-treatment method for measuring properties of powder samples with different analytical methods. The sample is distributed in a liquid of approximately equal refractive index, and the infrared spectrum is measured. Generally, the powder is dispersed in non-volatile liquid paraffin (Nujol) that has low absorption in the infrared region. To prepare a sample, pulverize approximately 10 mg sample powder in a mortar and pestle kept in a glove bag under argon/nitrogen atmosphere. Add one or two drops of liquid paraffin and mix to distribute the sample powder in the liquid paraffin. Apply the paste to a liquid cell (KBr crystal plate, etc.) and sandwich it under another cell plate. The characteristic C-H stretching frequency of liquid paraffin observed near 3000 to 2800 cm^{-1}, 1460 cm^{-1}, 1375 cm^{-1}, and 730 cm^{-1}in IR spectra. Infrared spectral measurements were performed on a Rigaku IR spectrometer within the range of 400 - 4000 cm^{-1}. Nujol method is applied for

XRD and Raman spectral measurements also.

2.5.2.3. Raman Spectroscopy

Raman spectroscopy is a spectroscopic technique used in chemistry to study vibrational, rotational and other low-frequency modes of molecules and solids. Since vibrational information is very specific for the chemical bonds in molecules, it therefore provides a fingerprint by which the molecule can be identified. The laser light interacts with phonons or other excitations in the system, resulting in the energy of the laser photons being shifted up or down. The shift in energy gives information about the phonon modes in the system. A sample is illuminated with a laser beam. Light from the illuminated spot is collected with a lens and sent through a monochromator. The process where most photons are elastically scattered is called Rayleigh scattering. Raman spectroscopy is based on the Raman Effect, which is the inelastic scattering of photons by molecules. The effect was discovered by the Indian physicist, C. V. Raman in 1928. Spontaneous Raman scattering is typically very weak, and as a result the main difficulty of Raman spectroscopy is separating the weak inelastically scattered light from the intense Rayleigh scattered laser light. The energy of the scattered radiation is less than the incident radiation for the Stokes line and the energy of the scattered radiation is more than the incident radiation for the anti-Stokes line. The energy increase or decrease from the excitation is related to the vibrational energy spacing in the ground electronic state of the molecule. Therefore, the wave number of the Stokes and anti-Stokes lines are a direct measure of the vibrational energies of the molecule [17].

Raman spectra were recorded on a Horiba JY Lab RAM HR 800 spectrometer excited with 633 nm lasers. While recording Raman measurements, to avoid any degradation of materials, a low-temperature setup (Linkam-Examine- THMS 600 setup connected to a TP94 temperature programmer and LN94 unit to cool the stage below ambient temperature using liquid nitrogen) was employed. Sample temperature was maintained below 0 °C to avoid any

degradation from atmospheric moisture.

2.5.2.4. Nuclear magnetic resonance spectroscopy (NMR)

Nuclear Magnetic Resonance (NMR) Spectroscopy is a powerful technique which is widely used as one of the key instrumental technique for the structure determination of compounds. NMR spectroscopy was discovered in 1945 by two groups independently: Purcell, Torrey and Pound detected weak radiofrequency signals from the nuclei of paraffin wax [18]; Bloch, Hansen and Packard observed signals of the same kind from water [19]. These two experiments were the beginning of NMR spectroscopy. Over the past three decades NMR spectroscopy has become a routine analytical technique for studying physical, chemical and biological properties of various compounds. NMR and magnetic resonance imaging (MRI) are applied in many different areas such as medicine, biology, chemistry and materials science, in particular for studying cells, bones, brain, protein folding, drug design, membranes, liquid crystals, surfaces of the materials, zeolites, polymers, colloids, catalysts, metals, phase transitions, cements, gasses, ceramics; and many other materials and processes [20]. As this technique is element-specific, it is possible to study atoms of interest without any interference from other atoms of similar atomic mass, unlike the X-ray diffraction technique.

NMR spectroscopy deals with the study of interaction of matter with electromagnetic radiation in the radio frequency range of hundreds of MHz NMR is based on a specific property of the atomic nucleus that it possesses a nuclear magnetic moment and can respond to an applied magnetic field. The majority of nuclei in the periodic table have a nuclear magnetic moment, which is proportional to the nuclear spin angular momentum *I*:

$$\mu = \gamma I \tag{2.3}$$

where the gyromagnetic ratio γ, is a constant, specific for each nucleus. The angular momentum of a nuclear spin is a vector and can point in any possible direction in the space.

When a magnetic field is applied to the spins, they start to precess (rotate) around the magnetic field axis. The frequency of this precession is called the Larmor frequency ω_0:

$$\omega_0 = -\gamma B_0 \qquad (2.4)$$

where B_0 is the external static magnetic field.

A radio-frequency (rf) pulse is an oscillating magnetic field of specific frequency ω_{rf} and duration, and it is applied to fulfil a resonance condition (Eq. 2.4). The radio-frequency pulses are applied in a direction perpendicular to the magnetic field B_0. If the rf pulse is set to be on resonance, then

$$\omega_{rf} = \omega_0 \qquad (2.5)$$

The oscillating magnetic field, B_1, is associated with the applied radiofrequency pulse and is perpendicular to B_0. The rf pulse flips the magnetization vector into the xy-plane (transverse plane). Spins will keep precessing around the magnetic field B_1, as they did around B_0, with a frequency,

$$\omega_1 = -\gamma B_1 \qquad (2.6)$$

where, ω_1 is called the nutation frequency. After the application of the rf pulse, the spins return to their thermal equilibrium state. Time interval, needed for reaching the thermal equilibrium, denoted by the time constant T_1, and the process is called spin-lattice relaxation. The precession of the transverse magnetization induces electric currents in the rf coils that can be detected: this is the NMR signal, so-called free induction decay, FID. This oscillating signal detected in the time domain can be transformed into the frequency domain by Fourier transformation. The peak maximum of the obtained spectrum corresponds to the Larmor frequency of the nuclei under observation.

2.5.2.4.1. Solid- state NMR Spectroscopy

NMR can be performed both in liquid and solid state. In liquids fast isotropic motions

result in spectra that are usually narrow and well resolved, as fast molecular tumbling in solutions averages all the orientation-dependent interactions. Liquid-state NMR is routinely used in academic and industrial research for simple compound identification and for advanced studies. Although liquid-state NMR is informative and very simple to perform, more information's about molecular dynamics and structure can be obtained from solid-state NMR. Solid samples, when compared to liquids, represent for NMR spectroscopy much more complex system. In liquids, molecule rapidly changes its position relative to the applied static magnetic field. As a consequence, orientation dependent interactions are averaged out, which results in narrow lines in NMR spectra. In solid samples isotropic motions are usually absent, and that results in broad, poorly resolved spectra, which is difficult to analyze. The main sources of broadening are chemical shift anisotropy, dipolar coupling and quadrupolar coupling. The experiment applied to suppress the anisotropic interaction in solid-state NMR spectroscopy is magic angle spinning (MAS).

2.5.2.4.1.1. Magic Angle Spinning (MAS)

Magic angle spinning (MAS) was introduced in solid state NMR to average out most of these anisotropic interactions present in the system (Figure 2.1). The molecular anisotropic interactions have orientation dependence in the form of $(3\cos^2\theta-1)$, where 'θ' is the angle which describes the orientation between the magnetic field and the spin interaction tensor. MAS remove the anisotropic parts of all interactions from the central spectrum and appear as spinning sidebands when the angle between external magnetic field and the sample rotation axis is adjusted to a value called magic angle 54.74° (i.e $3\cos^2\theta_R-1 = 0$). After MAS, the interactions that remain are the isotropic shifts and J coupling as in liquid samples and the spectrum obtained is simpler [21, 22].

2.5.2.4.1.2. Cross polarization magic angle spinning (CP/MAS)

Cross-polarization is a method for enhancing signal of low-abundant nuclei by

polarization transfer from abundant ones, usually protons. Polarization transfer from abundant (H) to rare nuclei (X) together with faster accumulation of signal which is enabled by interaction between rare and abundant spins makes the sensitivity of cross-polarization experiments almost 1000 times higher than obtainable from direct polarization. Therefore, CP serves as basic building block of most solid-state NMR experiments [23].

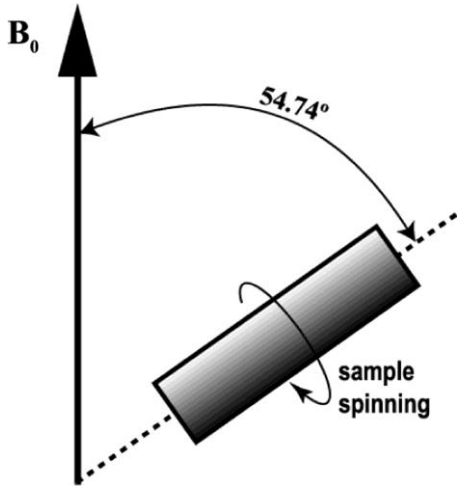

Figure 2.1: Magic angle spinning.

To establish the polarization transfer, the Hartmann-Hahn condition must be fulfilled:

$$\gamma_H B_H = \gamma_X B_X \quad \text{i.e. } \omega_{1H} = \omega_{1X} \tag{2.7}$$

γ gives the gyromagnetic ratios and B amplitudes of the radiofrequency (rf) field applied to proton channel and the heteronucleus X channel; ω_1 gives the nutation frequencies of the spins under these conditions. The polarization is transferred under simultaneous application of the two rf fields. The time for which the rf fields are on is called the contact time. For a given contact time, the signal intensity measured at constant rf amplitude B_H as a function of rf amplitude B_X (or at constant rf amplitude B_X as a function of rf amplitude B_H) determines the shape of Hartmann-Hahn matching profile.

The pulse sequence for a cross polarizations experiment is shown in Figure 2.2. In this sequence a 90° pulse is applied to the proton. Then it is allowed to evolve for some time. This is known as contact time. During the contact time, the cross polarization between proton and

the X nucleus (^{13}C, ^{15}N etc) takes place. Then the signal is detected by decoupling the proton. Since MAS averages out the chemical shift anisotropy (CSA), dipolar coupling to obtain narrow spectral lines, valuable structural information is lost due to the averaging of these anisotropic interactions. From CSA we can measure the orientational constraints in the molecules and from dipolar coupling we can measure the internuclear distance which is closely related to dynamics in molecule. Thus, one of the important areas in solid state NMR is to re-introduce these anisotropic interactions which are lost during magic angle spinning and then to measure them to obtain valuable structural information. This is broadly called recoupling of anisotropic interactions and this can be done by specially designed pulse sequences.

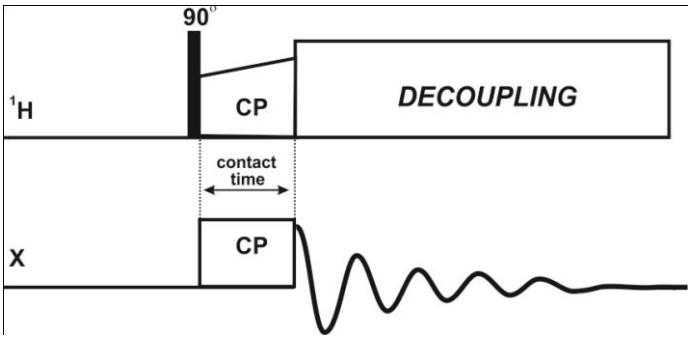

Figure 2.2: Schematic representation of a cross polarization pulse sequence.

2.5.2.4.1.3. ^{13}C 2D exchange NMR experiments

Two-dimensional (2D) NMR exchange spectroscopy has been introduced for the elucidation of molecular exchange processes [24]. It has been found that 2D exchange spectroscopy is of significance for the investigation of cross-relaxation [25-27], as well as for the study of chemical exchange network [24, 29]. The analysis of complex processes is greatly facilitated the recording informative 2D exchange maps. The essential concept of a 2D exchange experiment is illustrated in Figure 2.3. Spin diffusion between individual sites in solids is formally analogous to cross relaxation and chemical exchange in liquids [30-33] and can most conveniently be traced out by two-dimensional (2D) exchange NMR

spectroscopy, a method that has been used in liquids and has recently been applied to solids by Szeverenyi et al and by Suter and Ernst [34].

The basic form of a 2D exchange experiment to study molecular motions or chemical exchange; all pulses (shown as block with black colour) are 90° pulses. The experiment correlates changes of molecular orientation between t_1 and t_2 periods. Transverse magnetization is initially excited (via a 90° pulse or cross-polarization, labelled simply 'excitation' in the Figure 2.3) and allowed to evolve at its characteristic frequency, ω_1, during t_1.

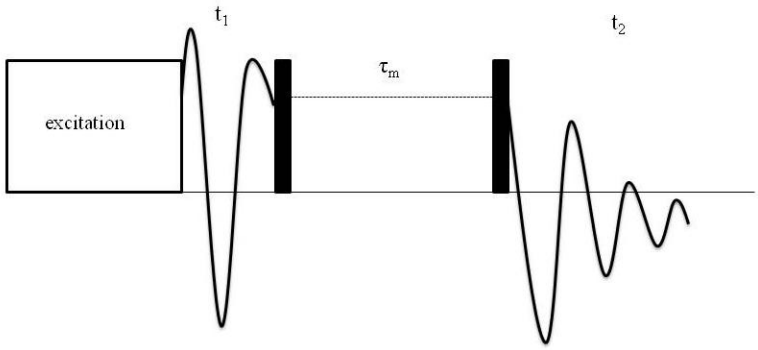

Figure 2.3: Schematic representation of a 2D exchange experiment.

The characteristic frequency in static solid samples is dependent on molecular orientations, as the spin interactions acting on the observed spin are anisotropic. At the end of t_1, a second pulse restores the magnetization to z (parallel to magnetic field, B_0), where it is stored for a mixing time τ_m, during which molecular reorientation may occur. Finally, another pulse reconverts the magnetization into observable transverse magnetization whose evolution, this time with offset frequency ω_2, is then recorded in free induction decay (FID). Subsequent processing of the resulting 2D dataset produces a correlation spectrum which shows how the observed spin's offset frequency changed from ω_1 in t_1 to ω_2 in t_2. Since molecular orientation can be directly correlated with offset frequency, the 2D spectrum represents a map describing the molecular reorientation between t_1 and t_2, i.e. during the mixing time, τ_m.

2.5.2.4.1.4. Separated Local Field Spectroscopy

Separated local field (SLF) spectroscopy is a powerful technique which measure dipolar interactions present in the system. It is a two dimensional NMR technique which separates the chemical shift of a low abundant nuclei S (^{13}C or ^{15}N) in one dimension and the dipolar coupling between this dilute spin S (^{13}C) and an abundant spin I (^{1}H) in the second dimension. The measurement of site-specific ^{1}H-^{13}C dipolar couplings provides a sensitive tool for elucidating structures and motions in solids at a molecular level through SLF NMR [35-37]. We have used the SLF techniques called the polarization inversion spin exchange at the magic angle (PISEMA). The pulse sequence of PISEMA is shown below [38, 39].

As shown in Figure 2.4, the ^{13}C are initially cross polarized using protons by a ramped CP sequence. Then the proton and carbon fields are aligned at the magic angle by 35^{0} pulses to both channels. The I-S coupling arise from the oscillations resulting from spin exchange between I and S during $t_{1,}$ this arises under double resonance conditions during Hartmann-Hahn condition is satisfied. During this time interval t_1 the homonuclear dipolar coupling between I spins is suppressed by frequency switched Lee-Goldburg sequence enabling an efficient polarisation transfer between the I and the S spin through the heteronuclear dipolar interaction. During the second time interval t_2 the H_{IS} is suppressed by a strong RF irradiation on I spin while the decay is detected in the S spin channel. Then we get a 2D spectrum with dipolar coupling in the indirect dimension and chemical shift of dilute spins in the direct dimension. Fourier transformation on f_2 dimension yields pure chemical shift spectrum where dipolar coupling is observed in f_1 dimension.

Solid state NMR experiments were carried out on a Bruker Avance 300 spectrometer operating at a static field of 7.04 T, resonating at 300 MHz for ^{1}H and 75.5 MHz for ^{13}C, equipped with 4 mm double resonance MAS probes. The operating frequencies for ^{1}H and ^{13}C were 300 and 75.4 MHz, respectively. The samples were packed into a 4mm zirconia

rotor and loaded into a Bruker's 4 mm MAS probe and spun about the magic angle (54.74°) at 8/10 kHz. The 90° pulses for proton and carbon were 2.6 (~96 kHz) and 3.0 (~83 kHz), respectively. The ^{1}H radio frequency (rf) field strength for heteronuclear two pulse phase modulation (TPPM) decoupling was carried out at 100 kHz.

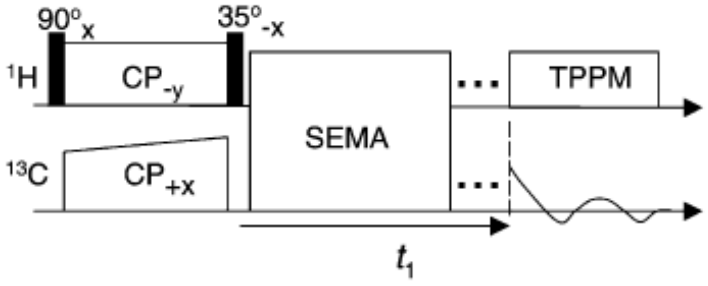

Figure 2.4: The pulse sequence of Sepearted Local Field-Polarisation Inversion Spin Exchange at Magic Angle (SLF-PISEMA) experiment.

All single-pulse excitation (SPE) experiments were done using a 30°flip angle and with a recycle delay of 5/20 s, and cross-polarization (CP) experiments were performed using a recycle delay of 3 s and a contact time of 2.5 ms using a standard ramp-CP pulse sequence with the RF power 83 kHz. All the chemical shifts were referenced to TMS by using adamantine as an external standard. Typically, 128-2048 scans were collected depending on the sensitivity of the sample. For the 2D exchange experiment, 512 experiments were collected with 16 scans in each experiment with a recycle delay of 2.5 s. Liquid state NMR experiments were carried out on a Bruker Avance 400 spectrometer operating at a static field of 9.4 T, resonating at 400 MHz for ^{1}H in a 5 mm tube.

2.5.2.5. Surface Area Determination by BET Method

The BET (Brunauer-Emmett-Teller) method is the most widely employed procedure to determine the surface area of the solid materials by using the BET equation:

$$P/V_{ads}\,(P_0\text{-}P) = 1/V_mC + [(C\text{-}1)/V_mC]_x\,(P/P_0) \qquad (2.8)$$

where P = adsorption equilibrium pressure, P_0 = standard vapour pressure of the adsorbent, V_{ads} = volume at STP occupied by molecules adsorbed at pressure P, V_m = volume of

adsorbate required for a monolayer coverage, and C = constant related to heat of adsorption.

To differentiate the adsorption mechanism between micro-pore and to that in meso and macro-pores, the *t-plot* analysis was developed by Lippens and de Boer and the same was applied [40]. The method consists of plotting the adsorption isotherm in terms of the volume of the adsorbate versus the statistical film thickness, *t*. The pore size distribution is obtained from the analysis of the desorption isotherms by applying the Barrett-Joyner-Halenda **(**BJH) expand model [41] which involves the area of the pore walls and uses the Kelvin equation to correlate the partial pressure of nitrogen in equilibrium with the porous solid to the size of the pores where the capillary condensation takes place.

The BET surface area and pore volume of the catalysts were determined by N_2 adsorption-desorption method at liquid N_2 temperature using Quantachrome Nova 1200 adsorption unit. Sample was degassed for about 2 hours till the residual pressure was $<10^{-3}$ Torr. Degassing temperature is equal to that of previous heat treatment. Indeed molecular adducts do not show meaningful surface area, since it cannot be heated above RT, which results in loss of alcohol molecules and hence a change in stoichiometry. The isotherms were analyzed in a conventional manner that includes the BET surface area in the region of the relative pressure P/P_0 = 0.05 to 1 with the assumption for the nitrogen molecular area in an adsorbed monolayer is 0.16 nm^2. The total pore volume of each samples were taken at P/P_0 = 0.95.

2.6. References

1. E.P. Moore, *Polypropylene Handbook*, Hanser, Munich, 22-24, 1996.
2. N. Kashiwa, *J. Polym. Sci.: Part A: Polym. Chem.* **42** (2004) 1
3. P. Galli, P.C. Barbe, L. Noristi, *Angew. Makromol. Chem.* **120** (1984) 73.
4. Z. Ma, L. Wang, W. Wang, L. Feng, X. Gu, *J. Appl.Polym. Sci.* **95 (**2005) 738.
5. Z. Ye, L. Wang, L. Feng, X. Gu, H. Chen, P. Zhang, J. Pan, S. Jiang, L. Feng, *J. Polym. Sci., Part A: Polym. Chem.* **40** (2002) 3112.

6. S. Ahmadjo, R. Jamjah, G.H. Zohuri, S. Damavandi, M. N. Haghighi, M. Javaheri, *Ir. Polym. J.* **16** (2007) 31.
7. S. Bhaduri, V. K. Gupta, U.S. Patent 6841633, 2005.
8. K. S. Thushara, R. Mathew, T. G. Ajithkumar, P. R. Rajamohanan, S. Bhaduri, C.S. Gopinath, *J. Phys. Chem. C.* **113 (**2009) 8556.
9. E. S. Gnanakumar, K. S. Thushara, D. S. Bhange, R. Mathew, T. G. Ajithkumar, P. R. Rajamohanan, S. Bhaduri, C. S. Gopinath, *Dalton Trans.* **40 (**2011) 10936.
10. V. D. Noto, S. Bresadola, R. Zannetti and M. Viviani, *Z. Kristallogr.* **204 (**1993) 263.
11. K. S. Thushara, E. S. Gnanakumar, R. Mathew, T.G. Ajithkumar, P.R. Rajamohanan, S. Bhaduri, C. S. Gopinath, *Dalton Trans.* **41** (2012) 11311.
12. K. S. Thushara, T. G. Ajithkumar, P. R. Rajamohanan, C.S. Gopinath (submitted to *Appl. Cata. A*).
13. K. S. Thushara, T. G. Ajithkumar, P. R. Rajamohanan, C.S. Gopinath (*submitted to RSC Advances*).
14. K. S. Thushara, E. S. Gnanakumar, R. Mathew, R. K. Jha, T. G. Ajithkumar, P. R. Rajamohanan, K. Sarma, S. Padmanabhan, S. Bhaduri, C. S. Gopinath, *J. Phys.Chem. C* **115** (2011) 1952.
15. E. S. Gnanakumar, K. S. Thushara, R. K. Gowda, S. K. Raman, T. G. Ajithkumar, P. R. Rajamohanan, D. Chakraborty, D. S. Bhange, C. S. Gopinath, *Dalton Trans.* **40** (2011) 10936.
16. P. Gabbott (Ed.) *Principles and Applications of Thermal analysis*, Wiley- Blackwell, 2007.
17. C. N. Banwell, E. M. McCash, *Fundamentals of Molecular Spectroscopy* Fourth Edition ed. Tata Mc-Graw-Hill Publishing Company limited.
18. E. M. Purcell, H. C. Torrey, R. V. Pound, *Phys. Rev.* **69** (1946) 37.
19. F. Bloch, W. W. Hansen, M. Packard, *Phys. Rev.* **70** (1946) 474.

20. M. H. Levitt, *Spin Dynamics: Basics of Nuclear Magnetic Resonance*, John Wiley and Sons Ltd, 2001.

21. E. R. Andrew, A. Bradbury, R. G. Eades, *Nature* **182** (1958) 1659.

22. I. J. Lowe, *Phys. Rev. Lett.* **2** (1959) 285.

23. S. R. Hartmann, E. L. Hahn, *Phys. Rev.* **128** (1962) 2042.

24. J. Jeener, B. H. Meier, P. Bachmann, R. R. Emst, *J. Chem. Phys.* **71** (1979) 4546.

25. S. Macura, R. R. Ernst, *Mol. Phys.* **41** (1980) 95.

26. K. Anil, R. R. Ernst, K. Wiithrich, *Biochem. Biophys. Res. Commun.* **95** (1980) 1.

27. K. Anil, G. Wagner, R. R. Ernst, K. W. Uthrich, *Biochem. Biophys. Res. Commun.* **96** (1980) 1156.

28. B. H. Meier, R. R. Ernst, *J. Am. Chem. Soc.* **101** (1979) 6441.

29. Y. Huang, S. Macura, R. R. Ernst, *J. Am. Chem. Soc.* **103** (1981) 5327.

30. J. Jeener, B. H. Meier, P. Bachmann, R. R. Ernst, *J. Chem. Phys.* **71** (1979) 4546.

31. B. H. Meier, R. R. Ernst, J. *Am. Chem. Soc.* **101** (1979) 6441.

32. S. Macura, R. R. Ernst, *Mol. Phys.* **41** (1980) 95.

33. Ani1 Kumar, R. R. Ernst, K. Wiithrich, *Eiochem. Eiophys. Res. Commun.* **95** (1980) 1.

34. D. Suter, R. R. Ernst, *Phys. Rev.* E **25** (1982) 6038.

35. M. J. Duer, *Introduction to Solid-State NMR Spectroscopy*, Blackwell, **2004**.

36. J. Grinshtein, C.V. Grant, L. Frydman, *J. Am. Chem. Soc.* **124** (2002) 13344.

37. D. McElheny, E. D.Vita, L. Frydman, *J. Mag. Reson.* **143** (2000) 321.

38. S.V. Dvinskikh, H.Zimmermann, A.Maliniak, D. Sandström, *J. Magn. Reson.* **164** (2003)165.

39. M. Hong, X. Yao, K. Jakes, D. Huster, *J. Phys. Chem. B* **106** (2002) 7355.

40. B. C. Lippens, J. H. de Boer, *J. Catal*. **4** (1965) 319.

41. E. P. Barret, L. G. Joyner, P. H. Halenda, *J. Am. Chem. Soc*. **73** (1951) 373.

Chapter 3

3. Studies of $MgCl_2$- Primary Alcohol Molecular Adducts

Part A: *Characterization and Catalytic Activity Studies of $MgCl_2$.6EtOH and $MgCl_2$.4(i-BuOH) and Corresponding Titanated Z-N catalyst*

3.1. Introduction

Most of the industrial processes for the production of polyolefin's are based on $MgCl_2$ supported heterogeneous Ziegler-Natta (Z-N) catalyst system. Development of proper catalyst system is a key factor for a successful polymerization industry, even though lots of challenges exist in the polymerization process and product development. In early stage of Z-N polymerization, active catalyst was prepared by ball milling $MgCl_2$ with $TiCl_4$ and electron donors [1-6]. It is difficult to achieve a uniform particle size of the active catalyst in ball milling method, which will be reflecting in the final property of the polymer. Therefore much attention has been given to the chemical conversion and regeneration method [7-9]. In chemical routes, active $MgCl_2$ has been prepared by elimination of Lewis base from $MgCl_2$.$(R)_x$ adducts (R = Lewis base or alkoxide) which were further treated with $TiCl_4$ to produce *super active catalyst* [10-12]. The performance of the final catalyst is based on the nature of the $MgCl_2$ precursors, $MgCl_2.(ROH)_x$, where R being $-C_2H_5$, $-HC(CH_3)_2$, $H_3C\acute{C}HC_2H_5$ etc. Reaction of $MgCl_2$ with alcohol forms molecular adducts, which undergo direct titanation (with $TiCl_4$) to synthesis Z-N catalyst. $MgCl_2$.nEtOH (n = 1 to 6) system has been studied extensively by different groups [13, 14]. Sozzani et al.[13] used solid state NMR as a versatile tool to study the various compositions and found the mixed phases of magnesium chloride with EtOH. In addition to ethanol, 1-hexanol, methanol, propanol, 2-ethyl-1-hexanol, 2-(2-ethylhexyloxy)ethanol, tetrahydrofuran, benzyl alcohol and isopropanol etc [5,15-26] have been tested as Lewis bases in the preparation of $MgCl_2$- based molecular adduct support for Z–N catalyst. It is to be noted that the number of reports available on well-

characterized single phase molecular adduct is limited to very few alcohols [14, 15-17]. The choice of the Lewis base influences the catalytic activity and the properties of polymer. By using azeotropic distillation method, a single phase molecular adducts with ethanol and isobutanol were prepared and reported in this thesis. Apart from the above; there is no literature report on the preparation, characterization and polymerization activity of Z-N catalyst supported on $MgCl_2$ with ethanol (EtOH) and isobutanol (i-BuOH).

A broad scope of our ongoing efforts on using different alcohols is how the activity of the Z-N catalyst varies with the nature of the molecular adduct. In this chapter, we chose two primary alcohols, but they differ by the number of CH_2 units and the chain structure. Although the difference is only two CH_2 units between ethanol and isobutanol, one belongs to linear alcohol and the latter one is branched. The aim behind the study is to understand how the increase in number of carbon atom and branching affect the property of the Z-N catalyst and its activity for olefin polymerization with respect to the nature of molecular adduct. Olefin polymerization activity of the Z-N catalyst derived from ethanol adduct shows comparable activity with commercial Z-N catalyst, in contrast, there is a steep decline in activity observed with Z-N catalyst prepared from isobutanol adduct.

It is also to be mentioned that the final Z-N catalyst does not contain any significant amount of alcohol, and this is true with all molecular adducts based Z-N catalysts. The purpose of using alcohol is to introduce $TiCl_4$ into the lattice of $MgCl_2$, as either $TiCl_3$ or $TiCl_2$. For this, triple layer structure found in α–$MgCl_2$ must be destroyed to introduce $TiCl_x$. As mentioned earlier, molecular adduct procedure has been adopted from 1980s to introduce $TiCl_x$. Indeed different alcohols present in the molecular adduct influences the introduction of $TiCl_x$ in different ways. Although the final catalyst does not contain any significant alcohol, it provides a way to introduce porosity, textural properties, exposing different crystal planes on the surface of $MgCl_2$, and Ti content; all of them influence the polymerization activity.

In this chapter, we discuss the characterization of a new molecular adduct Mg-*i*-BuOH and compare with MgEtOH. The above adducts have been employed as support material to prepare the final $TiCl_4$ incorporated $MgCl_2$. The main aim behind the present study is to understand the fundamental molecular level property of adduct, influence of the activity of the support when the size of the primary alcohol changes from ethanol to bulky group like isobutanol. Although extensive improvements on heterogeneous Z-N catalysts have been made, fundamental understanding is very limited due to the problems mentioned above as well as the proprietary nature of the catalysts. In order to understand the fundamental steps in the catalytic process, structure of the active centres and the role of the supporting surfaces are needed. To understand the molecular level property of the system both adduct and titanated catalysts have been subjected to systematic characterization. The present study is an attempt to explore how the presence of ethanol and isobutanol, in the initial molecular adduct, influences the final Z-N catalyst properties and its activity.

3.2. Results and discussion

3.2.1. Characterization of Molecular adducts (MgEtOH and Mg-*i*-BuOH)

3.2.1.1. Powder X-ray Diffraction

To explore the structural properties of the material, powder X-ray diffraction (PXRD) was recorded on a Philips X'Pert Pro powder X-ray diffractometer using Cu Kα radiation (λ = 1.5418 Å) with a flat sample stage in the Bragg-Brentano geometry. The diffractometer was equipped with a Ni filter and X'celerator as detector. The samples were scanned in the range 5–75^o 2θ and the scans were collected within a short time of ~2 minutes. All molecular adducts and titanated catalysts were protected with a thin layer of nujol or handled strictly under dry N_2 atmosphere to avoid any degradation due to interaction with atmospheric components. Figure 3.1 shows the PXRD patterns of anhydrous $MgCl_2$, MgEtOH and Mg-*i*-BuOH. XRD pattern of $MgCl_2$ exhibit strong peak at 2θ = 15.1° (003), 35° (004) and 50.4°

(110) indicating a cubic close packing with rhombohedral structure [27, 28]. (001) reflections below 2θ =10° characterize the molecular adducts formation with $MgCl_2$ and different alcohols (ROH= EtOH, *i*-BuOH). Absence of characteristic diffraction feature of $MgCl_2$ at 15.1° and (001) feature at lower 2θ value indicate the insertion of alcohol moiety between the central Mg^{2+} and chloride sphere leading to the adduct formation. For EtOH adduct, XRD pattern shows (001) feature at 9^o [14, 27-30]. However for Mg-*i*-BuOH, it appears at 7.7°. The above shift in (001) feature to lower 2θ value is due to the insertion of bigger alcohol moiety in the layered structure of $MgCl_2$ layers. Strong diffraction feature $<10^o$ for Mg-*i*-BuOH adduct highlights that it exhibits a layered structure due to *i*-BuOH stacking along the z-axis.

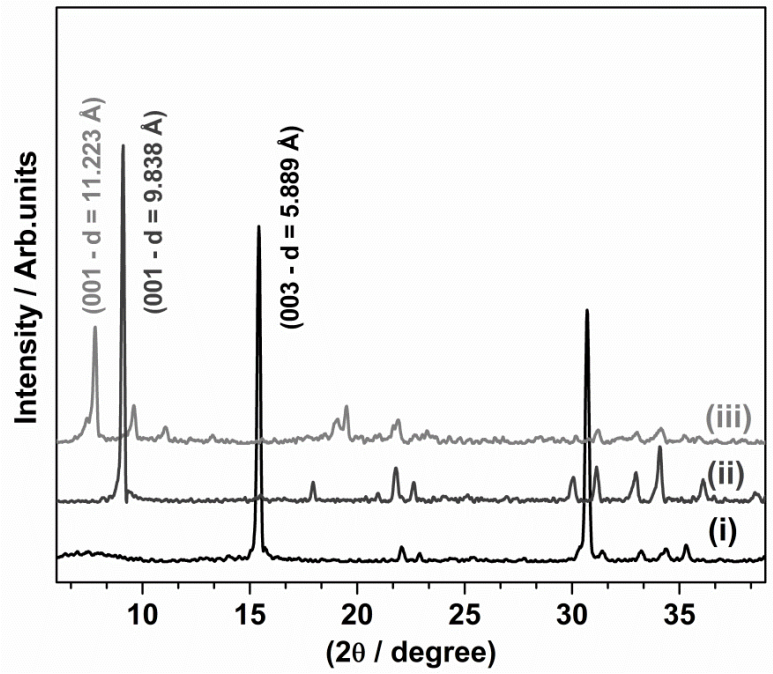

Figure 3.1: PXRD patterns (i) anhydrous $MgCl_2$ (ii) MgEtOH and (iii) Mg-*i*-BuOH.

XRD pattern clearly shows all (00z) features for MgEtOH adduct and exhibiting highly oriented crystalline nature compared to Mg-*i*-BuOH adduct. Depending on the size and the number of alcohol molecules coordinating to $MgCl_2$, the inter-planar spacing also changes. In the case of isobutanol adduct, the d_{001} is higher (11.223 Å) due to the large

molecular size compared to ethanol (9.838 Å). It is to be noted that Mg-*i*-BuOH is sensitive to temperature and preparative conditions, such as set to reflux time.

A significant change in splitting pattern in ^{13}C CP/MAS NMR has been observed with Mg-*i*-BuOH prepared under different set to reflux time. Nonetheless, adduct prepared by different set to reflux time doesn't affect the property of the final Z-N catalyst in any significant way, since all the alcohol molecules are removed during repeated washing. Detailed structural studies, especially by NMR, are reported in Part B.

3.2.1.2. Thermal Analysis

Figure 3.2 shows the results from TG/ DTA of MgEtOH and Mg-*i*-BuOH. TG-DTA is extensively used to study the weight loss of materials as a function of change in temperature, which provides an idea about stoichiometric ratio of material present in the system. The sample temperature was ramped from ambient to 300 °C at a rate of 10 °C/min under the flow of ultrahigh pure nitrogen (99.999%) at 40 mL/min. The well-defined weight loss and sharp DTA peaks indicate a systematic dissociation of alcohol molecules from the MgEtOH and Mg-*i*-BuOH adducts. In the case of ethanol adducts, the first ethanol molecule dissociates around the boiling point of liquid ethanol at 68 °C (weight loss from 100 to 88%) followed by sequential dissociation of the remaining five ethanol molecule (weight loss from 88 to 27%). The EtOH/$MgCl_2$ ratio was also identified to be 6 from the weight loss of the MgEtOH adduct due to the loss of EtOH molecules.

From the weight loss of Mg-*i*-BuOH adduct, it is calculated that dissociation of first *i*-BuOH molecules occurs at 80 °C. Dissociation of the remaining *i*-BuOH molecules coordinating to Mg^{2+} occurs at higher temperature. The molecule which dissociates at lower temperature is the one having weak interaction with the Mg^{2+} site. It is observed that 75% weight loss occurs up to 250 ^oC and no change in weight loss occurs above 250 ^oC. A simple calculation of four *i*-BuOH molecules (4 x 74) forming adduct with $MgCl_2$ (M.W = 95 g/mol)

fully explains the above observation and suggests that there are four *i*-BuOH molecules coordinating to $MgCl_2$; this is further confirmed by liquid NMR spectral results. Weight loss that occurs >100 ^oC indicates a relatively strong binding character of Mg^{2+} with *i*-BuOH in adduct. A sharp weight loss (38%) occurs between 85-120 ^oC with a distinct DTA peak at 112 ^oC suggesting a loss of two *i*-BuOH molecules. This may be due to a similar interaction of two *i*-BuOH with $MgCl_2$. Weight loss of fourth *i*-BuOH occurs in a broad temperature range between 120 and 250 ^oC. Above 250 ^oC, no weight loss was observed indicating only $MgCl_2$ remains after dissociation of all *i*-BuOH molecules. It is also to be noted that the weight loss of first three *i*-BuOH molecule is associated with endothermic DTA peaks, and the loss of fourth *i*-BuOH is associated with exothermic DTA peak.

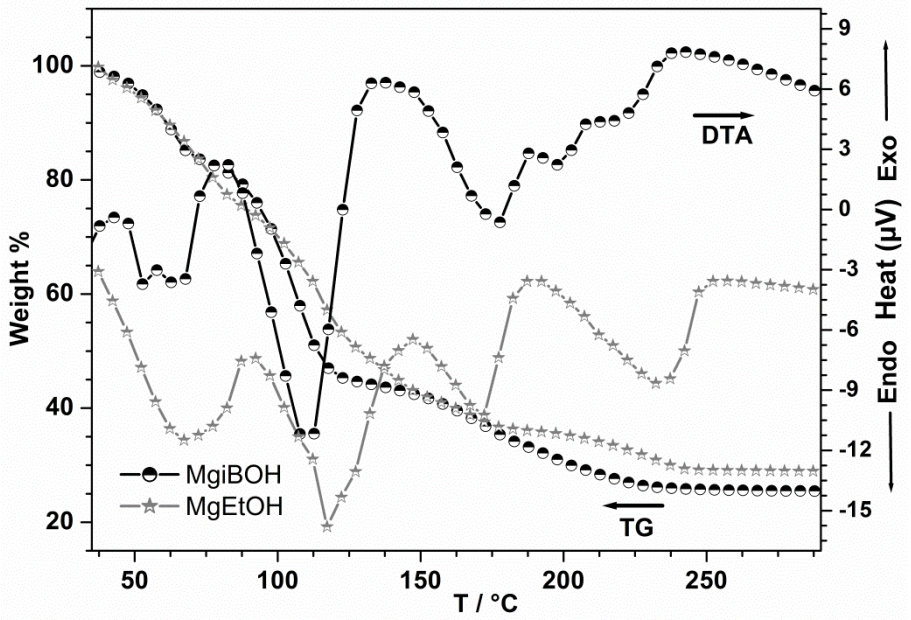

Figure 3.2: TG-DTA analysis of molecular adducts MgEtOH (—☆—) and Mg *i*-BuOH (—●—)

3.2.1.3. Solid state NMR

Figure 3.3 shows the ^{13}C CP/MAS and ^1H MAS NMR spectrum of MgEtOH and Mg-*i*-BuOH molecular adduct. ^{13}C CP/MAS of the MgEtOH adduct exhibits two sharp peaks: the peaks at 58.9 and 17.6 ppm correspond to -**C**H_2OH and **C**H_3 carbon, respectively.

The ^{1}H MAS spectrum of the MgEtOH adducts shows sharp peaks at 5.4, 3.6, and 1 ppm corresponding to-O**H**,-C$\mathbf{H}_2$-, and C$\mathbf{H}_3$ protons, respectively. The sharpness of the peaks is due to the high mobility of the ethanol molecules in the highly symmetrical environment [19, 31-33]. However, ^{13}C CP/MAS of Mg-*i*-BuOH shows methylene signal which appear as doublet at 69.2 and 68.8 ppm with a weak high field shoulder. The methine peaks also appear as a doublet with a chemical shift of 29.1 and 28.9 ppm. Besides, a weak signal at 28.3 ppm is also seen. For methyl group, the observed signals can probably be considered as a combination of four types of signals, the two inner peaks being split into doublet. The chemical shift values of methyl carbons are observed at 19.2, 18.7, 18.6, 18.3, 18.2 and 17.7 ppm (Figure 3.4).

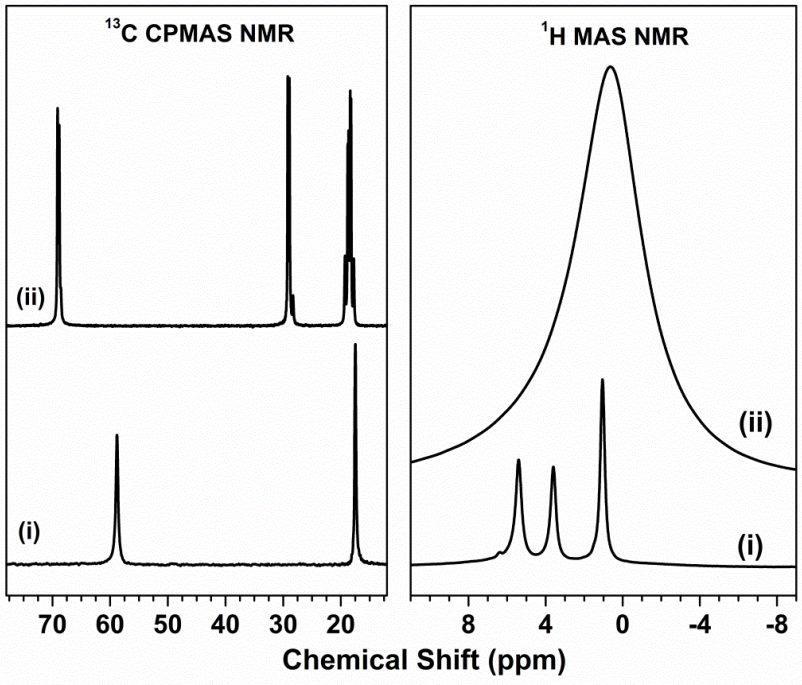

Figure 3.3: ^{13}C CP/MAS and ^{1}H MAS NMR spectra of molecular adducts, (i) MgEtOH, (ii) Mg-*i*-BuOH.

^{1}H MAS NMR of *i*-BuOH adducts shows a very broad peak which is due to the restricted mobility of the *i*-BuOH molecules coordinated to the Mg^{2+} site. Depending on the preparation time, especially set to reflux time of reaction mixture, structure of the molecular

adduct evolves slowly. Further the structure of molecular adducts undergoes reversible structural changes between ambient temperature and 100 ^oC [34]. Detailed XRD and NMR experiments are given in part B. NMR results reported in Figure 3.4 are obtained from samples with a set to reflux time of 3 hour in the preparation reported like other adducts, such as $MgCl_2$.6EtOH.

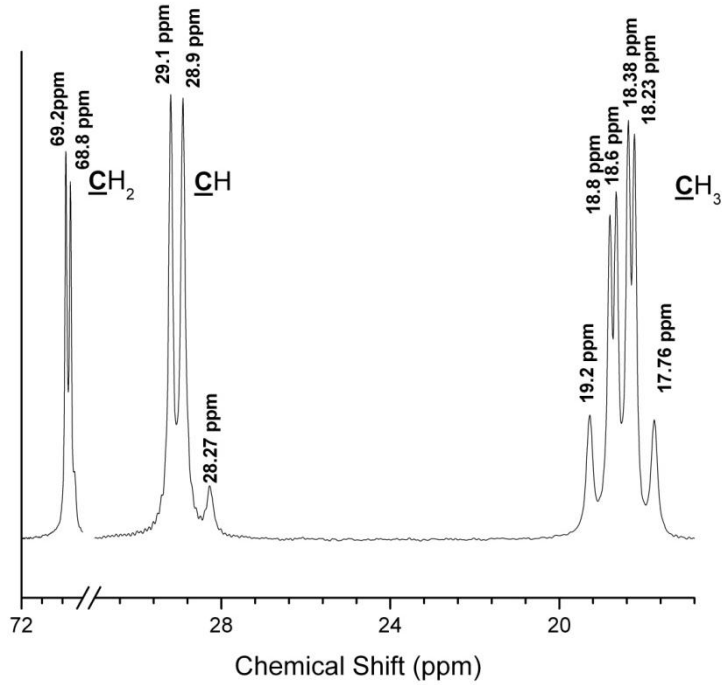

Figure 3.4: ^{13}C CP/MAS NMR spectra of molecular adduct, Mg-*i*-BuOH.

3.2.1.4. Raman Analysis

Figure 3.5 shows the Raman spectra of anhydrous $MgCl_2$, MgEtOH and Mg-*i*-BuOH. Raman spectra of $MgCl_2$ show a high intense peak at 243 cm^{-1} which has been assigned to the A_{1g} breathing mode of the $MgCl_6$ octahedra in the lattice [35-37]. Crystalline $MgCl_2$ belongs to the rhombohedral structure with D_{3d} space group and has a layered structure. Mg^{2+} is in a distorted octahedral configuration coordinated to six chlorine anions. In the Raman spectra of liquid ethanol, a broad and weak OH phonon mode observed at 3400-3100 cm^{-1} is due to the intermolecular hydrogen bonding. For ethanol, peaks at 430, 886, 1052, 1270, and 1094 cm^{-1} correspond to Raman modes associated with δ(CCO), symmetric CCO, anti symmetric CCO,

CH_2 twist + δ(COH), and CO stretch + CH_3 rock + δ (COH) modes, respectively [38]. After the adduct formation with $MgCl_2$, MgEtOH shows one extra peak at 684 cm^{-1} in addition to the features of liquid ethanol mentioned above. The above Raman mode at 684 cm^{-1} is due to the formation of the characteristic Mg-O_6 octahedron, and underscores the formation of the Mg-O bond between Mg and alcoholic oxygen [35, 39]. Similar behaviour is observed in the case of Mg-*i*-BuOH adduct also; however the characteristic Mg-O_6 breathing mode is shifted to 712 cm^{-1}. The above shift is attributed to the changes in the electronic environment around Mg^{2+} site and a possible strong interaction between *i*-BuOH and Mg^{2+}. In conclusion, disappearance of Mg-Cl peak and appearance of Mg-O_x octahedron Raman feature indicate that coordination of alcohol moiety to the system distort the $MgCl_2$ layered structure [34].

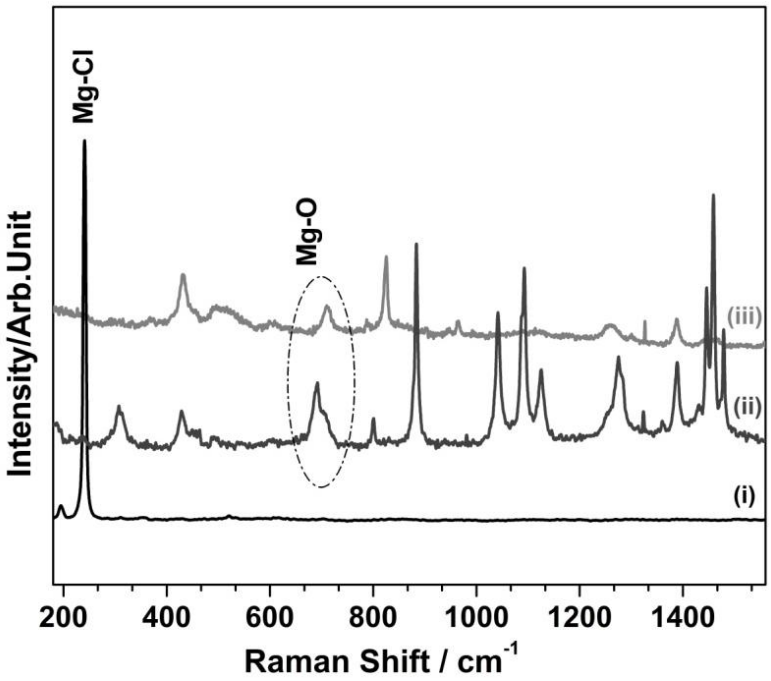

Figure 3.5: Raman spectra of (i) $MgCl_2$, (ii) MgEtOH and (iii) Mg-*i*-BuOH.

3.2.1.5. Scanning Electron Microscopy (SEM)

Figure 3.6 shows the SEM photograph of (a) MgEtOH, (b) and (c) Mg-*i*-BuOH respectively. The SEM photographs of MgEtOH clearly show the spherical shape of adduct with a diameter of 20-40 μm. In SEM images of Mg-*i*-BuOH adducts, particles are uniform

in size and exhibit one dimensional rod shape with an approximate length of 1 mm with a width between 10 and 30 μm. This adduct is highly crystalline and oriented in one direction. High intensity of oriented feature in XRD suggests that molecular adduct likely grows along z-axis. Aspect (length / width) ratio observed for the Mg-*i*-BuOH adduct is ~ 30-100 supports the unidirectional nature of as grown particles. Increase in the molecular size from EtOH to *i*-BuOH alters the interaction differently with $MgCl_2$ and leads to different morphology of adduct and catalyst.

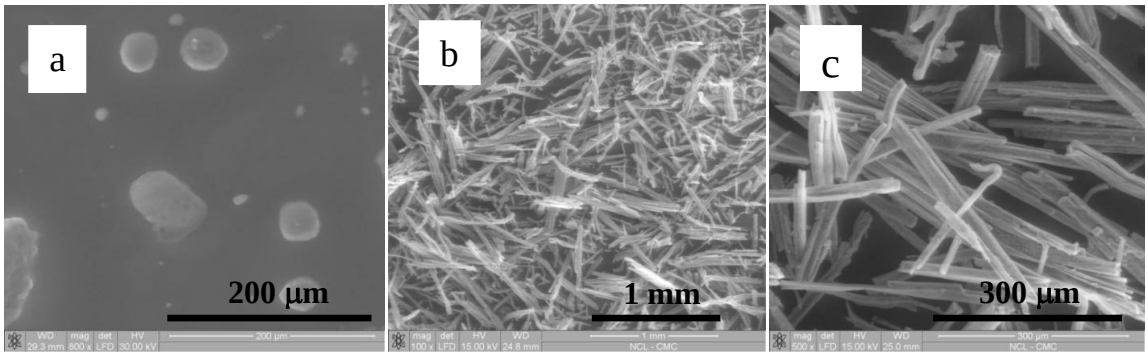

Figure 3.6: SEM images of (a) MgEtOH and (b) and (c) Mg-*i*-BuOH adduct.

3.2.2. Characterization of titanated adduct

3.2.2.1. Powder X-ray diffraction

MgEtOH and Mg-*i*-BuOH adduct were treated with $TiCl_4$ to prepare Z-N catalysts. Characteristic peaks for the molecular adduct disappear in the above Z-N catalyst (Figure 3.7). Powder diffraction data shows broad diffraction features between 15° and 23°, 29° and 34°, and 49° and 51°corresponding to structurally disordered δ-$MgCl_2$. The low-angle peak observed below 10° for MgEtOH and Mg-*i*-BuOH disappears, indicating the removal of EtOH and *i*-BuOH molecules upon titanation from the system; the same has been confirmed by solid state NMR, and it will be discussed later. The diffraction feature at about 16° is due to the stacking of Cl-Mg-Cl triple layers ((003) plane) along the crystallographic direction. XRD features at 29-34°(101/104) and 49-51° are also related to stacking faults in the triple

layers [35, 40]. The growth of $MgCl_2$ crystal was terminated by the surface incorporated $TiCl_4$ leading to assemblies of fine $MgCl_2$ crystallites that could be identified by the characteristic broad peaks in XRD analysis.

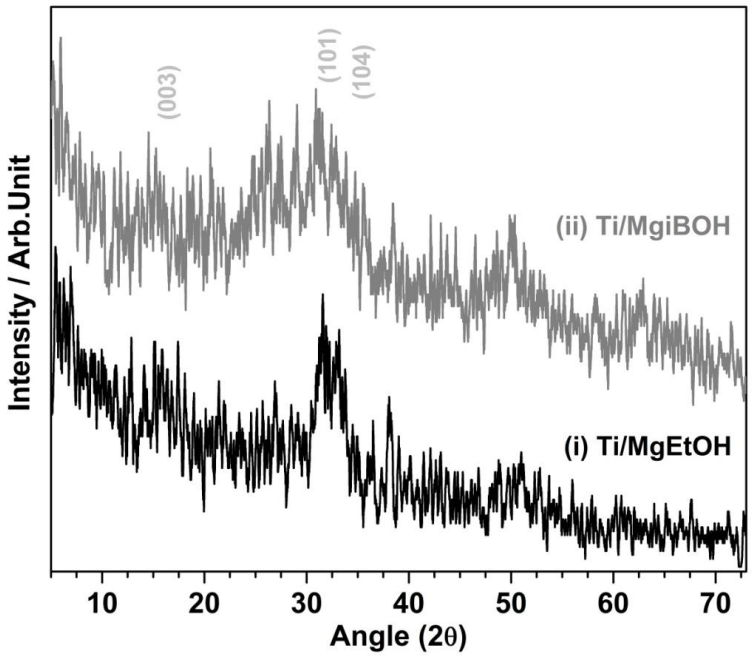

Figure 3.7: XRD patterns of Titanated catalyst (i) Ti/MgEtOH and (ii) Ti/Mg-*i*-BuOH.

3.2.2.2. Thermal Analysis

Thermal analysis of titanated catalysts, Ti/MgEtOH and Ti/Mg-*i*-BuOH also shows weight loss, and in particular DTA shows profound changes (Figure 3.8). For Ti/MgEtOH, there is no weight loss observed below 100 °C indicating a substantial removal of ethanol from the above catalysts. Nonetheless, weight loss observed above 100 °C may be attributed to the loss of any ethanol, trapped chlorinated ethers, and other solvent molecules from Ti/MgEtOH [41]. As compared to *i*-BuOH adduct, Ti/Mg-*i*-BuOH shows a significant difference in the TG/DTA results. There is no significant weight loss below 100 °C indicating no loss of any species from the Ti/Mg-*i*-BuOH catalyst. The weight loss associated with the Ti/Mg-*i*-BuOH catalyst at >100 °C might be due to the desorption of chlorobenzene (b.p. 131 °C) which has been used as the solvent in the titanation step. Some amount of hexane also gets adsorbed on the pore walls and it's not desorbed at its boiling point indicating the strong

interaction with the catalyst system. This result is supported further by NMR of the Ti/Mg-*i*-BuOH catalyst [34].

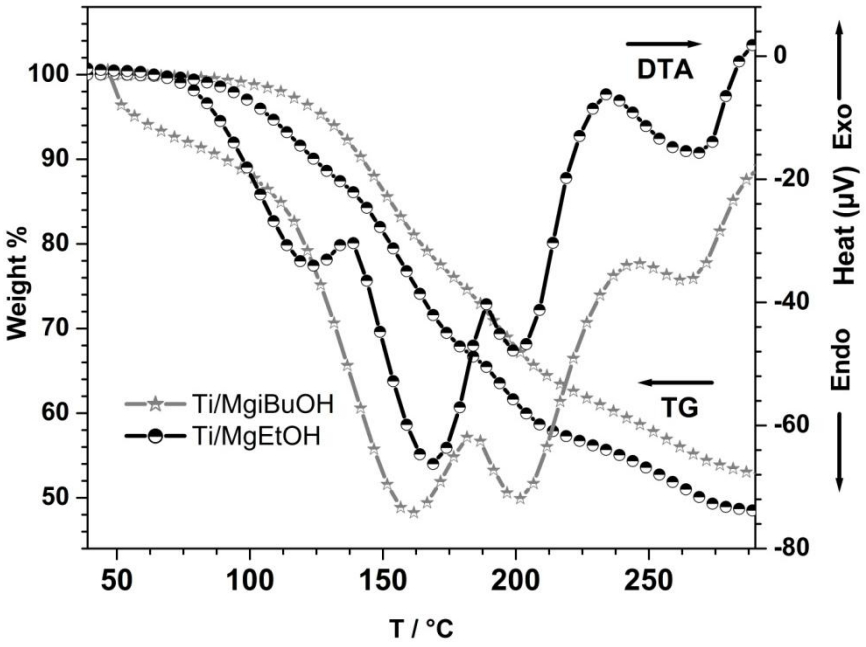

Figure 3.8: TG-DTA analysis of Titanated catalyst, Ti/MgEtOH and Ti/Mg-*i*-BuOH.

3.2.2.3.Solid- state NMR Spectroscopy

Figure 3.9 shows the ^{13}C CP/MAS and ^{1}H MAS NMR spectra of molecular adducts and corresponding titanated Z-N catalyst. ^{13}C CP/MAS spectra of Ti/MgEtOH show an additional peak at 87.6 ppm. This may be due to the formation of small amounts of chlorinated ether. The reaction between MgEtOH and $TiCl_4$ produces HCl, which in turn leads to the formation of chlorinated ethers. The latter remains trapped within the pores of the support and could be observed by ^{13}C CP/MAS NMR; weight loss in TG-DTA also corresponds to the loss of chlorinated ether molecules (see Figure 3.8). The ^{1}H MAS spectrum of Ti/MgEtOH show very sharp peaks at 8 and 2.5-1.6 ppm corresponding to protons from aromatic and ethyl species and chlorinated ethers, respectively [41].

The chemical shift value of *i*-BuOH adduct is also different from the titanated catalyst supported on Mg-*i*-BuOH. Absence of peaks at 69.2 and 68.8 ppm in Ti/Mg-*i*-BuOH supports the removal of *i*-BuOH from adduct upon titanation. Presence of aromatic carbon

features at 135 ppm is likely due to chlorobenzene, used for washing of titanated catalyst which remains trapped within the pores of the support and is seen by ^{13}C CP/MAS NMR. Peaks at 13.6, 20.9 and 32 ppm in the ^{13}C CP/MAS of Ti/Mg-*i*-BuOH are matching with the methylene peaks of n-hexane which is used for washing. The trapped hexane is seemingly strongly associated with the catalyst and is not desorbed at normal reaction conditions. This is supported by the weight loss observed at T = 120-300 ^{o}C observed in TG/DTA of Ti/Mg-*i*-BuOH (Figure 3.8).

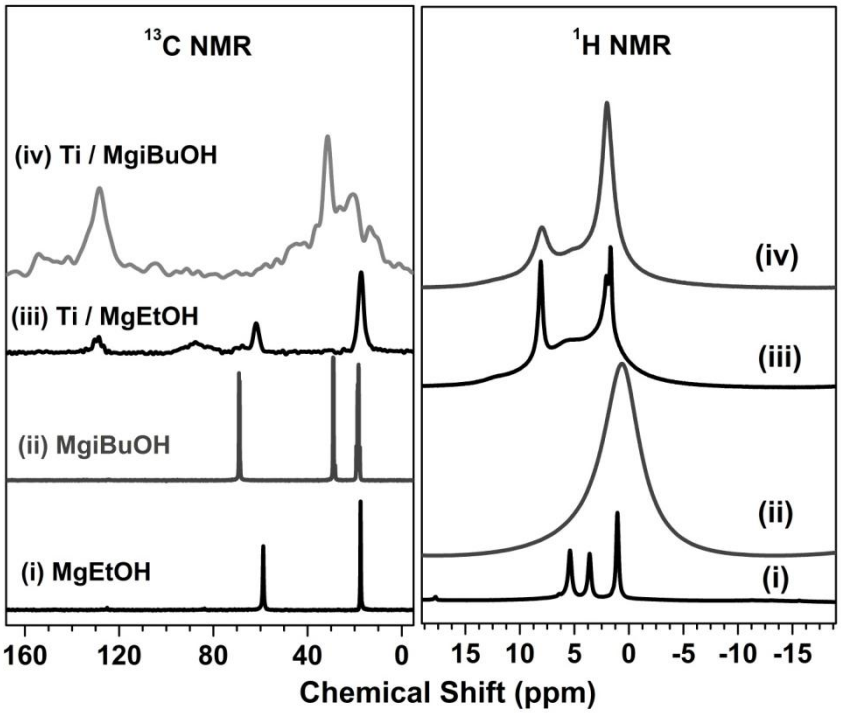

Figure 3.9: ^{13}C CP/MAS and ^{1}H MAS NMR spectra of molecular adducts (i) MgEtOH, (ii) Mg-*i*-BuOH, (iii) titanated catalyst Ti/MgEtOH, and (iv) Ti/Mg-*i*-BuOH.

3.2.2.4. Scanning Electron Microscopy (SEM)

The SEM images are shown in Figure 3.10 clearly show the spherical shape of both the titanated catalysts, Ti/MgEtOH and Ti/Mg-*i*-BuOH. However, there are some changes on the surface of the support after titanation. In the case of Ti/MgEtOH, the particle size has been reduced drastically from 20 to less than 10 μm upon titanation. Apparently, smooth surfaces of the pure adducts become significantly porous in the titanated catalyst. The porous

structure of the titanated catalysts is attributed to the removal of alcohol molecules from pure adducts, and this allows the creation of pores as well as the incorporation of $TiCl_3$ on the surface and pores. SEM images of titanated catalyst, Ti/Mg-*i*-BuOH exhibits spherical morphology with diameter of 100 μm. Higher magnification of surface of the titanated adducts shows highly porous in nature, particularly with macro-pores. A drastic change from one dimensional rod shape with Mg-*i*-BuOH to spherical shape after titanation is to be noted. This may be attributed to a disintegration of Mg-*i*-BuOH adduct with $TiCl_x$ incorporation into the $MgCl_2$ lattice.

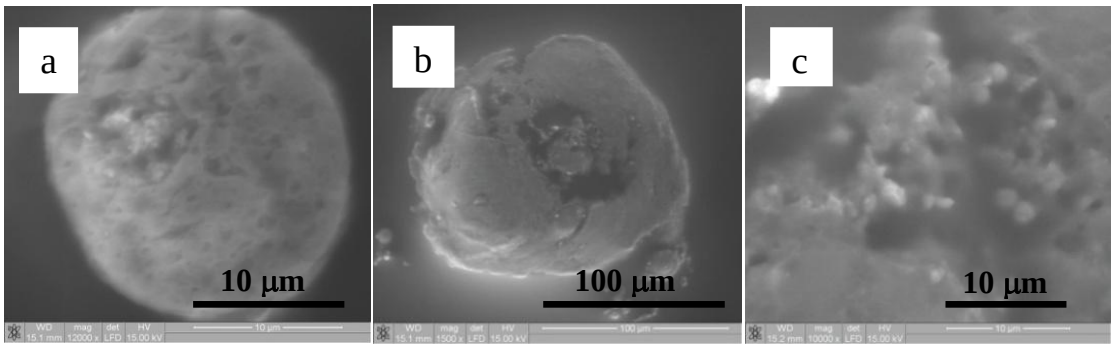

Figure 3.10: SEM images of (a) Ti/ MgEtOH and (b) and (c) Ti/ Mg-*i*-BuOH adduct.

Figure 3.11 shows the SEM images of polymer obtained from Ti/MgEtOH and Ti/Mg-*i*-BuOH. From SEM images it's clear that polymer exhibits spherical morphology, and replicating the morphology of the catalyst particle. Few particles are agglomerated which may be due to the conditions applied during polymerization reaction and the same leads to the cracks on the catalyst surface.

3.2.2.5. Textural Properties

Table 3.1 shows the BET surface area and pore volume of adducts and titanated catalysts. It is to be mentioned here that the surface area of as-prepared molecular adducts shows a negligible value of 1-2 m^2/g. Apart from the much less porosity of molecular adducts, they could not be degassed (before surface area measurement) at temperatures higher than 40 °C as it would lead to loss of ethanol molecules. Surface area and pore size

distribution measured through nitrogen adsorption isotherms on titanated catalysts are shown in Figure 3.12 b. Ti/MgEtOH show significantly high surface area (Table 3.1). Mg-*i*-BuOH does not show any significant surface area (< 1 m^2/g). Surface area of the Ti/Mg-*i*-BuOH was found to be very low (6.5 m^2/g) as compared to Ti/MgEtOH catalyst (55.3 m^2/g) [42]. Indeed, the high surface area of Ti/ME is likely due to the removal of all EtOH molecules and hence the creation of high porosity.

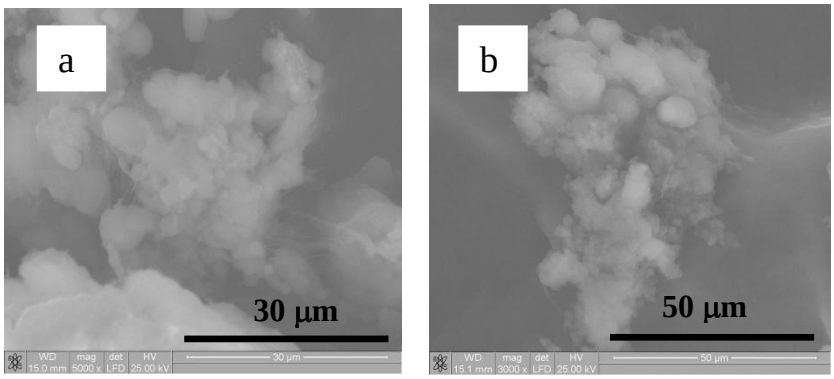

Figure 3.11: SEM photographs of Polyethylene obtained from (a) Ti/MgEtOH and (b) Ti/ Mg-*i*-BuOH.

Table 3.1: Textural characteristics of titanated catalysts.

Material	**Surface Area (m^2/g)**	**Pore Diameter (nm)**	**Pore Volume (cc/g)**
Ti/Mg-*i*-BuOH	6.485	2.32	0.014
Ti/MgEtOH	55.3	3.87	0.084

Adsorption isotherm and pore size distribution of titanated catalysts are shown in Fig. 3.12. Analysis of adsorption isotherms indicates type II and IV (H3) adsorption isotherms for Ti/Mg-*i*-BuOH and Ti/MgEtOH, respectively. An exponential increase in nitrogen adsorption observed for both catalysts at $P/P_o \sim 0.8$ is to be noted. This is attributed to the presence of macropores in Ti/MgEtOH catalysts, particularly with slit-type pores. The difference observed in adsorption isotherms between the above two catalysts is to be noted.

Indeed, the type II adsorption isotherm indicates an unrestricted monolayer-multilayer adsorption, which might be an important factor helping toward chain growth in polymerization.

Average pore diameter of Ti/Mg-*i*-BuOH catalyst is found to be 2.3 nm with a pore volume of 0.014 cc/g. Pore size distribution curve shows the various sizes of pores with a majority of them in the mesoporous regime (< 30 nm). It is evident from adsorption isotherm and SEM studies that Ti/Mg-*i*-BuOH exhibits pore size in all regimes from micro, meso to macro pores indicates a multimodel pores. Indeed exponential rise in adsorption isotherm > P/P_o ~ 0.9 supports the presence of macropores and N_2 filling of such macropores requires N_2 pressure greater than atmospheric pressure.

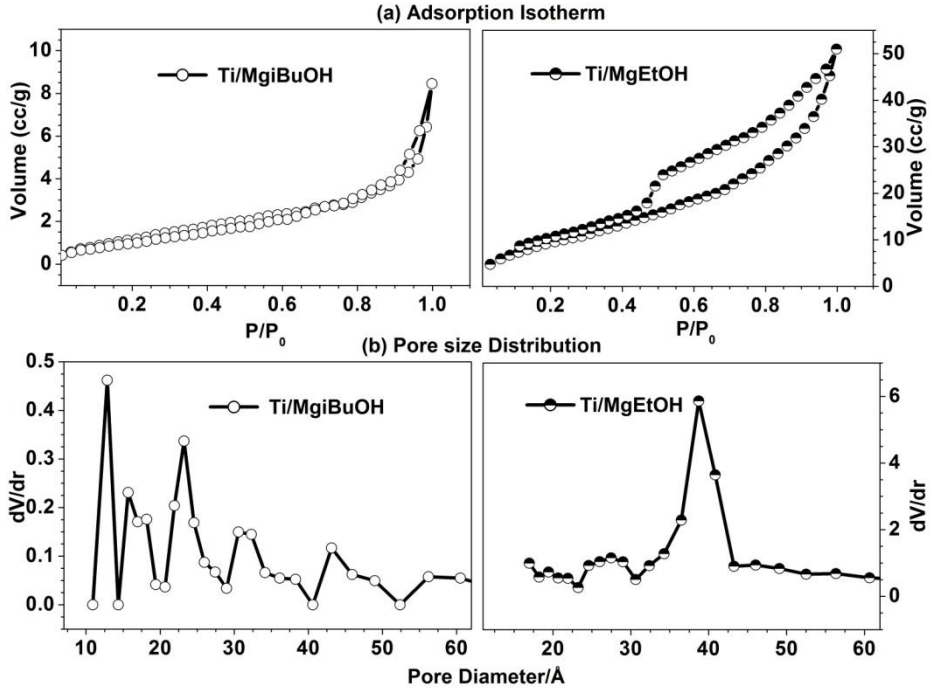

Figure 3.12: (a) Adsorption isotherms and (b) pore-size distribution of titanated catalysts, Ti/MgEtOH and Ti/Mg-*i*-BuOH.

3.3. Ethylene Polymerization

After the extensive characterization of molecular adduct and titanated catalyst, the activity of the catalyst was evaluated by ethylene polymerization (Table 3.2). Ethylene, rather

than propylene, polymerization was chosen as the benchmark for comparing the activities of MgEtOH and Mg-*i*-BuOH derived catalysts so that potential differences in energetics arising out of different orientations of propylene could be ignored. Ethylene polymerization was carried out with MgEtOH and Mg-*i*-BuOH molecular adducts supported Ti catalyst, as mentioned earlier, without any attempt to maximize the productivity by optimizing the experimental conditions. Triethyl aluminium (TEAL) was used as the cocatalyst. Higher yields (1300 g/g of catalyst) of polyethylene and productivity were obtained using MgEtOH rather than Mg-*i*-BuOH supported catalyst (see Table 3.2). The increase in activity of Ti/MgEtOH is due to high surface area, pore volume and pore size distribution [41].

Table 3.2: Catalytic performance of Ti/MgEtOH and Ti/Mg-*i*-BuOH for ethylene polymerization.

Support used for Catalyst preparation	**Wt % of Ti**	**Catalyst quantity (mmole of Ti)**	**TEAL/Ti ratio**	**Productivity of PE (g/g of catalyst)**
MgEtOH	11	0.228	100	1300
Mg-*i*-BuOH	17	0.354	50	300

Catalyst quantity = 0.1g; Al/Ti = 50 for MgEtOH support, Al/Ti = 100 for Mg-*i*-BuOH. Dry hexane has been used as solvent.

However, Ti/Mg-*i*-BuOH shows low activity (300 g/g catalyst) for ethylene polymerization, even at high Al/Ti ratio (100) [34]. Decreasing Al/Ti ratio decreases the activity significantly. Hard small lumps of polymer were obtained after polymerization with the above catalyst. It is likely that the pore of the active catalyst was blocked by hexane and it's not available for monomer insertion. It is evident from the peaks observed at 13.6, 20.9 and 32 ppm in the ^{13}C CP/MAS of Ti/Mg-*i*-BuOH are matching with the methylene peaks of n-hexane which is used for washing. Polymerization growth occurs likely, only on the external surface of the catalyst. Although pore size distribution exhibits micro and meso

pores, hardly any nitrogen adsorption occurs in those pores highlighting the unavailability of majority of them. As indicated above and supported by TG-DTA and NMR analysis of Ti/Mg-*i*-BuOH, aliphatic and aromatic species that are adsorbed inside the pores blocks the active sites. Further the large amount of Ti-content also indicates a low specific catalytic activity. Presence of less number of active titanium species (Ti^{3+}) in the system is also one of the reasons for decrease in activity.

3.4. Conclusions

Structural, spectroscopic, textural, and microscopic studies of MgEtOH and Mg-*i*-BuOH adduct and final catalysts have been thoroughly investigated by many techniques. XRD and NMR analysis shows the characteristic property of molecular adduct formation. In Raman spectra, MgO_6 breathing mode was observed at 712 cm^{-1} for Mg-*i*-BuOH, compared to 687 cm^{-1} for MgEtOH, indicating a significant increase in the interaction of *i*-BuOH with $MgCl_2$ and stronger electronic interaction. Introduction of bulky *i*-BuOH instead of EtOH as a Lewis base increases the complexity of the entire system. Changing the Lewis base affects the surface area, pore diameter, pore volume and % of Ti loading etc and finally the activity of Z-N catalyst. It is observed that changing the alcohol from simple to bulky, there is an overall change in electronic property of the active $MgCl_2$. Present studies gives some insight into the role of $MgCl_2$. nROH support in controlling the activity of the Z-N catalyst other than simply as a support for the dispersion of the Ti species for olefin polymerization. Polymerization of ethylene using titanated Mg-*i*-BuOH shows less activity compared to Ti/MgEtOH catalyst. The following factor results decrease in the activity of the titanated Mg-*i*-BuOH: (i) lower surface area, (ii) low pore volume and pore diameter, and (iii) absence of free Ti^{3+} species even though the catalyst contain high Ti wt % of the same. Present study gives an idea about the structural and electronic changes happen to the $MgCl_2$ support if the size of alcohol changes.

Part B: A Solid – State NMR investigations of Magnesium Chloride – Isobutanol adduct: A new Ziegler-Natta catalyst support

3.5. Introduction

The present generation Ziegler-Natta catalyst for the synthesis of polyolefin consists of titanium chloride as a catalyst, magnesium chloride as a support, an electron donor which may be an internal or external donor and trialkyl aluminium as cocatalyst. $MgCl_2$ supported Ziegler-Natta catalyst increases the rate of polymerization as compared to the traditional Ziegler-Natta catalyst for both ethylene and propylene polymerization. Ball milling, chemical conversion of MgO with chlorinating agent, recrystallization, spray crystallization etc are some of the common synthetic procedures used for the generation of active catalyst. In chemical methods, different Lewis bases such as alcohol, ether, amine, ester etc. were reacted with $MgCl_2$ which leads to a new generation of active Z-N catalyst.

Though a lot of research activities are going on in the area of Z-N catalyst system using different types of electron donors, hardly few findings are available on the role of $MgCl_2$ based support.$MgCl_2$ supported Z-N catalyst system has usually been characterized by XRD, IR, SEM, AFM, HRTEM, XPS, NMR and Raman techniques [15, 29, 42-46]. Among the alcohol adducts of $MgCl_2$, ethanol adduct ($MgCl_2$.nEtOH) has been studied significantly by different groups [44, 47, 48]. Di noto *et. al*. [48] used XRD and IR to elucidate the structure of the $MgCl_2$.nEtOH adduct. Somorjai et *al*. [35] used ultraviolet Raman spectroscopy to study $MgCl_2$ $(C_2H_5OH)_x$ adducts prepared over a wide composition range, x= 0.47 to 6. Vibration spectroscopy techniques could identify only the formation of metal – oxygen bond and difficult to distinguish the pure and mixed phases present in a system. Due to intrinsic complexity of the system, it is very difficult to understand its phase behaviour. The number of ROH/$MgCl_2$ ratio may vary from one to six and none of the described methods such as XRD, IR and Raman etc allow a reliable discrimination of pure phase

compounds from mixtures. Single crystal data is available only for few alcoholic adduct such as $MgCl_2$.6EtOH, $MgCl_2.6C_6H_{11}OH$ [27].

However, solid state NMR technique has emerged as one of versatile techniques to study phase and disorder behaviours of various systems, its application to Ziegler-Natta catalyst systems has been very limited. Terano *et al* [46] used solid-state ^{13}C NMR to study the state of ethyl benzoate, the electron donor, in $MgCl_2$-supported catalysts. Sormunen *et.al.* [49] studied heterogeneous Ziegler-Natta catalyst system containing mono and di ester internal donors by solid state ^{13}C NMR and observed changes in chemical shifts and line broadening as a result of complexation. Abis *et.al.* [42] reported NMR studies of aromatic ester - $MgCl_2$ / $TiCl_4$ systems. Solid state NMR of titanium and magnesium chloride complexes of ethyl acetate has also been reported by Clayden *et.al.* [50]. In a recent study Sozzani *et.al.* [13] applied multidimensional MAS NMR measurements to different stoichiometry of magnesium dichloride to ethanol. Our group has also been using solid state NMR as tool to characterize structure of various alcohol adducts of $MgCl_2$ [15, 16, 34, 41]. Part A of the third chapter discussed the formation of stoichiometric adduct of isobutanol with magnesium chloride (Mg-*i*-BuOH) under certain conditions, its characterization and activity for olefin polymerization. It has been observed that the formation of isobutanol adduct is very sensitive to the conditions of preparation. A detailed investigation has been carried out to explore a deeper understanding of the structure of Mg-*i*-BuOH adducts that has not been resolved until now, using solid state NMR especially variable temperature and Separated Local Field NMR experiments is described in Part B.

3.6. Results and Discussion

3.6.1. ^{13}C CP/MAS and ^{1}H MAS NMR study of Mg-*i*-BuOH

Figure 3.13 shows the ^{13}C CP/MAS spectrum of Mg-*i*-BuOH and isopropanol adduct (MgiPrOH) prepared by azeotropic set to reflux for 150 and 180 min. The spectrum is very

similar to the isopropanol adduct except for the presence of an additional methylene carbon. The methine (29.2 and 28.8pppm) and methylene carbons (69 and 68.8ppm) shows two equally intense signals while the methyl carbons, as in the case of $MgCl_2$. 4(iPrOH), shows four signals. In analogy with the isopropanol adduct this can be considered as adduct containing four isobutanol molecules, $MgCl_2$.4*i*-BuOH, with two sets of isobutanol. In each set the isobutanol molecules have equivalent arrangement.

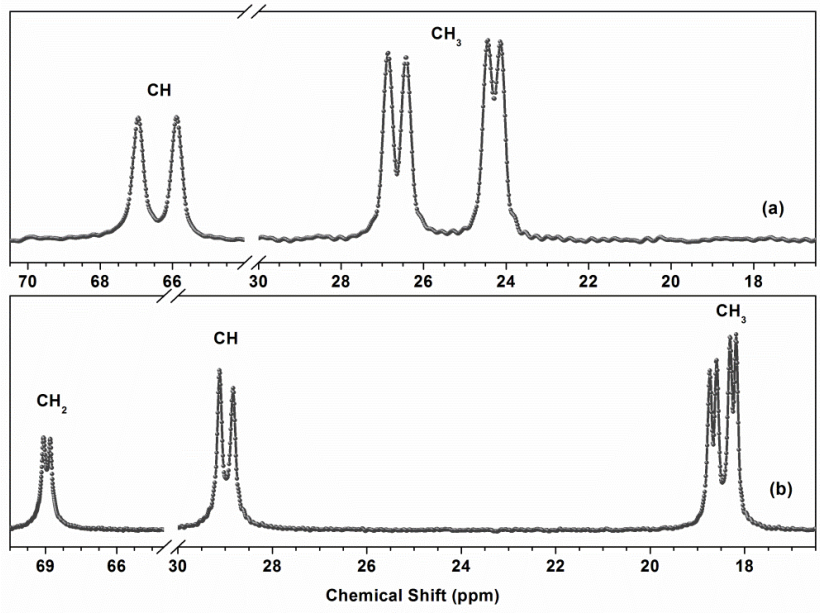

Figure 3.13: ^{13}C CP/MAS NMR spectra of molecular adduct, (a) MgiPrOH and (b) Mg-*i*-BuOH prepared at 150 min.

Mg-*i*-BuOH adduct obtained after 180 minutes azeotropic distillation (Fig 3.14b) showed additional signals of weaker intensities for all the carbons which are more prominent for the methyl and methylene carbons. It is interesting to note that the most deshielded and shielded methyl carbons appeared broader compared to the inner "doublets". These signals are attribute to the methyl groups belonging to two different isobutanol molecules in the adduct present in another phase. The methine carbon of this adduct showed, in addition to the two strong signals at 29.2 and 28.8 ppm, one weak signal at 28.2 ppm, the former one nearly overlapped with the shielded methine carbon (28.8 ppm) of the major phase. The presence of

two weak methine signals itself indicate that the additional phase in the system should also have at least two isobutanol molecules.

In the ^{13}C SPE (HPDEC) spectrum of this adduct the ratio of CH carbon at 28.2 ppm to CH_3 carbon at 19.3 and 17.8 has always been 1:2:2. A single unit of isobutanol molecule would have given a ratio of 1:1:1. For brevity we designate the minor phase as phase-1 and the major one as phase-2 (indicated as ph 1 in Fig 3.14 b).

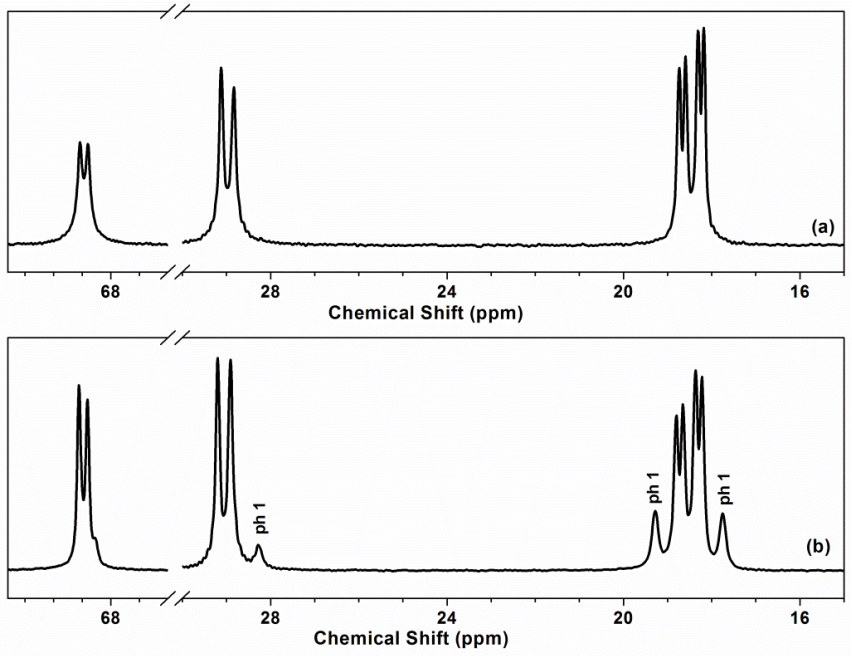

Figure 3.14: ^{13}C CP/MAS NMR spectra of molecular adduct, Mg-*i*-BuOH prepared at (a) 150 min and (b) 180 min.

In order to get deeper insight to this phenomenon of the presence of two different phases, we followed the formation of adduct as a function of set to reflux time. ^{13}C CP/MAS spectra of adducts formed at different set to reflux time are presented in Fig.3.15. It is interesting to note that the ratio between the inner (two doublets) and outer methyl peaks varies on increasing the set to reflux time. The phase-1 signal completely vanishes on set to reflux $MgCl_2$ and isobutanol for 150 min. It is observed that on further increase in set to reflux time the signals due to isobutanol molecules present in phase -1 reappeared. It may also be noted that phase-1 signals dominate at the initial stages and hence can be attributed to

the coordination of the isobutanol molecules to locations that are easily accessible. It is unlikely that these signals are arising from physisorption of the alcohol molecules as we could pick up the event by ^{13}C CP/MAS experiment.

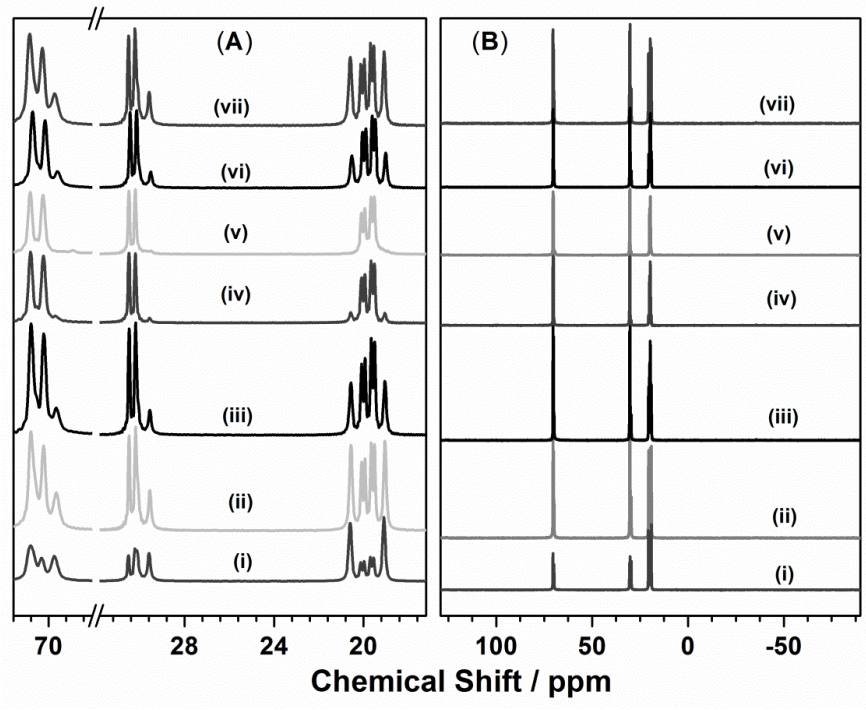

Figure 3.15: (A) ^{13}C CP/MAS NMR spectra of molecular adduct, Mg-*i*-BuOH prepared at (i) 5 min, (ii) 30 min, (iii) 60 min, (iv) 90 min, (v)150 min, (vi) 180 min and (vii) 240 min, (B) shows the full ^{13}C CP/MAS NMR spectra.

It is necessary for the molecular system to impart some sort of rigidity for achieving an effective cross polarization at the contact time (2 s) employed for the measurements. Only the isobutanol molecules which are strongly associated with $MgCl_2$ can hence be expected to exhibit cross polarization. Further, the broadness of signals of phase-1 also suggests lack of long range ordering or more amorphous nature of adduct, which is further supported by the XRD and SEM data (see sections 3.6.5 and 3.6.7).

It is well known that the ^{1}H MAS spectrum is very sensitive to the motional averaging of the molecules and the spinning speed employed for the measurements is not sufficient to average the strong ^{1}H-^{1}H dipolar coupling (50 to 100 KHz). The ^{1}H-^{1}H dipolar couplings are

completely averaged in liquid samples like isobutanol due to rapid molecular tumbling and give rise to very narrow ^{1}H signals.

Depending on the strength of association with matrix like $MgCl_2$, small molecules like isobutanol can achieve different degree of molecular motions. A strongly associated molecule will thus be more rigid; will show stronger ^{1}H-^{1}H dipolar couplings which cannot be averaged by MAS at moderate speeds and results in broader resonances. Signals of weakly bound molecules with partially averaged ^{1}H-^{1}H dipolar interactions can show narrow line under moderate spinning speeds at magic angle. The absence of narrow signals clearly demonstrates the rigid nature of the alcohol molecules present in phase-1. This is very clear from the spectra presented in Fig 3.16.

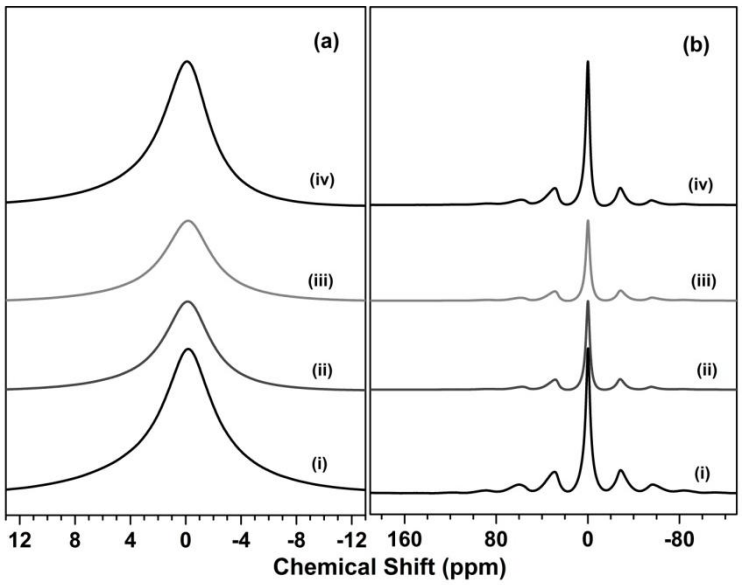

Figure 3.16: ^{1}H MAS NMR spectra of molecular adduct, Mg-*i*-BuOH prepared at (i) 5 (ii) 150 (iii) 180 and (iv) 240 min, (b) Full ^{1}H MAS NMR spectra as in panel (a).

Further, the presence of occluded *i*-BuOH can be confirmed form the ^{13}C SPE (HPDEC) spectrum wherein it is noticed that the chemical shift of these mobile molecules are slightly different from those of the rigid molecules (Figure 3.17). The origin of pahse-1 type of signals can thus be attributed to those isobutanol molecules interacting strongly with

$MgCl_2$ forming adduct, but without long range ordering. Considering the octahedral arrangement of $MgCl_2$, the most amenable locations available for coordination of alcohols molecules can be envisaged as those present along the Z axis. In additions to this, weaker signals belonging to phase -2 can also be seen in the ^{13}C CP/MAS spectrum of the sample collected after a set to reflux time of 5 minutes. These signals are sharper and hence likely to possess higher degree of ordering. In analogy with the $MgCl_2$ adduct of isopropyl alcohol, the most likely arrangements of isobutanol in this phase is along the XY plane. Decrease in the intensity of signals belonging to phase -1 in the ^{13}C CP/MAS spectra of samples collected at longer intervals of set to reflux suggests the likelihood of a meta stable phase which on further increasing in the set to reflux time moves over to phase-2 with better ordering. It is interesting to note at this point that the SEM images of adducts collected at longer set to reflux intervals also shows the presence of long range ordering. (See section 3.6.7).

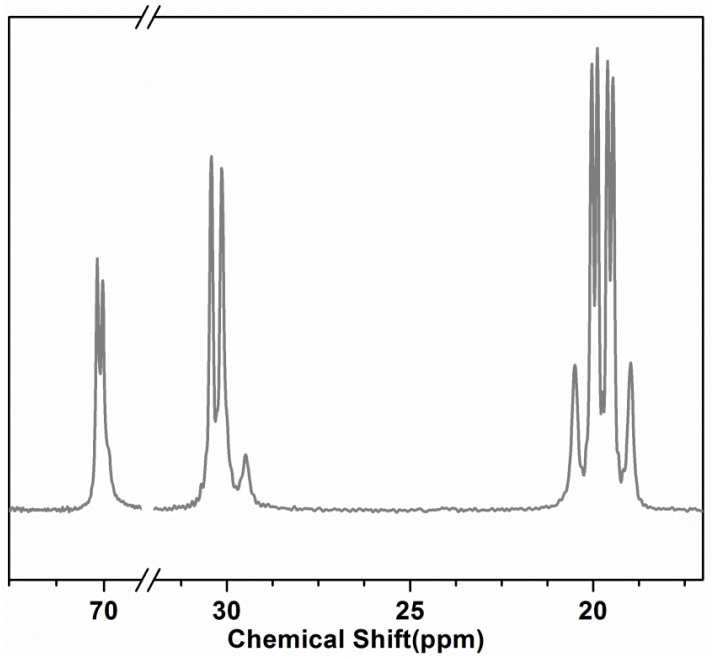

Figure 3.17: ^{13}C SPE (HPDEC) spectrum of Mg-*i*-BuOH prepared under 3 hr set to reflux.

3.6.2. Separated Local Field NMR Analysis

Peak broadness can be due to molecular motions having frequency of the order of spinning speed (a few KHz) or the ^{1}H decoupling field employed. In order to check this we

have carried out separated local field (SLF) experiment, which is a versatile tool to monitor C-H dipolar coupling to get information about molecular motions, especially of the order of hundreds of kHz. SLF is a two dimensional experiment based on cross polarization which display the carbon chemical shift on the F2 axis and a scaled C-H dipolar coupling on the F1 axis. When molecules undergo motions the C-H dipolar coupling also gets averaged and show a reduced value compared to a rigid system. In the SLF experiment, magnitude of the scaled C-H dipolar coupling extracted from the F1 dimension provides relative information about the molecular motions. We have carried out SLF measurement on the sample that containing both phases obtained after set to reflux for 180 min. The 2D plot and the slice projections are given in Fig.3.18. A comparison, for example for the methyl carbons itself, clearly shows that the C-H dipolar of carbons belong to phase -1 (outer signals) are larger than those of phase -2 (the inner signals) and hence have more restricted motions than the latter. Hence, it is evident that the broadness is not due to molecular motions.

3.6.3. Estimation of isobutanol molecule in adducts

^{13}C NMR measurements showed reappearance of phase-1 in adducts formed after 150 minutes of set to reflux time. This can either be due to migration of the alcohol molecules from phase-2 to the coordination sites corresponding to phase-1 or addition of more molecules of alcohol to the vacant coordination sites. In the latter case the total alcohol content should increase while in the former it should remain same. The alcohol content of various adducts prepared have been estimated by TGA and liquid NMR. It is observed that the alcohol content has not increased for adducts collected after a set to reflux duration of 150 minutes. The estimated alcohol content from liquid NMR is in good agreement with the valued obtained from TGA. It is surprising that $MgCl_2$-(*i*-BuOH) system cannot accommodate more than 4 molecules of alcohol and the alcohol molecules in $MgCl_2$.4(*i*-BuOH) system shows interesting dynamic nature during its preparation. Though the reason

for this behaviour is not very clear, the steric effect of the alcohol molecule may likely to play a crucial role.

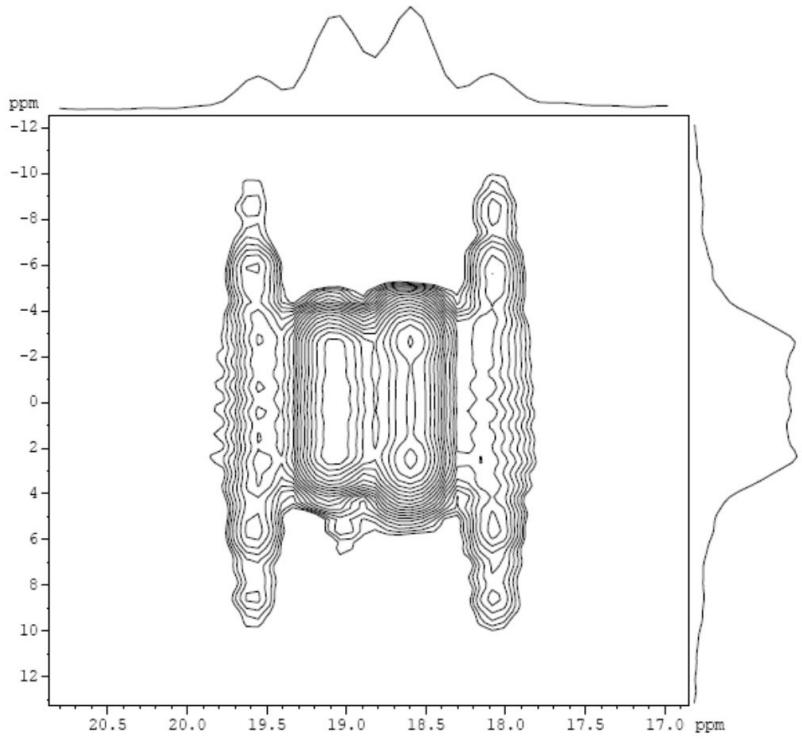

Figure 3.18: Separated Local Field (SLF) spectra of isobutanol adduct, Mg-*i*-BuOH.

3.6.4. Variable Temperature NMR analysis of Mg-*i*-BuOH

In order to get more insight to the dynamic nature of the system we have carried out *in situ* variable temperature (30 to 110^{o}C) ^{13}C CP/MAS measurements on the same batch of sample used for the SLF experiment having both the phases. The spectra obtained are shown in Figures 3.19 and 3.20. The striking feature is the complete disappearance of phase -1 carbon signals on heating at 50^{o}C. This clearly demonstrate that adducts of this type are not probably thermodynamically stable though are kinetically favoured. On increasing the temperature further, due to enhanced thermal motions, the inequivalene carbon sites of phase -2 tends to reduce and almost merges at 110^{o}C. On cooling, the phase -1 signal reappears. It is important to note that more of this environment is observed at room temperature on cooling indicating the larger population of the kinetically favoured phase.

The TG-DTA analysis of the sample showed that the dissociation of the first molecule of isobutanol is completed only at 80^{o}C. For the adduct under consideration, at 50^{o}C, three possibilities can be envisaged for the absence of phase-1 signals in the ^{13}C CP/MAS spectrum (Fig. 3.20): (i) the isobutanol desorbs and gets itself physically trapped in the matrix, (ii) It desorbs and migrates to the other phase, and (iii) both physical trapping and migration. More insight to the temperature behaviour is obtained from the ^{1}H NMR spectra collected at different temperature (Fig. 3.19). The ^{1}H NMR spectrum at room temperature is typical of a rigid system with broad peak (Figure 3.16 a (i)) at under the measurement conditions. At 50^{o}C the ^{1}H MAS spectrum clearly shows the existence of two types of environments via the broad one at a set of sharper signals. From the sharper signals it could also be able to identify all the four different environments of protons in isobutanol. These sharper lines are characteristic of motionally averaged isobutanol molecules. This observation suggests that these isobutanol molecules are indeed desorbed from adduct and has only very weak association, if any, with the $MgCl_2$ matrix. This is further confirmed from the ^{13}C CP/MAS NMR spectrum taken at 50^{o}C (Figure 3.20). ^{13}C Chemical shift of the methyl groups corresponding to sharper signal (19.6ppm) is different from the rest. This environment is not seen in the corresponding CP/MAS spectrum and confirms its origin. Besides, the area of this methyl environment observed at 50^{o}C nearly corresponds to the sum of areas of the outer signals at RT.

Observations from the variable temperature demonstrate that (i) Phase-1 environment is very sensitive to temperature. (ii) It desorbs at ~50^{o}C and get trapped in to $MgCl_2$ matrix and possess liquid like behaviour, and (iii) phase -2 is less sensitive to temperature range studied except the loss of inequivalene of the environments due to increase in molecular motion. (iv) On cooling, the desorbed alcohol molecules gets re-adsorbed on to the same sites and brings out the reversible nature of the events qualitatively, (v) Phase -1 is less stable

and are kinetically favoured.

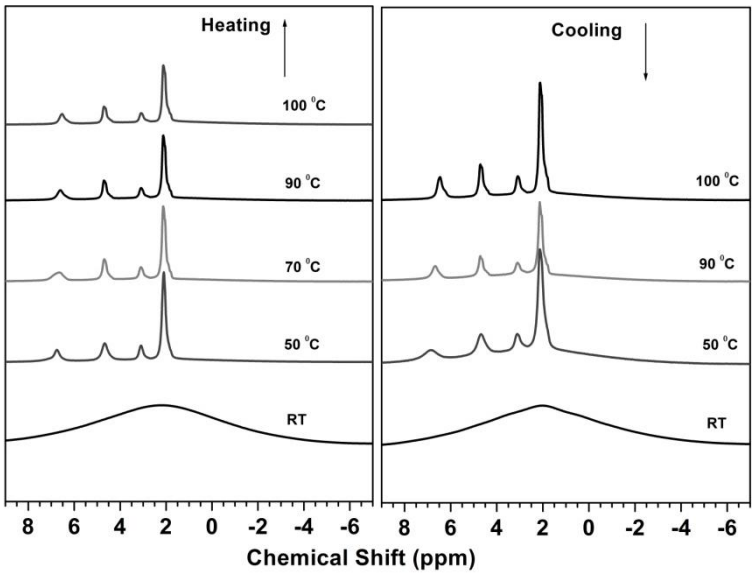

Figure 3.19: In-situ heating and cooling ^{1}H MAS NMR spectra of Mg-*i*-BuOH. The temperature varies from RT to 110 °C.

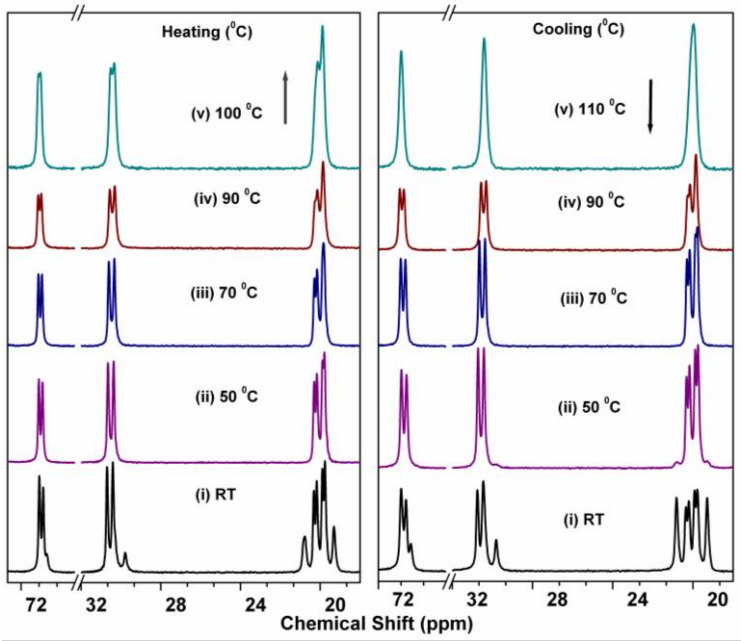

Figure 3.20 ^{13}C CP/MAS in-situ heating and cooling NMR spectra of Mg-*i*-BuOH. The temperature varies from RT to 110 °C.

3.6.5. XRD of Mg-*i*-BuOH adducts

Figure 3.21 shows the XRD pattern of isobutanol adduct prepared under different set to reflux conditions. A systematic evolution in the structure as well as crystalline nature of

adduct is clearly visible in the XRD pattern. The only variable here being the duration of set to reflux time. No peak at 2θ = 15.1° indicates that adduct formation started once the isobutanol is in contact with $MgCl_2$. However there is no interaction between $MgCl_2$ and isobutanol at RT and structure formation necessarily requires set to reflux time at T= 125 °C.

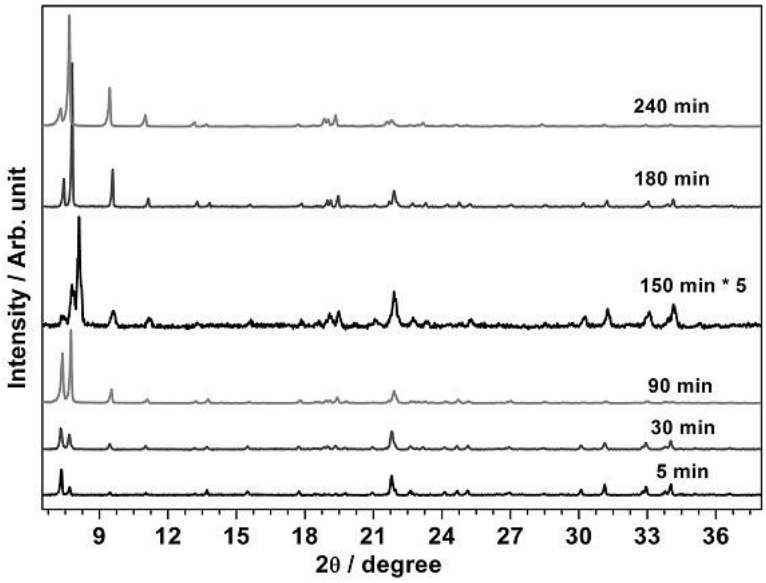

Figure 3.21: XRD patterns of Isobutanol adduct (Mg-*i*-BuOH) prepared by varying the set to reflux time.

At 5 min of set to reflux, the peak at 2θ = 7.4° shows high in intensity as compared to peak at 2θ = 7.8°. As the duration of set to reflux time increases, a noticeable increase in intensity of peak at 2θ ~ 9.5° is observed. Further, it is clear from the XRD data that the intensity ratio between peak at 2θ = 7.4 and 7.8 also increases with set to reflux time. This also support the conclusion made from the NMR studies that the alcohol molecules are initially coordinated to the Mg^{2+} through the easily accessible Z-axis sites and with increase in set to reflux time alcohol migrates to the sites available in the X-Y plane. The behaviour is seen up to 4 hrs of set to reflux and beyond that more alcohol molecules interact with $MgCl_2$, which is clearly visible in ^{13}C CP/MAS NMR.

3.6.6. Temperature Dependent XRD of Mg-*i*-BuOH

Non- ambient XRD experiment has been carried out under N_2 atmosphere in order to study the evolution of structural changes, while heating the sample from RT-200 ^oC and the results are shown in Figure 3.22. The data does not indicate any structural change in the system up to 70 ^oC though we have observed desorption of alcohol molecules by NMR even at 50 ^oC. At 90 ^oC, the characteristic peak of adduct disappear. At 90 ^oC and above, a peak at $2\theta = 15.5°$ start to evolve and shifts towards 15.1° indicating the presence of (003) feature of $MgCl_2$. Very similarly feature due to (006) plane of $MgCl_2$ evolves between 30 and 31°. These two features suggest the dealcoholation of the Mg-*i*-BuOH towards $MgCl_2$. Further the shift observed from higher angle to lower angle for (003) and (006) features indicate the association of $MgCl_2$ with increasingly lesser number of isobutanol molecules. Above feature due to $MgCl_2$ compares well with that of pure $MgCl_2$.

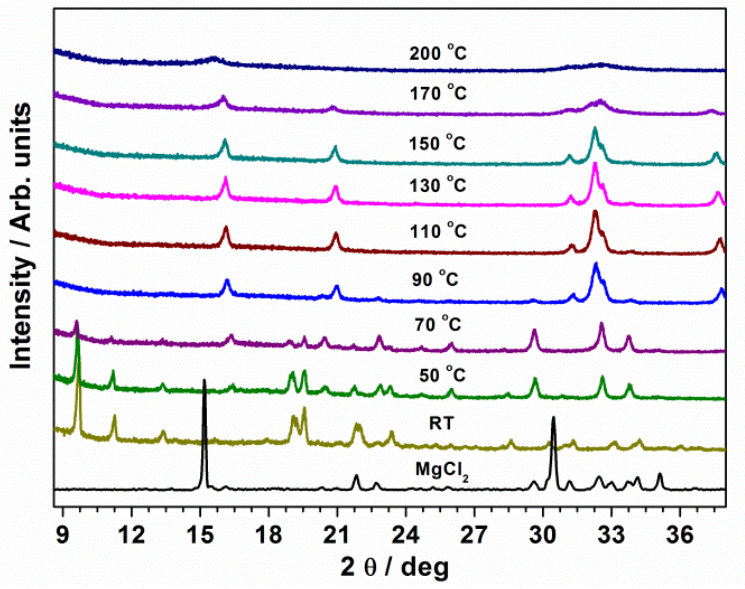

Figure 3.22: Non-Ambient temperature XRD patterns of Isobutanol adduct (Mg-*i*-BuOH) heating from RT to 200 ^oC.

3.6.7. Scanning Electron Microscopy

SEM images of isobutanol adduct prepared under different set to reflux times are shown in Figure 3.23.It is observed that perfect rod like shape formed gradually as the set to reflux time increases. At '5 min' set to reflux time, samples are in spherical shape. 30 minutes set to reflux results both spherical and fibre morphology. 3 hr set to reflux results molecular adduct with perfect rod shape. The growth of particles oriented in one particular direction and its start growing above 30 min of set to reflux. These rods are of few microns in length with a width of 8 μm.

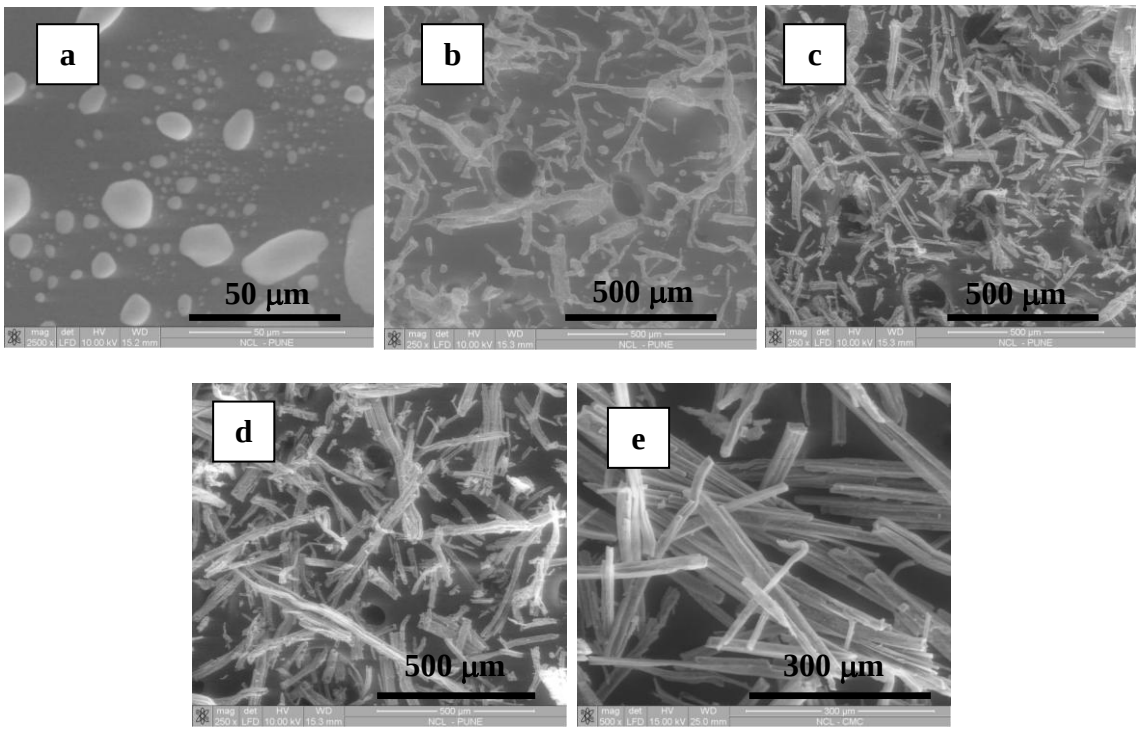

Figure 3.23: SEM images of isobutanol adduct, Mg-*i*-BuOH prepared under various set to reflux time of (a) 5 min, (b) 30 min, (c) 1 hr, (d) 2.5 hr, and (e) 3 hr.

3.7. Conclusions

A new Ziegler-Natta catalyst support material, $MgCl_2$.4(*i*-BuOH) has been synthesized and characterized thoroughly by solid-state NMR, XRD and SEM. Studies shows that, the system is sensitive to temperature and set to reflux time. Non- ambient XRD experiments reveals that system is stable up to 70 ^{o}C only after that characteristic feature of Mg-*i*-BuOH disappear indicating the structural disintegration. VT NMR experiments shows

that two phases are present in the system, one is kinetic and another one is thermodynamically stable. Due to the bulky nature of alcohol, kinetically stable (phase 1) adduct is forming at low set to reflux time and gets converted to thermodynamically stable phase 2. SLF experiments indicate that the outer methyl peaks are more rigid as compared to inner ones from the dipolar coupling values. SEM images of adducts prepared at different set to reflux time demonstrate the evolution of particle morphology from spherical to rod shape.

3.8. References

1. P.G. Barbe, G. Ceccin, L. Noristi, *Adv. Polym. Sci.* **8** (1981) 1.
2. E.P. Moore Jr., *Polypropylene Handbook: Polymerization, Hanser Publishers, New-York*, 1996.
3. E. Albizzati, G. Cecchin, J. C. Chadwick, G. Collina, U. Giannini, G. Morini, L. Noristi, L. Resconi, *In: Pasquini N (ed) Polypropylene handbook, (2nd edn. Carl Hanser Verlag), Munich*, (2005) Ch. 2.
4. U. Giannini, *Makromol. Chem. Suppl.* **5** (1981) 216.
5. J. S. Chung, J. H. Choi, I. K. Song, W.Y. Lee, *Macromol.* **28** (1995) 1717.
6. J. C. W. Chien, J.-C, Wu, C.-I. Kuo, *J. Polym. Sci. Polym. Chem. Ed.* **20** (1982) 2019.
7. D. N. T. Magalhaes, O. D. C. Filho, F. M. Coutinho, *Eur. Polym. J.* **27**(1991) 827.
8. R. N. Haward, A. N. Roper, K. L. Fletcher, *Polymer* **14** (1973) 365.
9. H. M. Park, W. Y. Lee, *Eur. Polym. J.* **28** (1992) 1417.
10. M. Vittadello, P. E. Stallworth, F. M. Alamgir, S. Suarez, S. Abbrent, C. M. Drain, V. D. Noto, S.G. Greenbaum, *Inorg. Chim. Acta.* **359** (2006) 2513.
11. G. Singh, S. Kaur, U. Makwana, R. B. Patankar, V. K. Gupta, *Macromol. Chem. Phys.* **210** (2009) 69.
12. E. Albizzati, U. Giannini, G. Collina, L. Noristi, L. Resconi, *In Polypropylene Handbook: Polymerization, Characterization, Properties, Applications;* Moore, E. P. Jr., (Ed. Hanser

Publishers) New York, 11 (1996).

13. P. Sozzani, S. Bracco, A. Comotti, Simonutti, R.; Camurati, I. *J. Am. Chem. Soc.* **125** (2003) 12881.
14. A. Andoni, J. C. Chadwick, S. Milani, J. W. H. Niemantsverdriet, P.C. Thüne, *J.Cata.* **247** (2007) 129.
15. K. S. Thushara, R. Mathew, T. G. Ajithkumar, P. R. Rajamohanan, S. Bhaduri, C. S. Gopinath, *J. Phys. Chem. C* **113** (2009) 8556.
16. E. S. Gnanakumar, K. S. Thushara, D. S. Bhange, R. Mathew, T. G. Ajithkumar, P. R. Rajamohanan, S. Bhaduri, C. S. Gopinath, *Dalton Trans.* **40** (2011) 10936.
17. V. D. Noto, S. Bresadola, R. Zannetti and M. Viviani, Z. *Kristallogr.* **204** (1993) 263.
18. Z. Ma, L. Wang, W. Wang, J. Wang, H. Yu, *Polym. Plast. Technol. Eng.* **44** (2005) 1475.
19. Z.-Y. Ye, L. Wang, L.-F. Feng, X.-P. Gu, H.-H. Chen, P.-Y. Zhang, J. Pan, S. Jiang, L.-X. Feng, *J. Polym. Sci., Part A: Polym. Chem.* **40** (2002) 3112.
20. M. C. Forte, F. M. B. Coutinho, *Eur. Polym. J.* **32** (1996) 223.
21. A. Parada, T. Rajmankina, J. Chirinos, *Polym. Bull.* **43** (1999) 231.
22. A. Parada, T. Rajmankina, J. J. Chirinos, A. Morillo, *Eur. Polym. J.* **38** (2002) 2093.
23. J. H. Choi, J. S. Chung, H. W. Shin, I. K. Song, W. Y. Lee, *Eur. Polym. J.* **32** (1996) 405.
24. V. K. Gupta, M. Ravindranathan, *Polymer*, **37** (1996) 1399.
25. H.-L. Rönkkö, H. Knuuttila, M. Linnolahti, M. Haukka, T. T. Pakkanen, P. Denifl, T.M. Leinonen, *Inorg. Chim. Acta*. **371** (2011) 124.
26. K. Seenivasan, A. Sommazzi, F. Bonino, S. Bordiga, E. Groppo, *Chem. Eur. J.* **117** (2011) 8648.
27. G. Valle, G. Baruzzi, G. Paganetto, G. Depaolit, R. Zannetti, A. Marigo, *Inorg. Chim. Acta*. **156** (1989) 157.
28. M. C. Forte, F. M. B. Coutinho, *Eur. Polym. J.* 32 (1996) 223. (b) F. Zaera, C. S.

Gopinath, *J. Mol. Catal. A* **167** (2001) 23.

29. J. C. J. Bart, W. Roovers, *J. Mater. Sci.* **30** (1995) 2809.
30. P. Sobota, *Coord. Chem. Rev.* **248** (2004) 1047.
31. D. N. T. Magalhase, O. D. C. Filho, F.M.B. Coutinho, *Eur. Polym. J.* **27** (1991) 827.
32. M. C. Forte, F. M. B. Coutinho, *Eur. Polym. J.* **32** (1996) 223.
33. R. Xu, D. Liu, S. Wang, N. Wang, B. Mao, *J. Mol. Catal. A* **263** (2007) 86.
34. K. S. Thushara, Edwin S. Gnanakumar, Renny Mathew, T. G. Ajithkumar, P. R. Rajamohanan, S. Bhaduri and C.S. Gopinath, *Dalton Trans.* **41** (2012) 11311.
35. C. R. Tewell, F. Malizia, J. W. Ager III; G. A. Somorjai, *J. Phys. Chem. B* **106** (2002) 2946.
36. Y. Jeong, D. Lee, *Makromol. Chem.* **191** (1990) 1487.
37. K. Balasubrahmanyam, *J. Chem. Phys.* **44** (1966) 3270.
38. F. R. Dollish, W. G. Fateley, F. Bentley, *Characteristic Raman Frequencies of Organic Compounds*; Wiley-Interscience: New York, (1974) p 443.
39. H.-L. Rönkkö, H. Knuuttila, P. Denifl, Leinonen, T.; Venäläinen, T. *J. Mol. Catal. A: Chem.* **278** (2007) 127.
40. P. Sobota, S. Szafert, *J. Chem. Soc. Dalton Trans.* **9** (2001) 1379.
41. K. S. Thushara, E. S. Gnanakumar, R. Mathew, R. K. Jha, T. G. Ajithkumar, P. R. Rajamohanan, K. Sarma, S. Padmanabhan, S. Bhaduri, C. S. Gopinath, *J. Phys. Chem. C.* **115** (2011) 1952.
42. L. Abis, E. Albizzati, U. Giannini, G. Giunchi, E. Santoro, L. Noristi, *Makromol. Chem.* **189** (1988) 595.
43. A. Andoni, J. C. Chadwick, H.J. W. Niemantsverdriet, P. C. Thüne, *Macromol. Rapid Commun.* **28** (2007) 1466.
44. S.H. Kim, G.A. Somorjai, *J. Phys. Chem. B* **106** (2002) 1386.

45. A.G. Potapov, G.D. Bukatov, V.A. Zakharov, *J. Mol. Catal. A: Chem.* **246** (2006) 248.

46. M. Terano, M. Saito, T. Kataoka, *Makromol, Chem., Rapid Commun.* **13** (1992) 103.

47. V. Di Noto, R. Zannetti, M. Viviani, C. Marega, A. Marigo, *Makromol. Chem.* **193** (1992)1653.

48. V. Di Noto, A. Marigo, M. Viviani, C. Marega, S. Bresadola, R. Zannetti, *Makromol. Chem.* **193** (1992) 123.

49. P. Sormunen, T. Hjertberg, E. Iiskola, *Makromol.Chem.* **191** (1990) 2663.

50. N. J. Clayden, S. Holmes, P. J. V. Jones, *J. Chem. Soc., Chem. Commun.* **19** (1988) 1289.

Chapter 4

4. Molecular adduct of $MgCl_2$ with Secondary and Tertiary Alcohols and Their Titanated catalyst: Structural, Spectroscopic and Catalytic activity study

4.1. Introduction

The polyolefin industries began in the 1950's, but the discovery of $MgCl_2$-supported $TiCl_x$ catalyst on 1968 brought about a breakthrough that led to a spectacular improvement in the productivity of the catalysts as well as polyolefin [1-9]. However, in spite of its enormous technological advancement, science of polyolefin making suffers from a serious drawback of poor molecular level understanding of the catalyst and support and their role in polymerisation [10-14]. Right support material with an excess of $TiCl_4$ can make it as *super active catalyst*. A common method of synthesizing the olefin polymerization catalysts involves the treatment of an alkanol adduct of $MgCl_2$ with an excess of $TiCl_4$, with or without an additive such as an ester [4-9]. The ethanol adducts, $MgCl_2$.xEtOH ($1 \leq x \leq 6$), have been studied significantly [15-16], but only $MgCl_2$.6EtOH (MgEtOH) has been characterized by single crystal X-ray crystallography. Recent studies with solid state NMR has shown the presence of mixed phases in materials formulated as $MgCl_2$.xEtOH (x = 1-3) [17] Thus isolation and unambiguous structural characterization of any alkanol adduct as a single phase solid with extended is an important problem that remains to be addressed. In order to explore any correlation that might exist between the activity of the titanated Z-N catalyst supported on $MgCl_2$ derived from molecular adducts with different size and nature of alcohol in the molecular adducts; we chose three different alcohols as Lewis base for the current study. Among these three different alcohols, one is branched three carbon secondary alcohol (isopropanol); second one is a linear secondary alcohol (2-butanol) and third is a branched tertiary alcohol (tert-butanol). An important point should be mentioned here is that, the Lewis

bases used for the molecular adduct formation does not directly participate in the final catalytic activity. These alcohols were washed away during the catalyst preparation. Catalytic activity of the $MgCl_2$ supported Z-N catalyst derived from isopropanol, 2-butanol and tertiary butanol adduct shows better activity than Z-N catalyst supported on MgEtOH. These molecular adduct shows significant changes in structural, textural and morphological properties. Indeed different alcohols in the molecular adduct leads to different textural properties and this influences the incorporation of $TiCl_x$ in the $MgCl_2$ lattice in different ways.

The main objectives of the current studies are the following: (i) to understand the molecular level property of the above mentioned molecular adduct and corresponding Z-N catalyst, (ii) to study how the property of adduct vary by changing alcohols from isopropanol to 2-butanol to tertiary butanol, (iii) effect of support in the structure and property of the Z-N catalyst in determining the activity in olefin polymerization. An emphasis is given to explore the fundamental difference in the molecular property of the adduct system by changing the nature of alcohols.

4.2. Characterization of Molecular adducts (MgiPrOH, Mg2-BuOH and MgtBuOH)

4.2.1. Powder X-ray Diffraction

Figure 4.1 shows the XRD patterns of anhydrous $MgCl_2$, MgiPrOH, Mg2-BuOH and MgtBuOH. $MgCl_2$ exhibits a cubic close packing structure which gives a strong XRD peaks at 2θ = 15.1° (003), 35° (004) and 50.4° (110) [15, 18]. Molecular adduct is formed via interaction between Mg^{2+} and alcoholic oxygen. As a result, insertion of alcohol in between the Cl-Mg-Cl triple layers leads to an increase in the interplanar distance (or decrease in 2θ value) for all molecular adduct compared to $MgCl_2$. High intensity 001 reflections below 10° characterize the molecular adducts formation due to easy alcohol interaction on the z-axis of

layered structure, in addition to x/y axis, of rhombohedral $MgCl_2$. All the molecular adduct exhibits a high intense diffraction feature at $2\theta < 10°$.

XRD pattern of MgiPrOH adduct shows a characteristic low angle peak at 9.95°, and it is attributed to 001 reflection. High intensity (001) reflections <10° characterize the molecular adducts formation due to easy alcohol interaction along the *z*-axis of layered structure of rhombohedral $MgCl_2$. Characteristic changes in d-values of (001) plane of $MgCl_2$ with the adducts supports the above conclusion.

Intense peak at 8.9° for Mg2-BuOH indicate the formation of molecular adduct with oriented crystallites along (00z) direction. Increase in the d-spacing due to insertion of 2-butanol indicating the removal of Cl-Mg-Cl triple layered structure.

MgtBuOH shows a high intense peak at $2\theta = 9°$ which is similar to 2θ of MgEtOH. The solubility of $MgCl_2$ in tertiary butanol is very low, in order to make a homogeneous solution, a few drops of methanol was added. The number of coordinating alcohol to the Mg^{2+} site reduced from ethanol to tertiary butanol due to steric hindrance factor. It is to be noted that $MgCl_2$.nROH molecular adduct is a prerequisite to introduce $TiCl_x$ in the $MgCl_2$ lattice support. All alcohol molecules are removed from at the introduction of $TiCl_x$ into molecular adducts, to prepare $TiCl_x$/ $MgCl_2$ catalyst. Presence of secondary or tertiary alcohol with different chain length exerts different influence on the incorporation of $TiCl_x$ on $MgCl_2$. Indeed this leads to different catalytic activity and it depends on the nature of molecular precursor.

Peaks at $2\theta > 20^o$ in the XRD of adducts show similar behaviour as that of anhydrous $MgCl_2$. In the case of MgiPrOH, the powder samples are free flowing in nature. Molecular adduct with 2-butanol shows entirely different morphology, needle shape which is visible to naked eyes (shown in inset of Figure 4.1). Even though 2-butanol belongs to secondary alcoholic group and a four carbon chain alcohol, '2θ' value for ethanol and 2-butanol adducts

are similar. In addition to XRD, Raman analysis also carried out to confirm the molecular adduct formation. Low intensity peak at 712 cm^{-1} in Raman spectra exhibits the characteristic Mg-O vibration mode for molecular adduct.

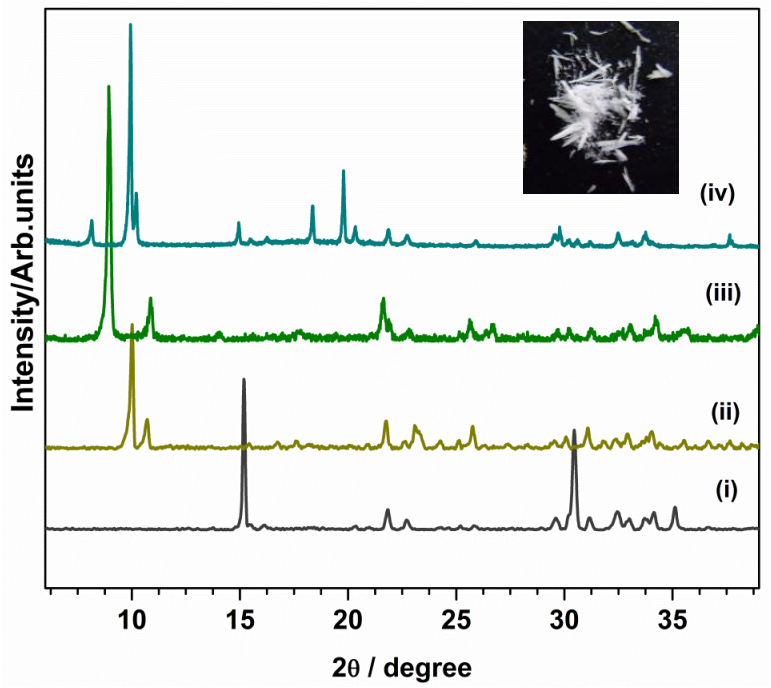

Figure 4.1: XRD patterns (i) anhydrous $MgCl_2$ (ii) MgiPrOH (iii) Mg2-BuOH and (iv) MgtBuOH (Inset shows the photograph Mg2-BuOH molecular adduct with one-dimensional needle or rod shape).

4.2.2. Thermal Analysis

Figure 4.2 shows the results from TG-DTA analysis of MgiPrOH, Mg2-BuOH and MgtBuOH adducts. The sample temperature was ramped from ambient to 300 °C at 10 °C/min under the flow of UHP nitrogen (99.999 %) at 40 ml/min. The well-defined weight loss and sharp DTA peaks indicates a systematic dissociation of isopropanol (iPrOH) molecules from adduct one by one. First iPrOH molecule dissociates at 77 °C (weight loss from 100 to 82 %) followed by another at 100 °C (weight loss from 82 to 64%). As the boiling point of iPrOH is 82 °C, it is clear that the association of above two iPrOH molecules to $MgCl_2$ is weak. However, broader transitions >100 °C indicates a relatively strong binding

character of iPrOH in adduct with possibly some molecular reorganisation. iPrOH/$MgCl_2$ ratio was identified to be 4 from the weight loss of MgiPrOH adduct due to loss of iPrOH molecules (~72%). No weight loss was observed above 245 °C, and it is reasonable to assume that only $MgCl_2$ remains >245 °C. The thermal analysis data indicates that the iPrOH molecules that dissociate <100 °C are weakly bound to the $MgCl_2$ lattice compared to the other two molecules that dissociates > 100 °C [19].

Thermal analysis data of Mg2-BuOH shows that dissociation of 2-butanol molecules starts gradually from 35 ^{o}C and above. First two 2-butanol molecules dissociates quickly from the system. Dissociation of 2-butanol at T < 100 ^{o}C indicates a relatively weak binding character of Mg^{2+} with 2-BuOH in adduct. It is to be noted the boiling point of 2-BuOH is 100 °C and dissociation of 2-BuOH from adduct < 100 °C underscores the weak binding. TG data reveals that there is a sharp decrease in the weight loss around 100 °C (~ 50 %). The weight % calculation shows that, 55% weight loss corresponds to the dissociation of three 2-butanol moiety which is coordinating weakly to the Mg^{2+} site. Remaining alcohol dissociates slowly between 150 and 220 ^{o}C respectively. The 2-BuOH/$MgCl_2$ ratio was found to be four which is further supported by liquid NMR spectral results (4 x 74 g/mol of 2-BuOH with $MgCl_2$ with (M.W = 95 g/mol)) [20].

The loss of tertiary butanol from MgtBuOH starts from 50 °C onwards in the thermal analysis. Liquid NMR results shows that the number of alcohol coordinating is less compared to other alcoholic adduct which is further supported by TG-DTA analysis. From the weight loss, the tBuOH/$MgCl_2$ ratio was found to be two. However, four distinct DTA features accompanied with weight loss features suggesting a continuous reorganisation of adduct, likely to form new structures. Temperature dependent NMR studies are suggested to understand the dynamic behaviour.

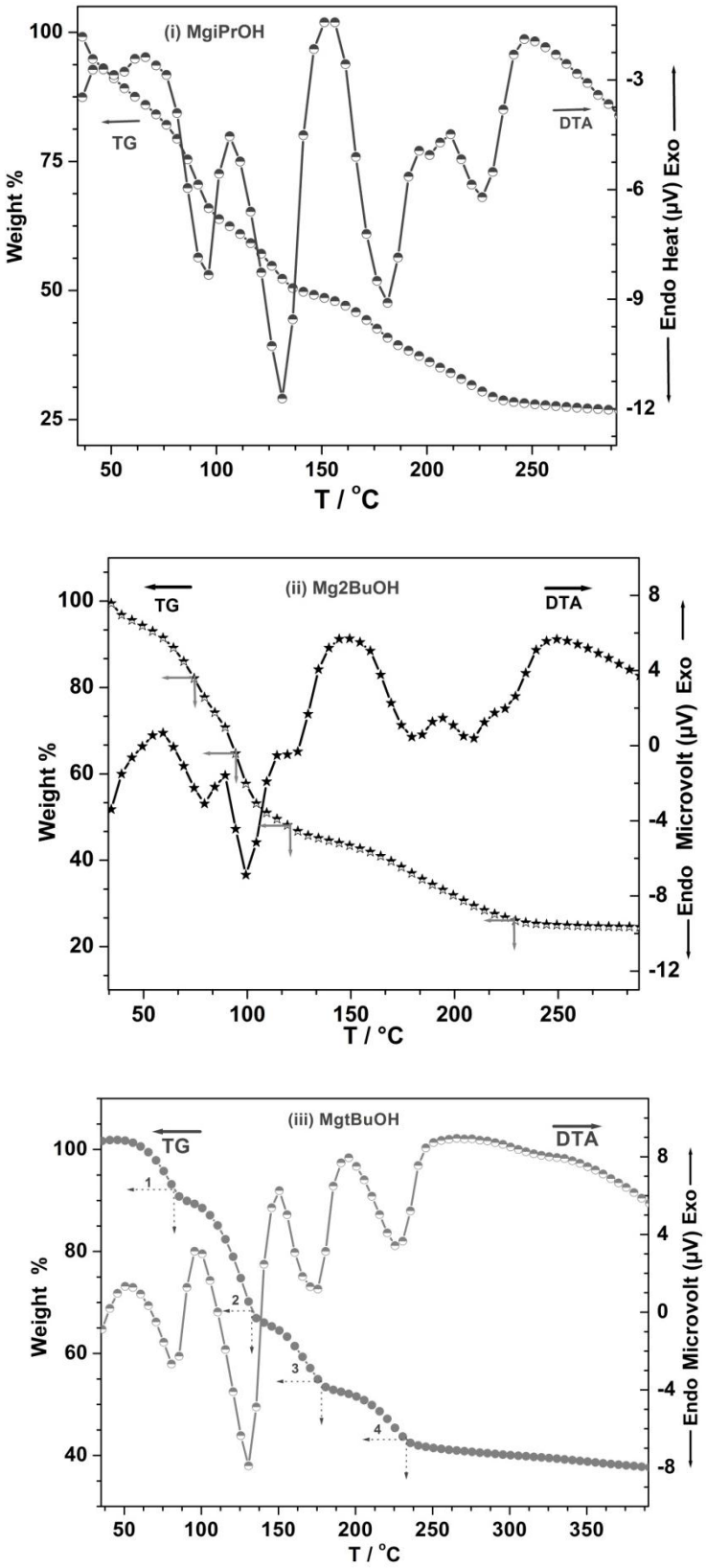

Figure 4.2: TG-DTA analysis of molecular adducts (i) MgiPrOH (ii) Mg2-BuOH and (ii) MgtBuOH.

4.2.3. NMR Spectroscopy

4.2.3.1. Liquid NMR Spectroscopy

NMR spectral measurement was carried out to find the composition of MgiPrOH, Mg2-BuOH and MgtBuOH adduct according to the procedure published by Sozzani et. al [21] Weighed amount of adduct was dissolved in 1 ml of D_2O. Small and known amount of THF is added as a reference compound. ^1H NMR spectra was recorded and the mole fraction of alcohol is estimated from the ^1H integrals and used for the calculation of stoichiometry of iPrOH, 2-BuOH and tBuOH in MgiPrOH, Mg2-BuOH and MgtBuOH adduct, respectively. ROH/$MgCl_2$ molar ratio is found to be 3.8, 3.9 and 1.9 which is in very good agreement with TG-DTA results supporting the adduct compositions are $MgCl_2$. 4(i-PrOH), $MgCl_2$.4 (2-BuOH) and $MgCl_2$. 2(tBuOH), respectively.

4.2.3.2. Solid- State NMR Spectroscopy

When Lewis base is varied from linear to branched, a different mode of interaction of alcohol to the Mg^{2+} site is noticed. ^{13}C CP/MAS spectrum of the MgiPrOH adduct (Figure 4.3) shows four equally intense methyl and two methine signals around 24-27 and 65-67 ppm, respectively. In an octahedral environment around the Mg^{2+} ion, where two out of six coordination sites are occupied by Cl^-, only a *cis*- arrangement of the two Cl^-can give two magnetically inequivalent methine and four magnetically non-equivalent methyl carbons (Figure 4.4).

To prove unequivocally that both sets of isopropyl signals have their origin in an adduct having a single phase; ^{13}C 2D exchange NMR experiments [22] have been carried out. The ^{13}C 2D exchange spectra of MgiPrOH adduct have been measured at two different mixing times (2 and 200 ms) are given in Figure 4.5. At 2 ms mixing time, cross peaks are seen only between the methyl groups belonging to the same molecule, which are probably undergoing slow rotation around the C-C bond. Longer mixing time showed cross peak

between the two methine carbons and also between the methyl pairs. These weak 'inter-units' cross peaks obtained unequivocally confirms that the ^{13}C signals of adduct is exclusively from a single entity or from a single phase. The NMR results are thus consistent with TG analysis, which suggests a composition of the $MgCl_2$ adduct with four iPrOH molecules.

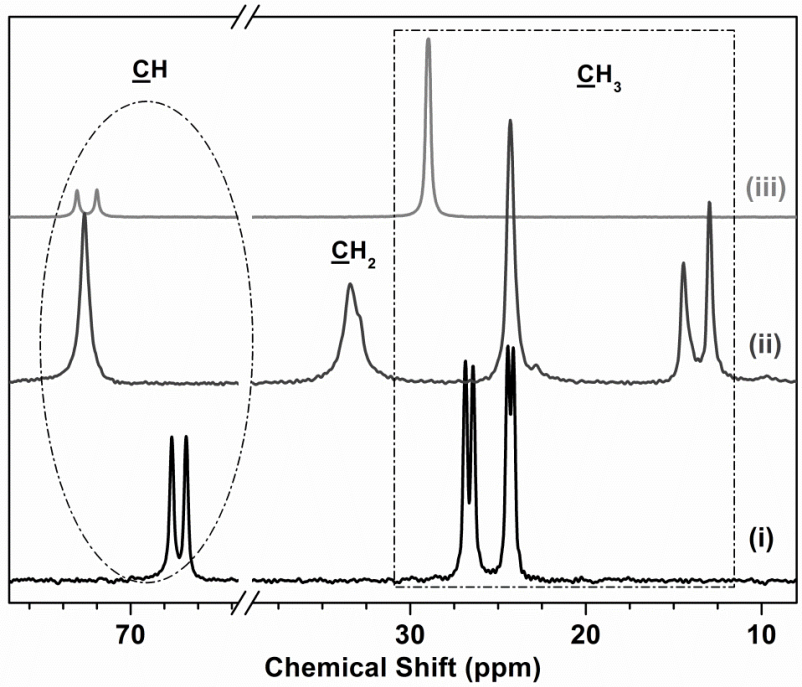

Figure 4.3: ^{13}C CP/MAS NMR spectra of (i) MgiPrOH (ii) Mg2-BuOH and (iii) MgtBuOH.

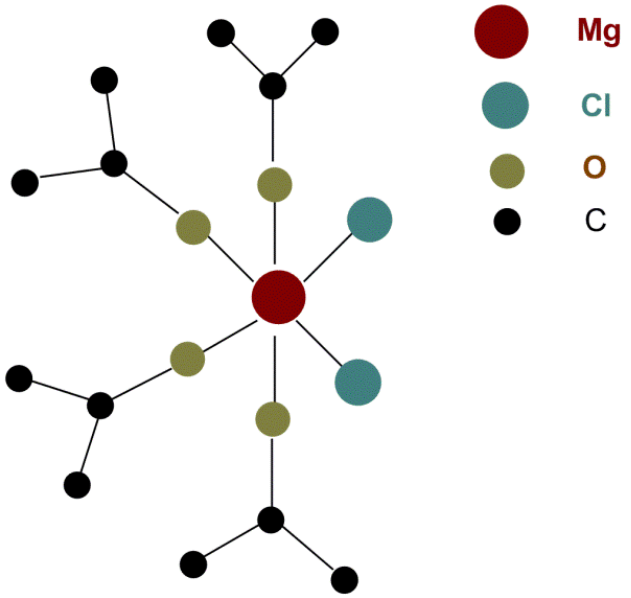

Figure 4.4: Schematic representation of cis-arrangement of MgiPrOH.

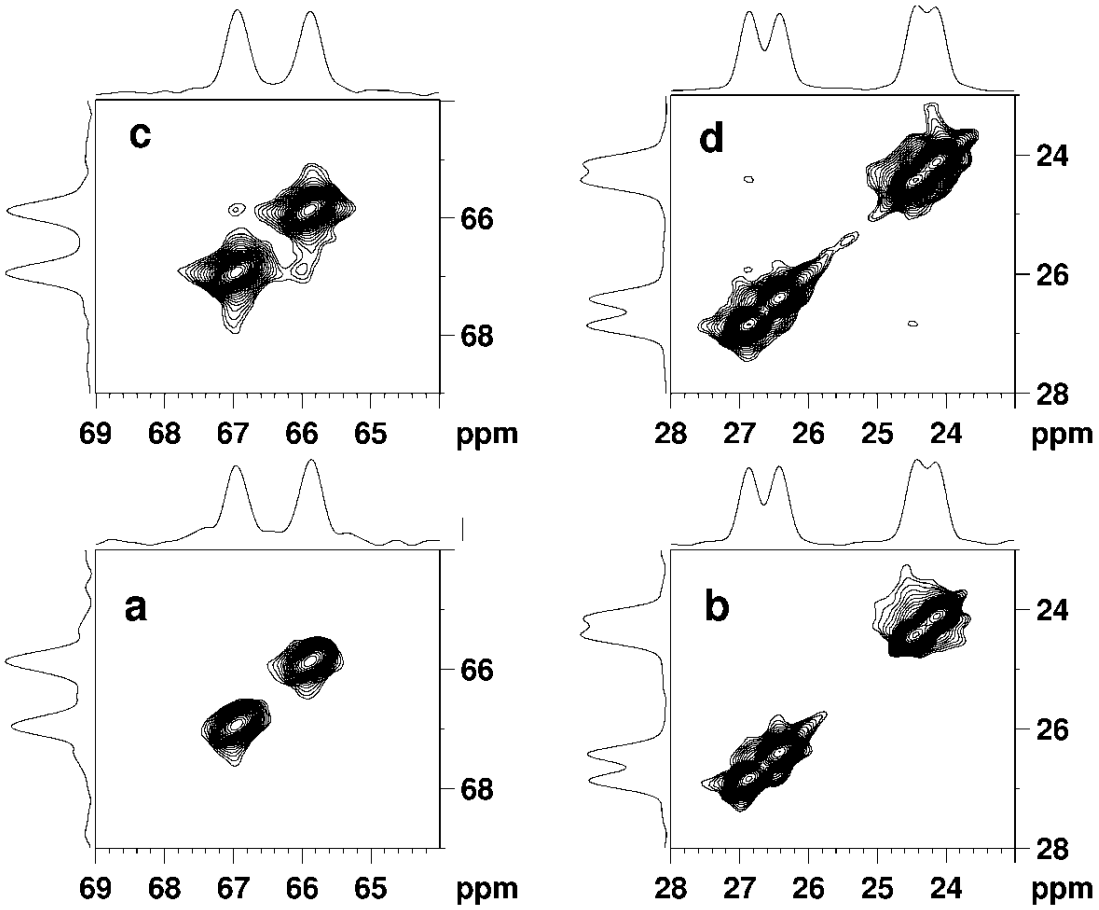

Figure 4.5: 2D exchange NMR contours of MgiPrOH with mixing time of 2 ms (a and b), and 200 ms (c and d).

Further support comes from the intensity ratios of the CH and CH_3 carbons of a fully relaxed DD MAS spectrum that clearly shows that the four methyl signals belong to two isopropyl moieties (Figure 4.6). The in-equivalence of the methyl groups of an isopropyl group points to a motional restriction of the alcohol molecules on coordination to Mg^{2+}. This is also confirmed from the large broadness of the ^1H MAS spectrum even at a spinning speed of 33 kHz, unlike the ^1H MAS spectrum of the MgEtOH, which shows well resolved ^1H peaks at 8 kHz. The extent of in-equivalence seen, as indicated by the chemical shift separation of the high and low field methyl doublets (Figure 4.7), are also found to be different, the latter being more [19].

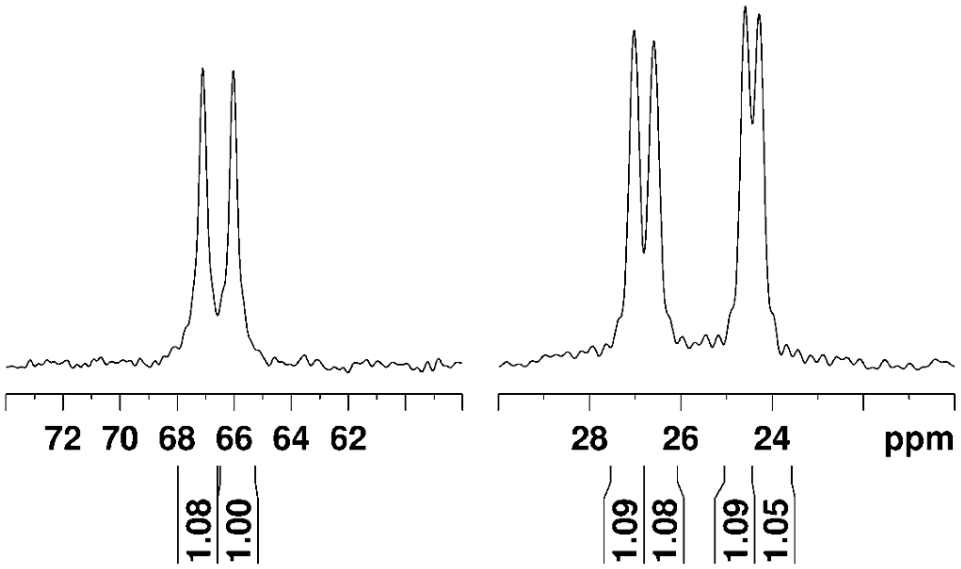

Figure 4.6: Intensity ratios of the CH and CH_3 carbons estimated from a fully relaxed (60 s delay) DD MAS spectrum of MgiPrOH adduct.

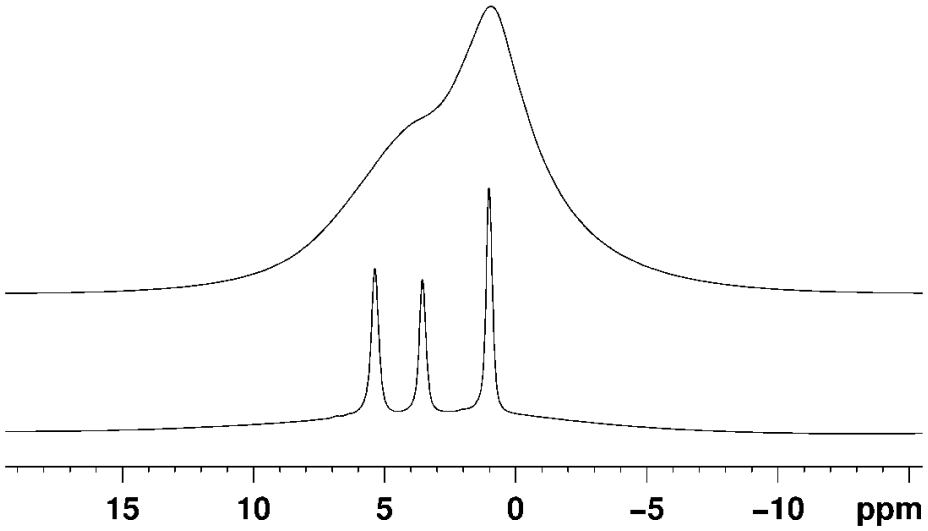

Figure 4.7: ^{1}H MAS spectrum obtained from MgEtOH adduct (lower trace at 8 kHz) which shows well resolved peaks compared to MgiPrOH adduct (upper trace at 30 kHz).

Analysis of ^{13}C CP/MAS spectra of Mg2-BuOH adduct is shown in Figure 4.3. Spectra of Mg2-BuOH show five signals; CHOH peak appears at 69.7 ppm, CH_2 carbon peak at 29.6 ppm. Out of two methyl groups, methyl group attached directly to carbon atom bearing hydroxyl group shows a chemical shift value of 20.6 ppm. The second methyl group which is three bonds away from hydroxyl group shows two signals appearing at 10.6 and 9.2

ppm. The single pulse MAS (HPDEC) spectrum of this adduct, collected with sufficient relaxation delay, showed that these two methyl signals possess same area and the chemical shifts are different from that of any non-coordinated (free) 2-butanol molecules (Figure 4.8). The combined area observed for these signals is equal to the areas observed for each of the other three carbon signals. Considering four 2-BuOH molecules in the molecular adduct, each of the two methyl signals at 10.6 and 9.2 ppm in 2-butanol molecules of Mg2-BuOH can be attributed to two different sets of 2-butanol molecules. It is interesting to note that, unlike the case of MgiPrOH, the non-equivalent nature is manifested mainly for the carbon located farthest from the OH group, the site of coordination. Two of the methyl groups in adduct are likely to be close to the stack of Cl–Mg–Cl triple layer along the crystallographic direction. Hence, as in the case of MgiPrOH, two types of 2-butanol molecules can be envisaged for Mg2-BuOH also. The broadness of other carbon signals compared to MgiPrOH (Figure 4.3), suggest that the chemical shift difference is not sufficient enough to be resolved at the magnetic field used for the measurement. The observation of two types of 2-butanol molecules in Mg2-BuOH is also in agreement with the XRD data.

Two types of carbon peaks are observed for MgtBuOH adduct in ^{13}C CP/MAS spectra (Figure 4.3). Peak at 28.9 ppm corresponds to the methyl carbon, 72.5 and 73.9 ppm for tertiary carbon atom. The doublet peaks at higher chemical shift indicate the presence of two magnetically in equivalent sites. Liquid NMR and TG/DTA analysis support this conclusion.

4.2.4. Raman Analysis

Figure 4.9 shows the Raman spectra of (i) MgiPrOH, (ii) Mg2-BuOH and (iii) MgtBuOH. Raman spectra of $MgCl_2$ show a high intense peak at 243 cm^{-1} which has been assigned to the A_{1g} breathing mode of the $MgCl_6$ octahedra in the lattice [24]. After the adduct formation with alcohols, characteristic peak for the $MgCl_2$ disappears and a new peak formed at ~ 710 cm^{-1}, and underscores the formation of the Mg-O bond between Mg and

alcoholic oxygen [19, 20].

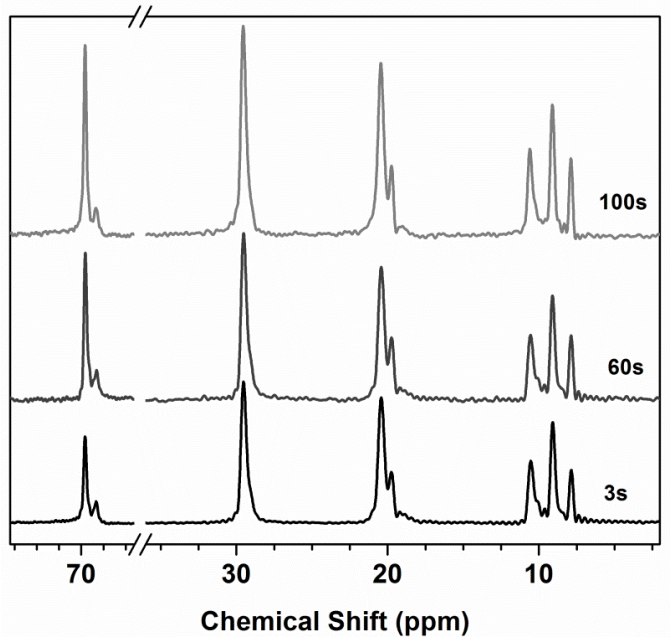

Figure 4.8: HPDEC spectra of Mg2-BuOH at different relaxation delay (d1) = 3 s, 60 s and 100 s.

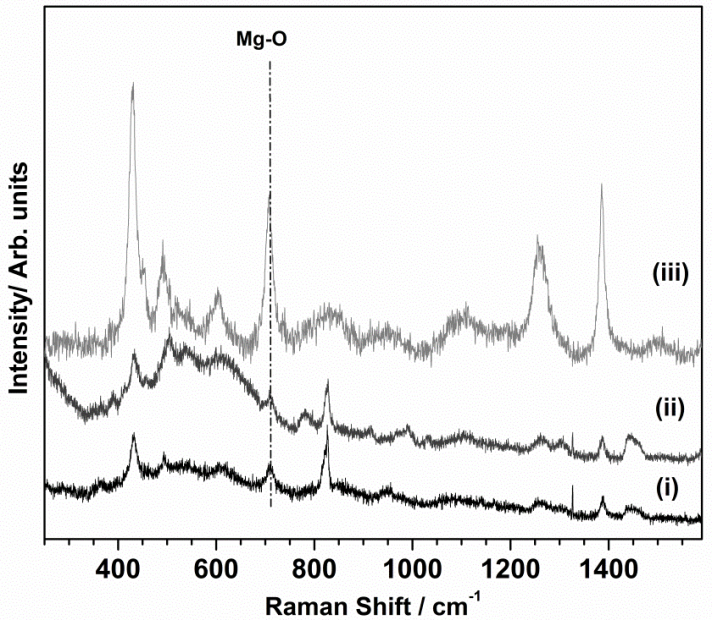

Figure 4.9: Raman spectra of (i) MgiPrOH, (ii) Mg2-BuOH and (iii) MgtBuOH.

For MgiPrOH, Mg2-BuOH system, the Mg-O bond observed at 712 cm^{-1}, but for MgtBuOH adducts, peak observed at little lower wavenumber, 708 cm^{-1}. The decrease in the Raman shift for MgtBuOH gives an idea about the weak electronic interaction between Mg^{2+}

and tertiary butanol. As compared to other alcoholic adduct, the number of tertiary butanol coordinated to $MgCl_2$ is two.

4.2.5. Scanning Electron Microscopy (SEM)

To understand the morphology of MgiPrOH, Mg2-BuOH and MgtBuOH adduct, SEM images at various magnifications were taken (Fig.4.10). MgiPrOH also shows spherical morphology with a diameter of 20-30 μm. Molecular adduct formation of $MgCl_2$ with isomeric forms of n-butanol, such as 2-butanol, isobutanol and tertiary butanol prepared via azeotropic distillation shows rod shape morphology in SEM analysis. As compared to isobutanol adduct, 2-butanol adduct shows porous nature. SEM measurements of 2-BuOH adduct at lower magnification (250 x, Figure 4.10(b)), revealed a fiber morphology with 300-600 μm in diameter. System morphology is homogeneous in the entire scanning area. A bundle of fibers are held together in any rod is clear from the images. Further, SEM measurements at higher magnification (2500 x, Fig. 4.10 (c)) revealed highly porous nature of the adduct material.

SEM images of MgtBuOH at two different magnifications were shown in Figure 4.10 (d and e). Lower magnification (500 x) images exhibits network of fibers. At higher magnification of 10000 x, each bundle is made of small nano particles and each particles shows more or less same morphology with a close packed arrangement.

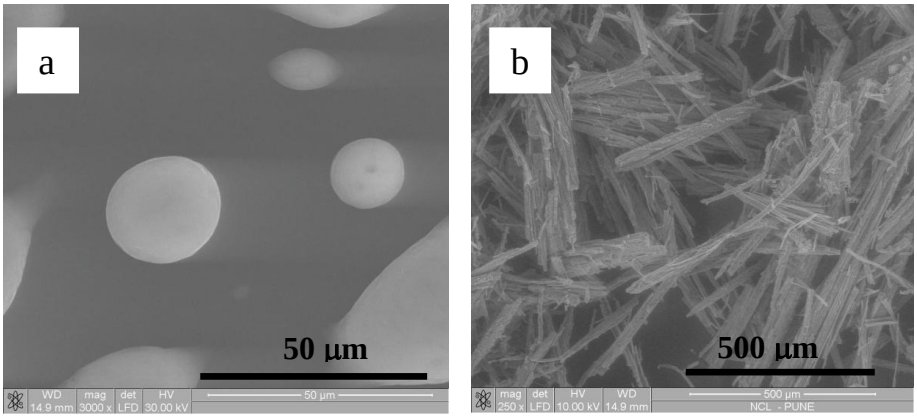

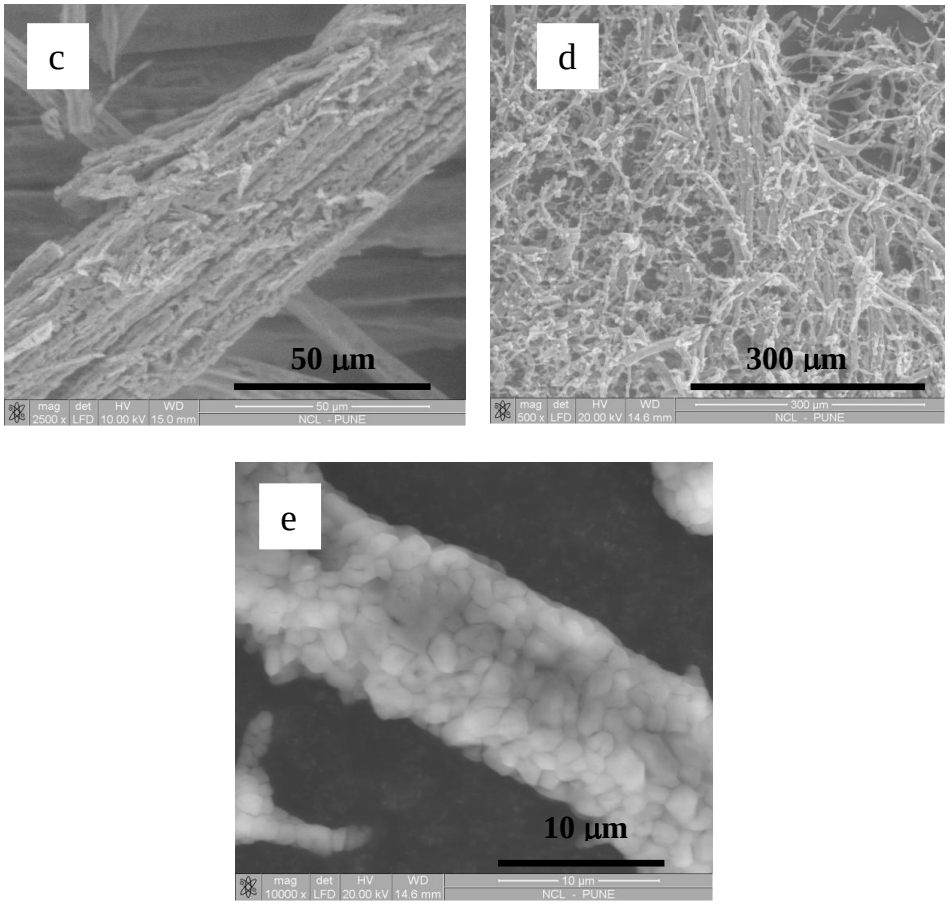

Figure 4.10: SEM images of (a) MgiPrOH (b) and (c) Mg2-BuOH and (d) and (e) MgtBuOH adduct.

4.3. Characterization of Titanated Catalyst

4.3.1. Powder X-ray diffraction

Figure 4.11 shows XRD pattern recorded for Ti/MgiPrOH, Ti/Mg2-BuOH and Ti/MgtBuOH. Broad peaks indicate the short range ordered nature of the material. From XRD pattern it is clear that characteristic features of above mentioned alcoholic adduct (Fig 4.1) disappears during the preparation of active catalyst with $TiCl_4$.

A broad halo peak is observed for Ti/MgiPrOH at 2θ = 15-22°. Z-N catalyst derived using 2-Butanol shows broad peak with 2θ = 13 – 22^o indicate the formation of more disordered $MgCl_2$ (δ-form) than α and β-$MgCl_2$. The broad peak is related to the stacking of Cl–Mg–Cl triple layers along the crystallographic direction. Activity of the catalyst is

increased due to the formation of δ-$MgCl_2$ even though the % of titanium is high. After reaction with $TiCl_4$, the crystalline nature of the material got reduced or it becomes more amorphous which results a broad peak in XRD. The same trend is observed for Ti/MgtBuOH catalyst also. The extent of active form of $MgCl_2$ varies with alcohols that will determine the final activity of the catalyst.

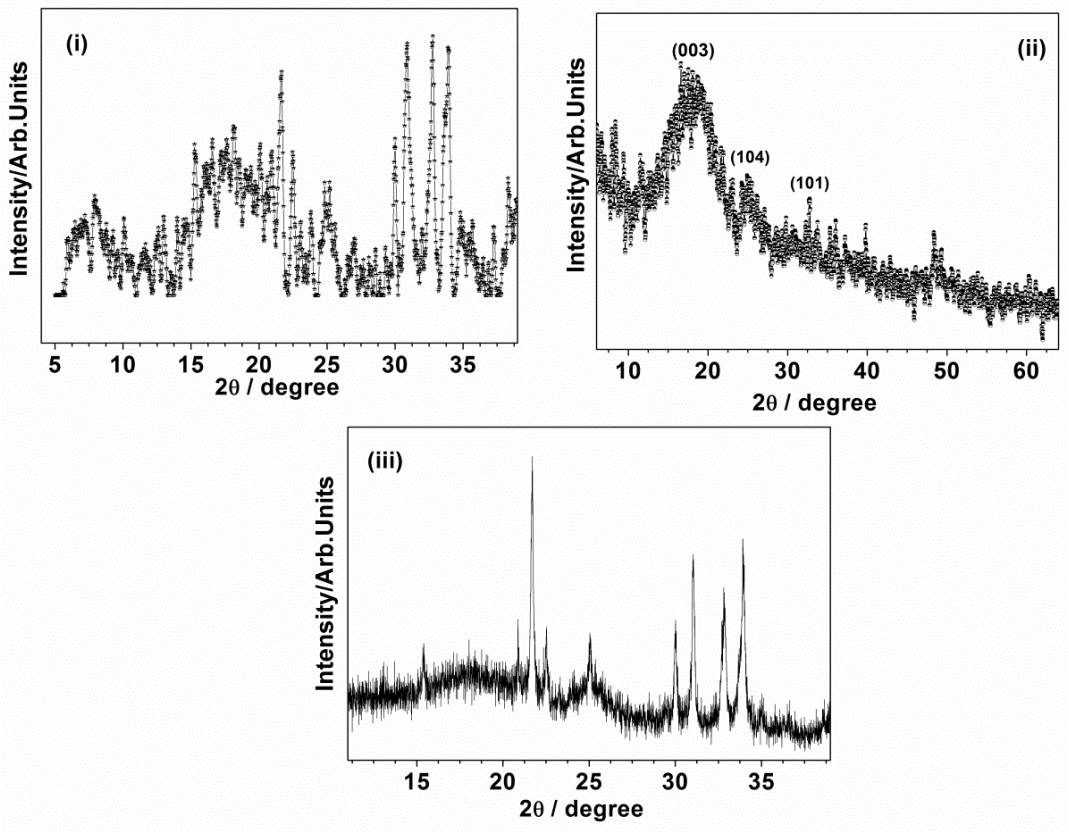

Figure 4.11: XRD patterns of Titanated catalyst (i) Ti/MgiPrOH (ii) Ti/Mg2-BuOH and (iii) Ti/MgtBuOH.

4.3.2. Thermal Analysis

Thermal analysis of titanated catalysts, Ti/MgiPrOH, Ti/Mg2-BuOH and Ti/MgtBuOH shows weight loss, and in particular DTA shows profound changes (Figure 4.12). As compared to the alcoholic adduct, titanated catalyst shows significant difference in the TG/DTA results. Analysis of thermal peak indicates that there is no significant weight loss below 100 °C indicating no loss of any species from the above mentioned titanated

catalysts. The weight loss associated with the Z-N catalyst at >100 °C might be due to the desorption of chlorobenzene (b.p.131 °C) which has been used as the solvent in the titanation step. Some amount of hexane also gets adsorbed on the pore walls and it's not desorbed at its boiling point indicates the strong interaction with the catalyst system. This result is supported further by NMR of the Z-N catalysts.

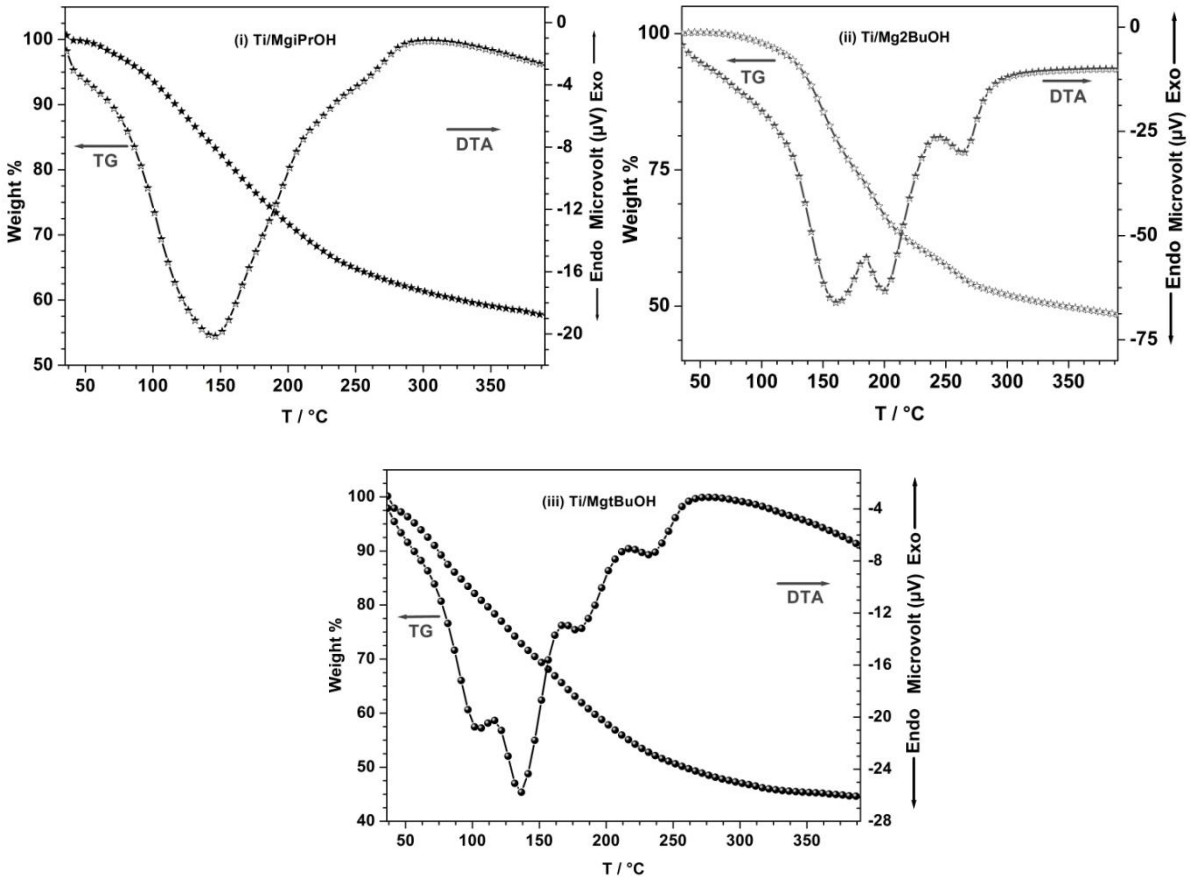

Figure 4.12: TG-DTA analysis of Titanated catalyst, (i) Ti/Mg2-BuOH and (ii) Ti/MgiPrOH and (iii) Ti/MgtBuOH.

4.3.3. Solid- state NMR

^{1}H MAS NMR spectra of titanated Z-N catalysts are shown in Figure 4.13 and it shows two peaks with a chemical shift value at 8 and 2 ppm corresponds to chlorobenzene and hexane respectively. These solvents were used during the catalyst preparation and for final washing purpose. Due to the porous nature of the catalyst, significant amount of solvents get trapped inside the pores and remained there. This is further supported by TG-

DTA analysis of Z-N catalyst.

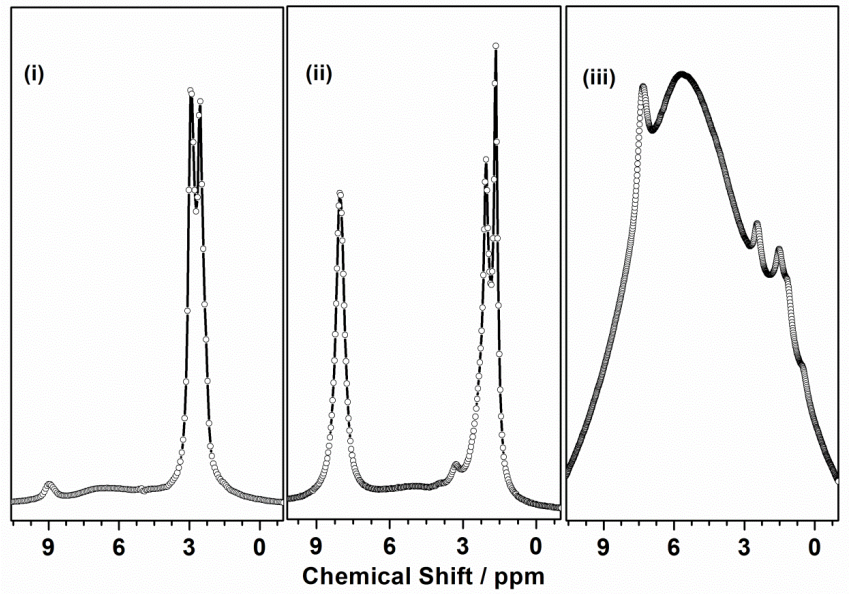

Figure 4.13: ^{1}H MAS NMR spectra of (i) Ti/MgiPrOH (ii) Ti/Mg2-BuOH and (iii) Ti/MgtBuOH.

^{13}C CP/MAS NMR of Ti/Mg2-BuOH is shown in Figure 4.14. In the case of Ti/MgiPrOH and Ti/MgtBuOH, there is no carbon peak observed in the ^{13}C CP/MAS NMR spectra. This indicates that the solvents trapped inside the pores are physically adsorbed on the surface of the catalyst. There is no peak observed that corresponds to alcohol molecules indicates that all alcohols are washed away during the catalyst preparation.

The peaks shown in ^{13}C CP/MAS of Ti/Mg2-BuOH arise from the solvent trapped inside the pores of the catalyst. Chemical shift value of 130 ppm is due to the presence of chlorobenzene which is used during the catalyst preparation. There is a broad halo peak centered at 30 ppm is likely due to hexane molecules present in the pores of Z-N catalyst. The trapped hexane and chlorobenzene is coordinated with the catalyst and the weight loss pattern observed in TG/DTA of Ti/Mg2-BuOH at T = 120-300 ^{o}C, indicates the above trapped molecules are likely to be present in the catalyst under reactions conditions. Z-N catalyst supported on $MgCl_2$ derived from ethanol adduct also contains trapped solvents but ^{13}C NMR

spectra of Ti/MgtBuOH didn't show any impurities.

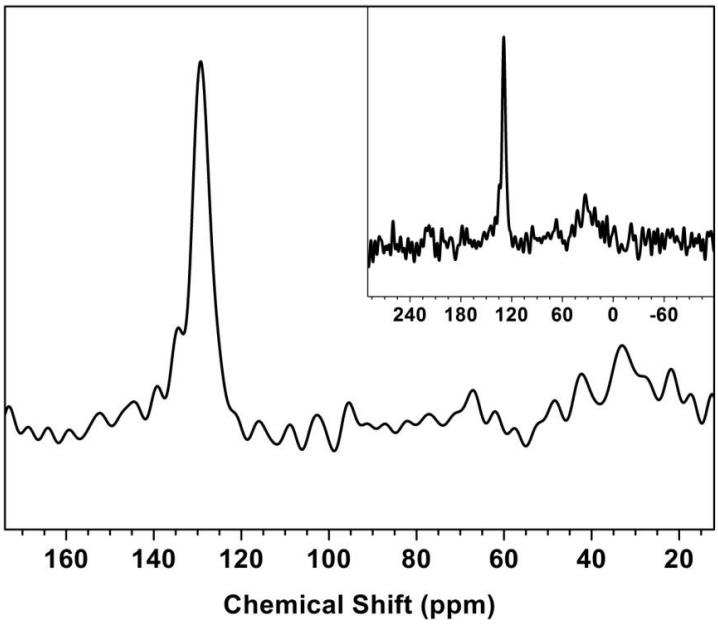

Figure 4.14: ^{13}C CP/MAS NMR of Ti/Mg2-BuOH catalyst (Full spectra shown in inset).

4.3.4. Scanning Electron Microscopy (SEM)

Figure 4.15 shows the SEM images of the Ti/MgiPrOH, Ti/Mg2-BuOH and Ti/Mg2-BuOH. Active Z-N catalyst derived from 2-butanol adduct shows spherical morphology with fibrous network. At higher magnification (6000x), SEM image reveals that spherical particle is made up of fibers. Size of the Z-N catalyst particle is ~ 50 μm. In general, polymer replicates the morphology of the Z-N catalyst. In the case of Mg2-BuOH derived catalyst, virgin adduct shows fibre/rod morphology but the catalyst shows fibrous nature within spherical particles. SEM images of resulting polyethylene obtained from Ti/Mg2-BuOH exhibits spherical morphology with a diameter of 5 μm (Fig. 4.16). PE obtained from Ti/MgiPrOH and Ti/MgtBuOH show irregular shape.

In SEM analysis, Ti/MgiPrOH catalysts didn't show any specific morphology. One part of the scanned area of Ti/MgiPrOH (fig. 4.15 b) exhibits a heterogeneous combination of rod and spongy spherical shape. In some areas, a bundle of fibres are observed and on its surface spongy type structure are forming. In the case of Ti/MgtBuOH, catalyst replicates

the morphology of the adduct material. Catalyst exhibits rod shape morphology with 10-20μm in length.

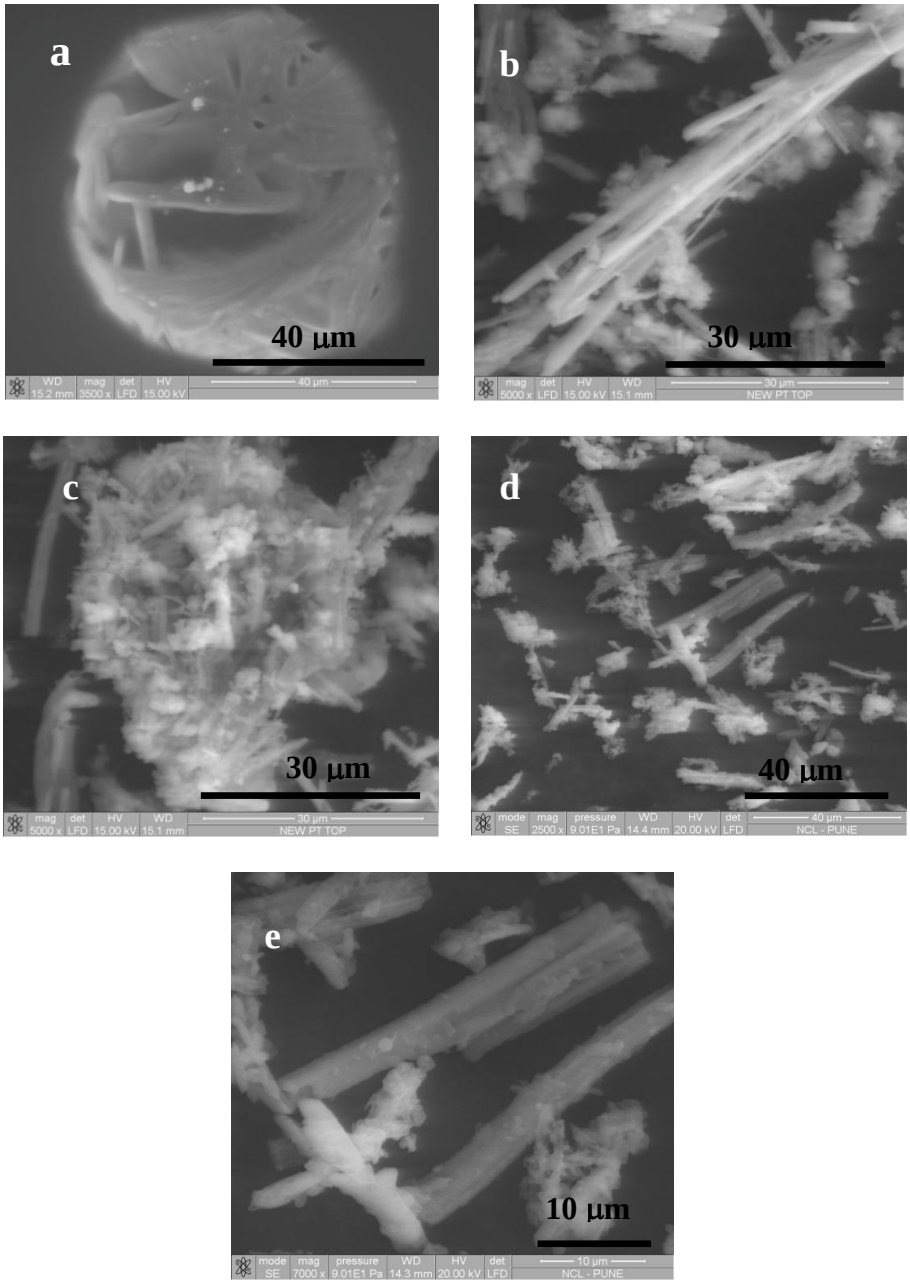

Figure 4.15: SEM images of Titanated catalyst (a) Ti/Mg2-BuOH (b and c) Ti/MgiPrOH and (d) and (e) Ti/MgtBuOH.

4.3.5. Textural Properties

Adsorption isotherm and pore size distribution of titanated catalyst shown in Figures 4.17 and 4.18. A type II adsorption isotherm was observed for Ti/MgiPrOH and

Ti/Mg2-BuOH. There is no saturation occurs even at high P/P_0 indicating the presence of macrospores. Pore size distribution analysis of Ti/Mg2-BuOH shows bimodal pore size distribution of 15 and 40 Å respectively. Pore size distribution of Ti/MgiPrOH shows a wide range from 40 to 70 Å.

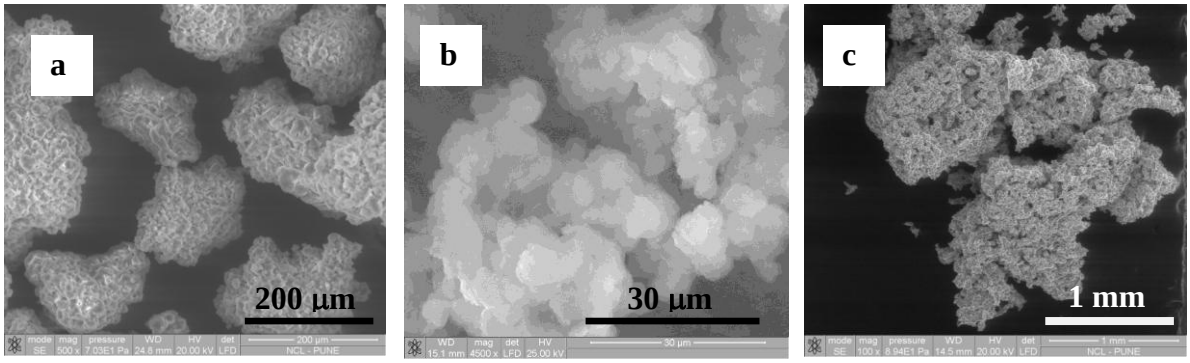

Figure 4.16: SEM images of PE obtained from Titanated catalyst (a) Ti/MgiPrOH (b) Ti/Mg2-BuOH, and (c) Ti/MgtBuOH.

Textural properties are investigated by N_2 adsorption isotherm and the result is shown in Table 4.1. Among a series of Z-N catalyst derived from $MgCl_2$ molecular adduct with different alcohols, Ti/MgiPrOH shows high surface area of 197 m^2/g. Ti/Mg2-BuOH also shows significantly high surface area (120 m^2/g) than the commercially available heterogeneous Z-N catalyst supported on magnesium chloride ethanol adduct.

Among the above mentioned catalyst, titanated catalyst supported on isopropanol adduct is having high pore volume value of 0.973 cc/g. The Ti/Mg2-BuOH catalyst shows pore diameter and pore volume of 3.85 nm and 0.269 cc/g respectively. The activity of the Ti/Mg2-BuOH is comparable with that of commercially available Ti/MgEtOH but less in activity with Ti/MgiPrOH for ethylene polymerization [23]. High surface area of these catalysts might be one of reasons for increase in activity for ethylene polymerization. The percentage titanium loading varied with Z-N catalyst derived from different adduct. The % of Ti loading of Ti/MgiPrOH, Mg2-BuOH and MgtBuOH are 11, 23 and 7.8 % respectively. Even though Ti loading was high, productivity for polyethylene is not affected.

Table 4.1: Textural properties of Z-N catalyst derived from MgiPrOH, Mg2-BuOH and MgtBuOH (BJH method).

Catalyst	Surface Area (m^2/g)	Pore Diameter (nm)	Pore Volume (cc/g)
Ti/MgiPrOH	196.7	6	0.973
Ti/Mg2-BuOH	120	3.85	0.269
Ti/MgtBuOH	170.45	4.78	0.774

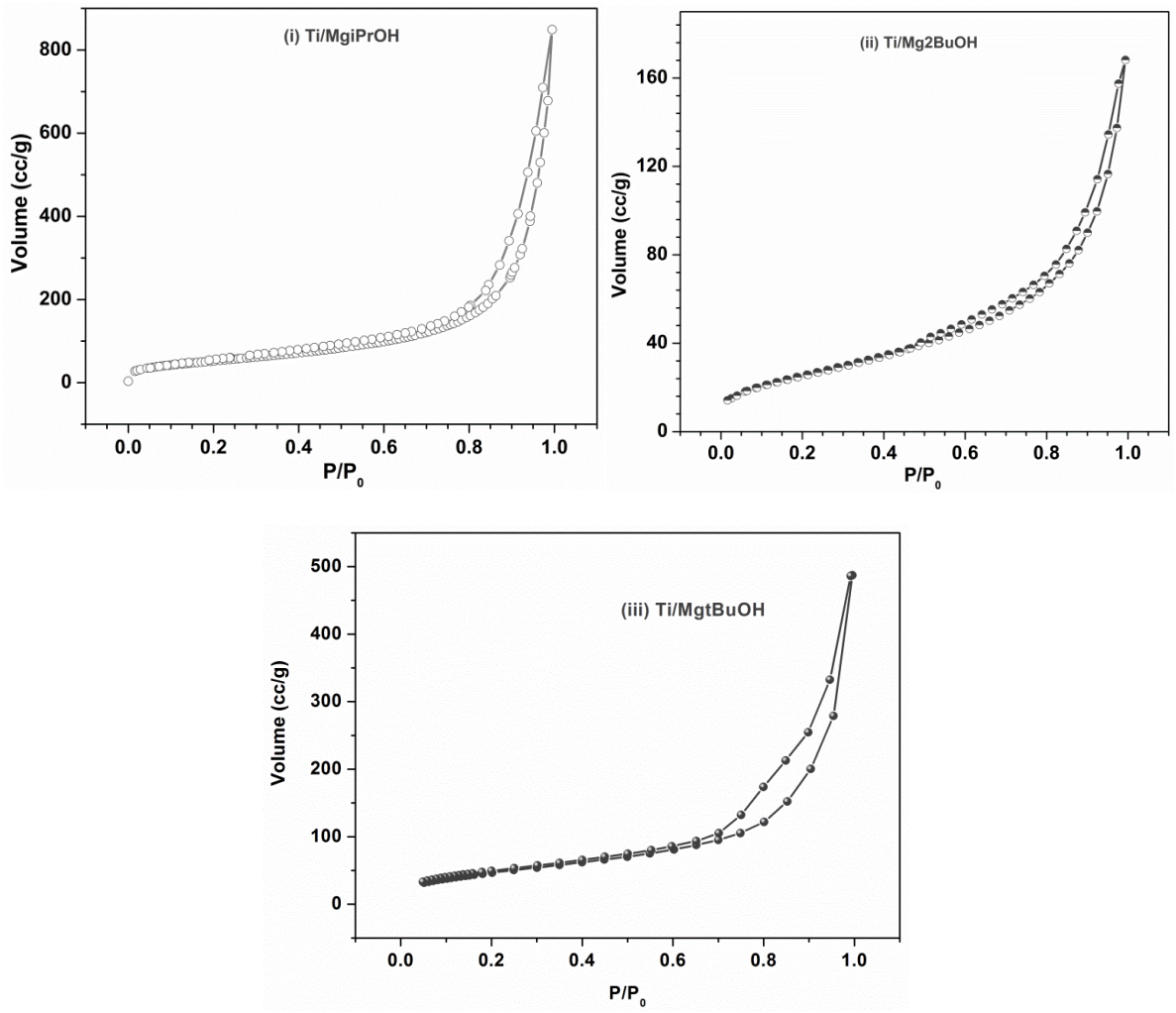

Figure 4.17: Adsorption Isotherm of (i) Ti/MgiPrOH (ii) Ti/Mg2-BuOH and (iii) Ti/MgtBuOH.

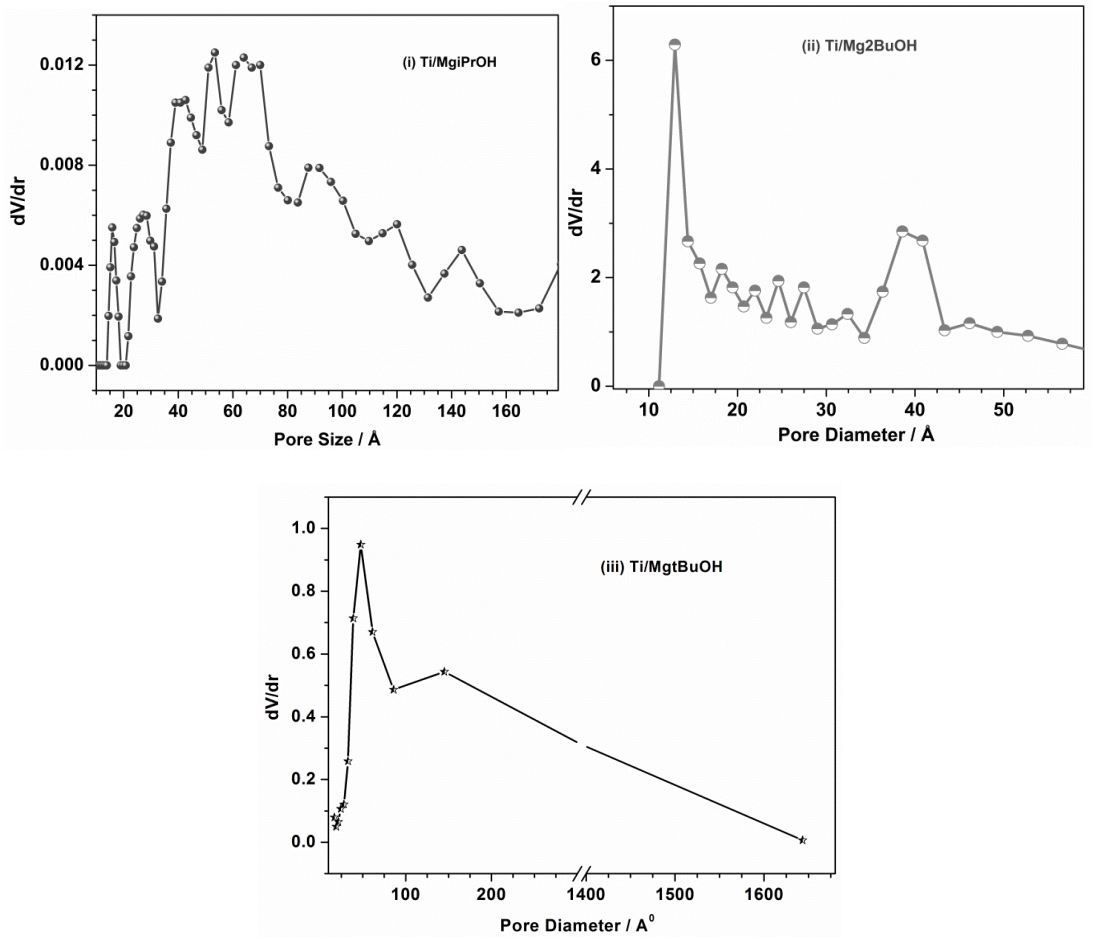

Figure 4.18: Pore size distribution of titanated catalysts, (i) Ti/MgiPrOH (ii) Ti/Mg2-BuOH and (iii) Ti/MgtBuOH.

4.4. Ethylene Polymerization

Titanation of $MgCl_2$-based adducts and their performance evaluation for ethylene polymerization was shown in Table 4.2. The activity of the Z-N catalyst supported on MgiPrOH, Mg2-BuOH and MgtBuOH towards ethylene polymerization is described below:

4.4.1. Ti/MgiPrOH

Ethylene polymerization was carried out with MgiPrOH derived catalyst, with triethylaluminum as the cocatalyst, Ultrahigh molecular weight polyethylene (UHMWPE) with MW (7 million by Margolie's equation, and 4.8 million by ASTM equation) was obtained with high yield (14 kg/g catalyst or 5.75 kg/mmol of Ti) that shows that the productivity is comparable to or better than many commercial catalysts. Polymers like

UHMWPE which are almost insoluble in solvents (even at high temperature) used for GPC analysis cannot be characterized using such techniques for their molecular weight and related characteristics. Hence, the molecular weight is calculated based on the intrinsic viscosity of a 0.02 % solution of same in decalin (tetrahydronaphthalene) determined at 135 °C using an Ubbelohde viscometer. The two equations normally used for calculating the viscosity based molecular weight are as follows:-

$$M = K[\eta]\alpha \qquad (4.1)$$

Where M is the molecular weight, η is the intrinsic viscosity, the constant K = 53700 and constant α = 1.37. The ASTM equation (ASTM D-4020-01a) uses the value for α as 1.37 and Margolie's equation uses the value for α as 1.39.

Characterization of UHMWPE has been carried out by ^{13}C CP/MAS NMR as the product could not be dissolved even at 135 °C for many hours in solvent like ortho dichlorobenzene/trichloro benzene (ODCB/ TCB) which is conventionally used for microstructure determination by ^{13}C solution state NMR. ^{13}C CP/MAS spectrum of the UHMWPE sample clearly indicated the presence of highly crystalline domains compared to a commercial high density polyethylene (HDPE) sample.

Table 4.2: Titanation of $MgCl_2$-based adducts and their performance evaluation for ethylene polymerization with triethyl aluminium as cocatalyst.

Catalyst	Wt % of Ti	PE (g/g of catalyst)
Ti/MgiPrOH	11	UHMPE, 14000
Ti/Mg2-BuOH	23	1300
Ti/MgtBuOH	7.8	8120

Catalyst quantity = 0.1g for Ti/Mg2-BuOH and Ti/MgtBuOH; 0.01 g for Ti/MgiPrOH; Al/Ti = 50 for MgiPrOH support, Al/Ti = 20 for Mg2-BuOH.and Al/Ti = 150 for MgtBuOH. Dry hexane has been used as solvent.

4.4.1.1. ^{13}C CP/MAS study of UHMWPE obtained using Ti/MgiPrOH

Comparison of ^{13}C CP/MAS spectra of PE obtained in the reaction using MgiPrOH adduct as support and a commercial HDPE is shown in Figure 4.19. The ^{13}C CP/MAS spectrum of the polyethylene obtained is very similar to the one reported for UHMWPE [14] and can be interpreted in terms of signals arising from an amorphous and different crystalline domains. The broad signal at the highest field (31.3 ppm) is from the polymer chains of the amorphous domain (A). The rest, including the strongest peak at 33 ppm (C2B) and the weak shoulder at 34.4 ppm (C3) are attributed to the polymer chains in one of the orthorhombic phases (orthorhombic II) and monoclinic phase, respectively. In addition, two more signals from crystalline domains are envisaged form the relaxation measurements [26]. One of these, with a chemical shift very close to the main crystalline all *trans* configuration and a faster relaxation rate is more amorphous like (C2A), while the other one with a chemical shift ~33.5 ppm is more crystalline like, which is attributed to another orthorhombic phase (C1). It is very clear from the spectra that the sample prepared with MgiPrOH support is less amorphous in nature and also has more monoclinic phase. A deconvolution of the ^{13}C CP/MAS spectral data using DIMFIT [27] showed a decrease in the A, C2A components and increase in C,C1 and C2B components for the sample compared to the commercial HDPE sample. The details of deconvolution are given in the following Table 4.3.

4.4.2. Ti/Mg2-BuOH

Ethylene polymerization has been carried out as a test reaction to study the activity of the Ti/Mg2-BuOH catalyst. Triethylaluminium is used as a co catalyst. Polymerization activity of Ti/Mg2-BuOH has been compared with that of Ti/MgEtOH and Ti/MgiPrOH catalyst in Table 4.2. Titanium loading was high for Ti/Mg2-BuOH (23 %) as compared to 11% in Ti/MgEtOH and 11% in Ti/MgiPrOH.

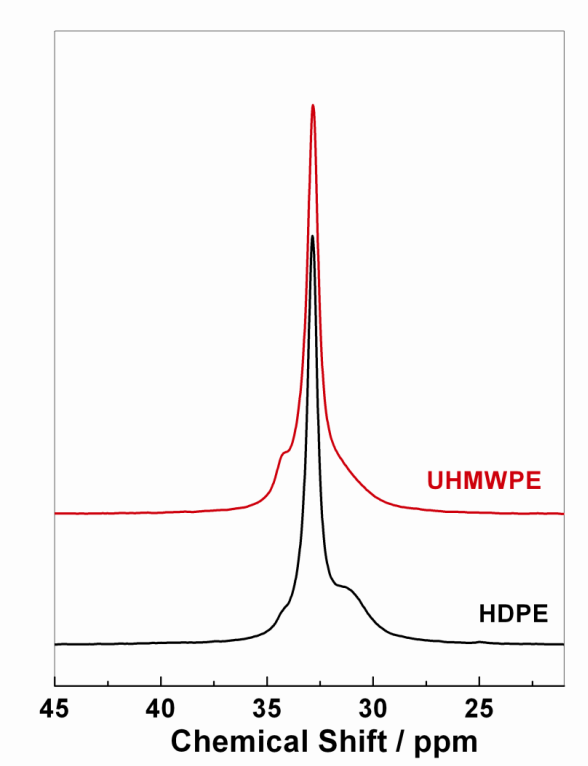

Figure 4.19: Comparison of ^{13}C CP/MAS spectra of PE obtained in the reaction using MgiPrOH adduct as support (upper trace) and a commercial HDPE (lower trace).

Table 4.3: The details of deconvolution of components in HDPE and UHMWPE.

Component	g/l	HDPE		UHMWPE	
		Peak Position (ppm)	Ratio (%)	Peak Position (ppm)	Ratio (%)
A	0.27	31.30	24.32	31.30	13.66
C1	0.22	33.50	5.71	33.50	4.91
C2B	0.20	32.85	58.81	32.84	67.69
C2A	0.00	32.85	8.29	32.85	6.72
C3	0.05	34.42	2.87	34.48	7.02

The polymerization activity of the $MgCl_2$ supported Z-N catalyst derived from ethanol and 2-butanol adduct shows similar nature even though Ti/Mg2-BuOH possess high surface area. This indicates that catalyst with high surface area is not mandatory to get high

polymerization activity. In fact, large surface area of Ti/Mg2-BuOH catalyst leads to very high impregnation of $TiCl_x$ active species on $MgCl_2$ surface. Even though Ti loading was high, the productivity for polyethylene polymerization is not higher than the Ti/MgEtOH, suggests the specific activity of active titanium species is likely to be lesser than the commercial catalyst. 1300 g of polymer was produced for a gram of catalyst, which is similar to the one obtained for commercially available catalyst. The reason for the comparable catalytic activity between Ti/Mg2-BuOH and commercial catalyst is attributed to the following: In spite of its high titanium content, Ti/Mg2-BuOH shows a comparable activity as that of commercial catalyst suggesting a lower specific activity towards olefin polymerization. In Z-N catalysts partial reduction of the catalytically active $Ti^{4+/3+}$ to Ti^{2+} in a side reaction with TEAL is known to be one of the main catalyst deactivation pathways. In the case of Ti/Mg2-BuOH, high surface area and larger pores with high pore volume makes the catalytically active $Ti^{4+/3+}$ sites more accessible to TEAL resulting in over-reduction and deactivation. Above type of electronic interaction limits the activity of the catalyst and hence a pore-size optimization might lead to an improvement in activity.

4.4.3. Ti/MgtBuOH

Ti/MgtBuOH catalyst has been screened for ethylene polymerization using three different co-catalysts to study the effect of cocatalyst in determining the activity. Ethylene polymerization activity results of catalysts with different co-catalysts at 5 atm pressure shown in Table 4.4.

Among the three cocatalyst, Et_3Al results highest polymerization activity of 8120g/ g of catalyst. The reason is due to high reducing nature of Et_3Al as compared to Me_3Al for the generation of active Ti^{3+}/ Ti^{2+}. There is a decrease in polymerization activity which was observed when switching the cocatalyst from Et_3Al to iBu_3Al, this might be due to increase in the percentage reduction of Ti^{4+} which make the catalyst inactive for olefin polymerization.

In general, the difference in polymerization activity with different cocatalyst could be due to different active sites formation. Overall performance of Ti/MgtBuOH was much better than the commercial Ti-MgEtOH catalyst. The possible reason could be due the very high surface area (170.45m^2/g) of Ti/MgtBuOH and lesser content of active TiClx species over the catalyst.

Table 4.4: Ethylene polymerization activity results of catalysts with different co-catalysts at 5 atm pressure.

S. No	Support	Ti wt% (mmol)	Co-catalyst	Condition	PE Yield (g/g of catalyst)
1	MgtBuOH	7.8 (0.16)	Me_3Al	75^{o}C, 5atm	4320
2	MgtBuOH	7.8 (0.16)	Et_3Al	75^{o}C, 5atm	8120
3	MgtBuOH	7.8 (0.16)	iBu_3Al	75^{o}C, 5atm	6976
4	MgEtOH	11 (0.23)	Et_3Al	75^{o}C, 5atm	1300

4.5. Conclusion

MgiPrOH, Mg2-BuOH, MgtBuOH and their titanated catalysts have been thoroughly investigated by different structural and spectroscopic techniques. $2\theta < 15^o$ in XRD indicate the formation of molecular adduct. The peak at ~ 710 cm^{-1} in the Raman spectra further support the adduct formation. Solid-state NMR was used as a major tool to understand the structural property of the molecular adduct and final Ziegler-Natta catalyst. The number of coordinating alcohols in MgiPrOH, Mg2-BuOH and MgtBuOH was calculated from liquid NMR and TG-DTA analysis. The major findings from these materials are the following:

Characteristic feature of $MgCl_2 \cdot 4(CH_3)_2CHOH$, with a secondary alcohol (iPrOH) is that it showed two different sets of magnetically in equivalent isopropanol, high polymerization activity and selectively to UHMWPE. This titanated catalyst shows higher surface area among all other catalyst we prepared with different alcohols.

Formation of porous shaped with fibrous nature is the special feature of Mg2-BuOH. Activity of this catalyst for ethylene polymerization is comparable with the commercially available Z-N catalyst derived from $MgCl_2$.6EtOH (MgEtOH) adducts. The aforementioned Z-N catalyst exhibits a high surface area of 120 m^2/g. The reason for the increase in the activity of Ti/Mg2-BuOH can be due to (i) high surface area which in turn increase the dispersion of active Ti species, (ii) large pore volume and pore diameter. Our study shows that, secondary alcohols with linear and branched structure of alcohols didn't inhibit the activity of the catalyst. Instead of that indirectly these alcohols changes the electronic and textural properties of the Z-N catalyst.

A new molecular adduct of $MgCl_2$ with a tertiary alcohol (MgtBuOH) has been synthesized and structural insights of adduct has been revealed by various spectroscopic and morphological characterization methods. The polymerization activity of Z-N catalyst supported on MgtBuOH exhibits much better performance in terms of activity and polymer property compared to commercial Ziegler Natta catalyst. To study the effect of cocatalyst, ethylene polymerization was tested with three different types of trialkyl aluminium compounds. The best activity was observed with triethylaluminium with a polymer yield of 8120 g /g of catalyst.

4.6. References

1. K. Ziegler, H. G. Gellert, K. Zosel, W. Lehmkuhl, W. Pfohl, *Angew. Chem.* **67** (*1955*) 424.
2. K. Ziegler, E. Holzkamp, H. Breil, H. Martin, *Angew. Chem.* **67** (1955) 541.

3. G. Natta, *J. Polym. Sci.* **16** (1955) 143.
4. N. Kashiwa, H. Fujimura, Y. Tokuzumi, *Japan Patent 1031698*, 1968.
5. P. Pino, R. Mülhaupt, *Angew. Chem.* **92** (1980**)** 869.
6. P. C. Barbe`, G. Cecchin, L. Noristi, *Adv. Polym. Sci.* **81**(1987) 1.
7. E. Albizzati, U. Giannini, G. Balbontin, I. Camurati, J. C. Chadwick, T. Dall'Occo, Y. Dubitsky, M. Galimberti, G. Morini, A. Maldotti, *J. Polym. Sci., Part A: Polym. Chem.* **35** (1997) 2645.
8. E. Albizzati, U. Giannini, G. Collina, L. Noristi, L. Resconi, In *Polypropylene Handbook: Polymerization, Characterization, Properties, Applications*; E. P. Moore, Ed.; Hanser Publ., Jr.: NY, (1996) p 11.
9. N. Kashiwa, *J. Polym. Sci., Part A: Polym. Chem.* **42** (2004) 1.
10. E. Magni, G. A. Somorjai, *Surf. Sci.* **345** (1996**)** 1.
11. S. H. Kim, G. A. Somorjai, *J. Phys. Chem. B* **106** (2002) 1386.
12. M. Boero, M. Parrinello, S. Hüffner, H. Weiss, *J. Am. Chem. Soc.* **122** (2000) 501.
13. V. Busico, M. Causa, R. Cipullo, R.Credendino, F. Cutillo, N. Friederichs, R. Lamanna, A.Segre, V. V. A. Castelli, *J. Phys. Chem. C* **112** (2008) 1081.
14. A. Andoni, J. C. Chadwick, S. Milani, J. W. Niemantsverdriet, P. Thüne, *J. Catal.* **247** (2007) 129.
15. P. Sobota, *Coord. Chem. Rev.* **248** (2004) 1047.
16. G.Valle, G. Baruzzi, G. Paganetto, G. Depaolit, R. Zannetti, A. Marigo, *Inorg. Chim. Acta* **156** (1989) 157.
17. P. Sozzani, S. Bracco, A. Comotti, R. Simonutti, I. Camurati, *J. Am. Chem. Soc.* **125** (2003) 12881.
18. C. J. Bart, *J. Mater. Sci.* **30** (1995) 2809.
19. K. S. Thushara, R. Mathew, T. G. Ajithkumar, P. R. Rajamohanan, S. Bhaduri, C. S.

Gopinath, *J. Phys. Chem. C* **113** (2009) 8556.

20. K. S. Thushara, T. G. Ajithkumar, P. R. Rajamohanan, C.S. Gopinath (submitted to *Appl. Cata. A*).
21. P. Sozzani, S. Bracco, A. Comotti, R. Simonutti, I. Camurati, *J. Am. Chem. Soc.* **125** (2003) 12881.
22. P. Caravatti, J. A. Deli, G. Bodenhausen, R. R. Ernst, *J. Am.Chem. Soc.* **104** (1982) 5506.
23. K. S. Thushara, E. S. Gnanakumar, R. Mathew, R. K. Jha, T. G. Ajithkumar, P. R . Rajamohanan, K. Sarma, S. Padmanabhan, S. Bhaduri, C. S. Gopinath, *J. Phys. Chem. C.* **115** (2011) 1952.
24. C. R. Tewell, F. Malizia, J. W. Ager III, G. A. Somorjai, *J. Phys.Chem. B* **106** (2002) 2946.
25. K. Atsushi, Y. Ohta, H. Yasuda, M. Murano, *Poly. J.* **22** (1990) 455.
26. Z. Lili, G. Chen, E. W. Hanser, *Macromol. Chem. Phys*. **206** (2005) 246.
27. D. Massiot, F. Fayen, M. Capron, I. King, S. L. Calve, B. Alonso, J. O. Durand, B. Bujoli, Z. Gan, G. Hoatson, *Magn. Reson. Chem*. **40** (2002) 70.

Chapter 5

5. Characterization of Esterified $MgCl_2$. nROH (R= ethyl, isopropyl, isobutyl and 2-butyl) with Benzoyl Chloride and their Catalytic Activity Studies for Ethylene Polymerization

5.1. Introduction

$MgCl_2$-supported titanium catalysts for the polymerization of olefins have had spectacular success in simplifying the polymerization process and improving polymer quality. The basis for the development of the high-activity supported catalysts [1] lay in the discovery of "activated" $MgCl_2$ being able to support $TiCl_4$ and give high catalyst activity for both ethylene and propylene polymerization. After the name of the discoverers, these solid catalysts are usually referred to as Ziegler and Ziegler-Natta (Z-N) catalyst, respectively. In the mid-1970s, it was discovered that certain Lewis bases, when present as an integral part of the $MgCl_2$ support and/or when added from outside during polymerization, are capable of significantly increasing the stereospecificity of propylene polymerization. These Lewis bases, typically an ester or ether, are called electron donors (ED) and when incorporated in $MgCl_2$ as an integral part of the support are referred to as the internal electron donors (IED). They bind strongly to $MgCl_2$, and their basic function is to control the amount and distribution of $TiCl_4$ on the support [2-12]. In contrast, external electron donors (EED) are EDs that enhance stereospecificity in the presence of the correct IED and are added externally during the polymerization reaction. Although innumerable organic compounds have been tested as potential IEDs and EEDs, only a few combinations were found to give satisfactory results. Understanding how the activated surface of magnesium chloride can influence the properties of the active sites has turned into a great challenge for the techniques of surface science, spectroscopy, and computational methods [13-15]. It is generally believed that the IED blocks particular sites on the $MgCl_2$ surface which otherwise, upon coordination with $TiCl_4$, would generate precursors of non stereo specific active sites [6, 10, 11]. Spitz et al. [12]

recently reported that IED might have no direct role in the active site formation; however, it stabilizes the $MgCl_2$ crystallites. One of the main reasons for this uncertainty regarding the role of IED is that the majority of the experimental information available in the literature comes mainly from detailed analysis of the microstructure of polypropylene, rather than the support and/or the catalyst itself. The difficulties in interpreting data from propylene polymerization experiments also arise from the fact that a widely used IED such as ethyl benzoate (EB) is eluted from $MgCl_2$ supported titanium catalyst under the general polymerization conditions. Furthermore, there is enough evidence to suggest that there are multiple modes of interactions between IED, EED, cocatalyst (alkyl aluminium complexes), and the active Ti sites [16-23]. Thus, direct investigation of the active species on the catalyst is an extremely complex problem even if other difficulties such as complexity of the constitution, low content of the active sites in the catalyst, high sensitivity to oxygen and moisture in the ambient conditions are ignored.

The aim of the present chapter is to understand the molecular level properties of $MgCl_2$.nROH adduct with IED as structural and an integral part of support by subjecting them to spectroscopic and other techniques. Ethyl Benzoate (Est) and its analogues are known to be highly effective as donors for modifying Z-N catalyst and thus have many advantages [24] over Z-N catalyst supported on $MgCl_2$ derived from $MgCl_2$.6EtOH (ME). However, nothing is known about the structural properties of esterified- ethanol (Est-ME), isopropanol (Est-MiP), isobutanol (Est-MiB) and 2-butanol(Est-M2B). Detailed structural and comparative studies on esterified $MgCl_2$ with corresponding alcohol adduct are therefore important steps towards the overall goal of a better understanding of the role of IED. This chapter discusses the comparative data on the activities of Ziegler catalysts made by using these supports. First part of the thesis discussed about the molecular level properties of the esterified adduct with ethanol, isopropanol, isobutanol and 2-butanol adduct with benzoyl

chloride as esterifying agent. Out of these different esterified compounds, we randomly chose few adducts for catalytic activity studies. Esterified adducts (Est) prepared using ethanol (ME), isopropanol (MiP), isobutanol (MiB) and 2-butanol (M2B) are designated as Est-ME, Est-MiP, Est-MiB, Est-M2B and the corresponding titanated catalysts as Ti/Est-ME and Ti/Est-MiP, respectively.

5.2. Results and discussion

5.2.1. Characterization of Esterified MgEtOH, MgiPrOH, Mg2-BuOH and Mg-*i*-BuOH Molecular adducts

5.2.1.1. Powder X-ray Diffraction

Figure 5.1 shows the XRD patterns of (i) ME (ii) MiB (iii) M2B (iv) Est-ME (v) Est-MiB and (vi) Est-M2B. A thorough analysis of XRD pattern indicates that 2θ value of adducts varies depending on the amount of alcohol in $MgCl_2$ [25-28]. The corresponding '2θ' values for ME, MiP, MiB and M2B are 9°, 9.95°, 7.7° and 8.9°.

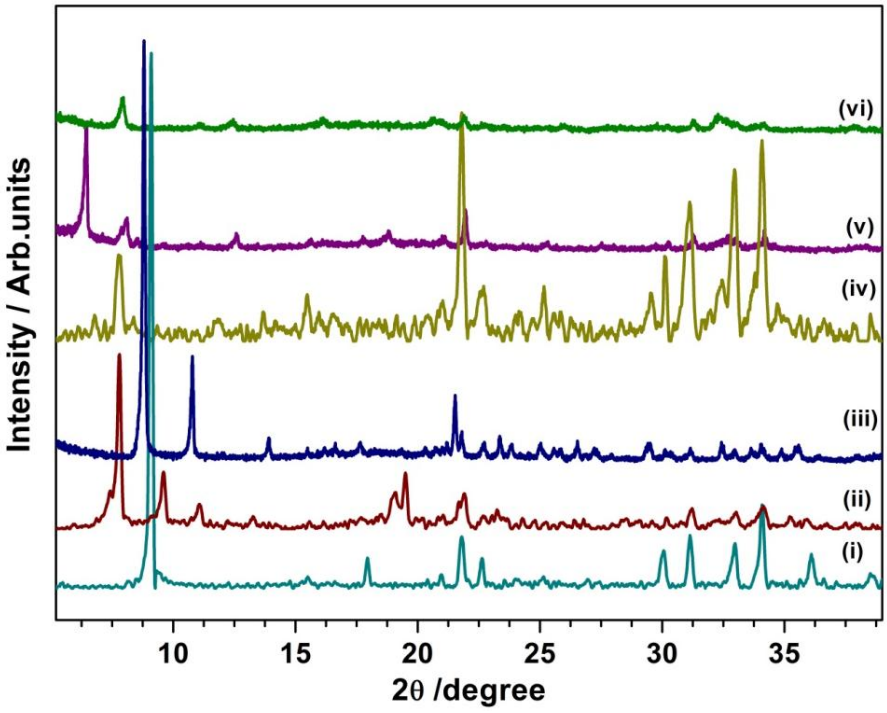

Figure 5.1: XRD patterns (i) ME (ii) MiB (iii) M2B (iv) Est-ME (v) Est-MiB and (vi) Est-M2B.

The XRD pattern of the esterified adduct shows a characteristic low-angle peak as compared to $MgCl_2$.nROH and hence an increase in the d-value of the (001) plane. This low angle peak characterizes the esterified molecular adduct formation indicating the ester formation that occurs along the z-axis of ME, MiP, MiB and M2B. Indeed, this is the preferred route due to the lowest steric hindrance along the z-axis of the layered structure of $MgCl_2$. Based on the bulky nature of the ester formed via reaction of benzoyl chloride with alcohol adduct, there is a change in the peak position of XRD pattern. For Est-ME, Est-MiB and Est-M2B, the diffraction pattern appears at a 2θ value of 7.8°, 6.45° and 7.89° but for Est-MiP no characteristics peak was observed.

5.2.1.2. Thermal Analysis

Figure 5.2 shows the results from TG-DTA of (i) Est-ME (ii) Est-MiP (iii) Est- MiB and (iv) Est-M2B. In the case of Est-ME, the first ethanol molecule dissociates at 89 °C (weight loss from 100 to 90%), indicating the stronger binding force between EtOH and $MgCl_2$ in Est-ME. Indeed, the weight loss trend observed is significantly lower up to 130 °C with the Est-ME adduct compared to ME, again highlighting that EtOH is bound relatively stronger in the former. However, between 130 and 245 °C, the remaining four-ethanol molecule dissociates. Weight loss in Est-ME corresponds to the dissociation of five EtOH molecules in total. No weight loss was observed >245 °C, and it is reasonable to assume that $MgCl_2$ with one molecule of ester remains >245 °C.

TG-DTA analysis of Est-MiB, Est-MiP and Est-M2B follows a more or less similar trend. Due to the strong interaction of alcohols with $MgCl_2$, the first alcohol molecule dissociate at a higher temperature (150 °C). Above 250 °C, no weight loss was observed for the esterified adducts. In all the above mentioned adducts, the weight % calculation shows that out of 'n' coordinated alcohol molecules only one is esterified during the reaction with benzoyl chloride. This observation is further supported by NMR analysis.

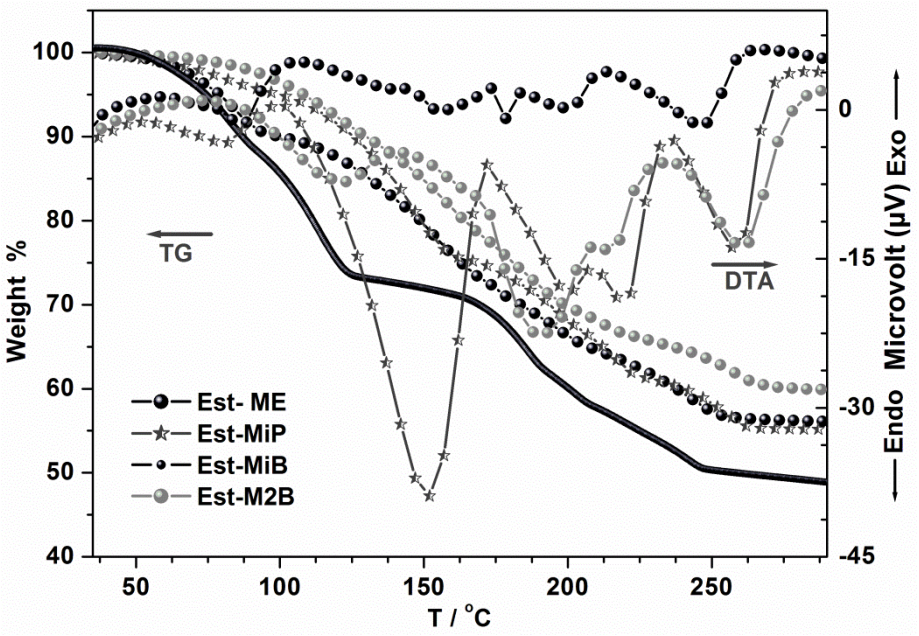

Figure 5.2: TG-DTA analysis of (i) Est-ME (ii) Est-MiP, (iii) Est- MiB and (iv) Est- M2B.

5.2.1.3. IR Spectroscopy

IR spectra of (i) Est-ME (ii) Est-MiB (iii) Est-MiP and (iv) Est-M2B are given in Figure 5.3. IR spectroscopy is one of the most common spectroscopic techniques used to determine the chemical functional groups in the sample and IR is very much sensitive to carbonyl groups. Nujol method was used to measure the IR spectrum of esterified adduct. High intense peaks observed at 2980- 2900 cm^{-1} and 1500-1300 cm^{-1} for all samples are due to C-H stretching of nujol and absorption band at 3450 cm^{-1} is due to O-H stretching. Ethyl benzoate (EB) (liq.) displays the $\nu_{C=O}$ peak at 1720-1730 cm^{-1}, while BC shows the ν_{OC-Cl} peak at 1780 cm^{-1} in addition to the above [27]. Indeed, the esterified adduct shows the $\nu_{C=O}$ feature at 1730 cm^{-1} directly supporting the ester formation. The esterified adduct shows C-O-C_{str} and O-C=O $_{asym}$ signals at 1167 and 1106 cm^{-1}, respectively.

5.2.1.4. Solid - State NMR Spectroscopy

The ^{13}C CP/MAS spectra of (i) Est-ME (ii) Est-MiB (iii) Est-MiP and (iv) Est-M2B are shown in Figure 5.4. Formation of the esterified adduct was further supported by solid-state NMR. The presence of the peak at ~160-180 ppm is due to the carbonyl carbon of the ester group.

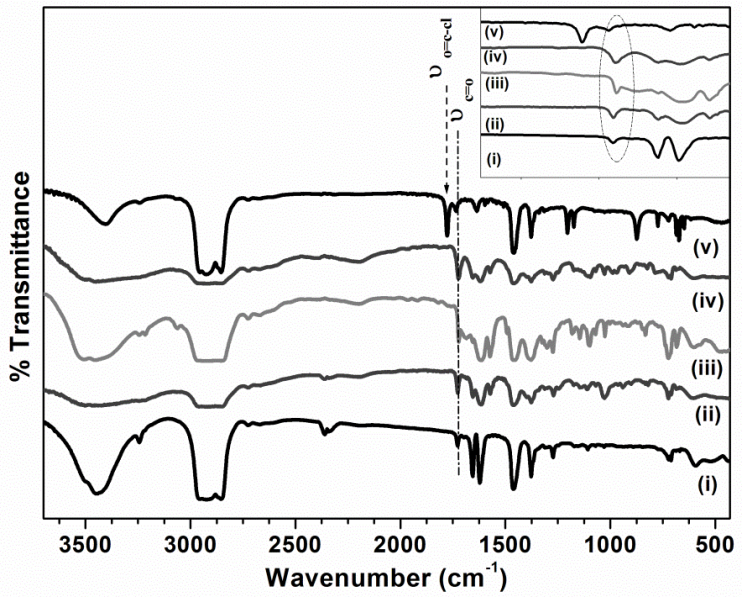

Figure 5.3: IR spectra of esterified molecular adducts, (i) Est-ME (ii) Est-MiB (iii) Est-MiP (iv) Est-M2B and (v) Benzoyl Chloride (BC). Strong C-H vibrational features around 3000 and 1500 cm^{-1} are due to nujol. Ester formation is supported by the observation of the carbonyl feature at 1730 cm^{-1}.

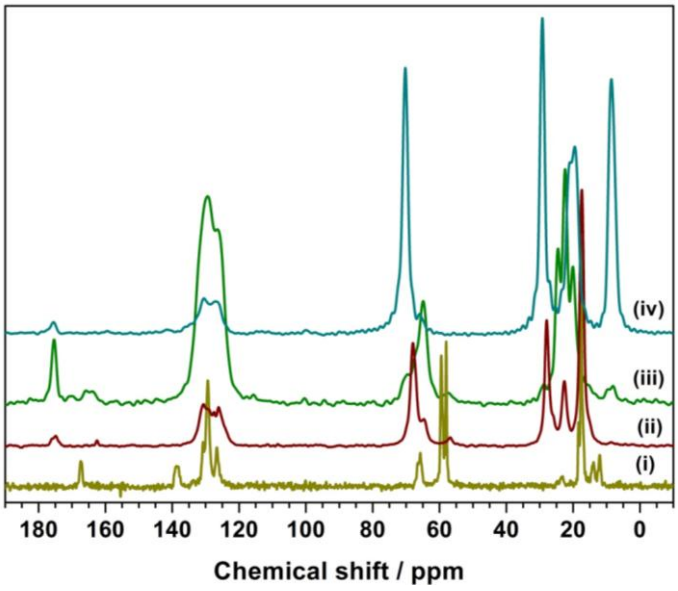

Figure 5.4: ^{13}C CP/MAS NMR spectra of (i) Est-ME (ii) Est-MiB (iii) Est-MiP and (iv) Est-M2B.

From the ^{13}C SPE-MAS spectrum, it is confirmed that only one alcohol is converted to the corresponding ester out of 'n' coordinating alcohols. The chemical shift value of the

each esterified adduct shows a slight change due to the changes in the electron density around the system. The corresponding chemical shift value of C=O peaks for esterified adduct are the following - 167.3 ppm (Est-ME), 175.3 (Est-MiP), 175.7 (Est-MiB) and 175.7 (Est-MiB).

5.2.1.5. Raman Spectroscopy

Figure 5.5 shows the Raman spectra of anhydrous $MgCl_2$, ethanol (liquid), ME, Est-ME, and EB (liq.). Raman spectra of $MgCl_2$ show a high intense peak at 243 cm^{-1} which has been assigned to the A1g breathing mode of the $MgCl_6$ octahedra in the lattice [29, 30]. Crystalline $MgCl_2$ belongs to the rhombohedral structure with D3d space group and has a layered structure. Mg 2p is in a distorted octahedral configuration coordinated to six chlorine anions. In the Raman spectra of liquid ethanol, a broad and weak OH phonon mode observed at 3400-3100 cm^{-1} is due to the intermolecular hydrogen bonding. For ethanol, peaks at 430, 886, 1052, 1270, and 1094 cm^{-1} correspond to Raman modes associated with δ(CCO), symmetric CCO, antisymmetric CCO,CH_2 twist + δ(COH), and CO stretch + CH_3 rock + δ (COH) modes, respectively [31]. After the adduct formation with $MgCl_2$, ME shows one extra peak at 684 cm^{-1} in addition to the features of liquid ethanol mentioned above. The above Raman mode at 684 cm^{-1} is due to the formation of the characteristic MgO_6 octahedron, and underscores the formation of the Mg-O bond between Mg and alcoholic oxygen [27, 29]. In the case of esterified adduct, the Mg-O phonon mode shifted to a little higher value of 700 cm^{-1} which is due to the presence of the aromatic ester moiety in the adduct. This is in good agreement with TG/DTA results discussed earlier. In the Raman spectrum of liq. EB, the C=O breathing mode appears at 1717 cm^{-1}; however, the C=O breathing mode of Est-ME shifted to 1703 cm^{-1} due to the coordination with $MgCl_2$. A shift in the Raman features of Est-ME, compared to ME, also underscores the changes in the structural and electronic environment.

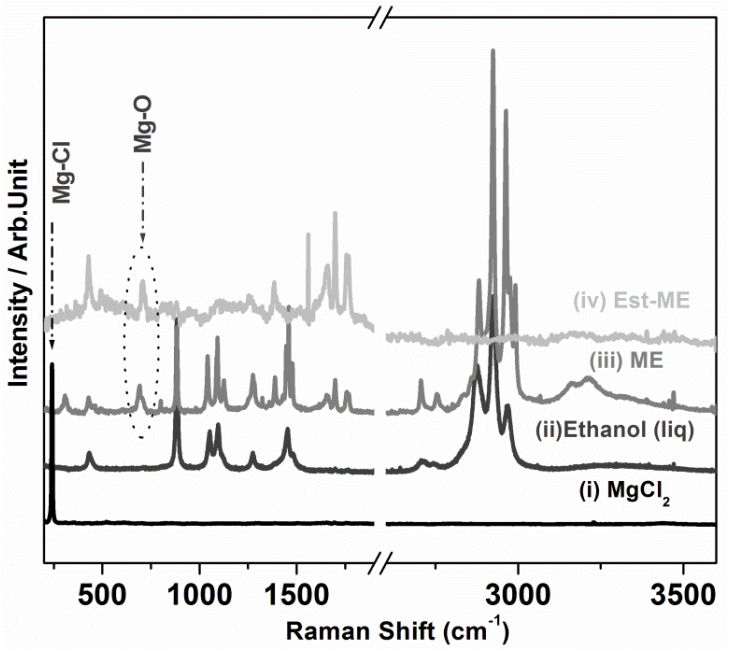

Figure 5.5: Raman spectra of standard compounds, (i) $MgCl_2$ and (ii) ethanol (liquid), and molecular adducts, namely, (c) ME and (d) Est-ME.

5.2.1.6. Scanning Electron Microscopy (SEM)

Figure 5.6 shows the SEM photograph of Est-ME and (b) Est-MiP (c) Est- MiB and (d) Est-M2B respectively. The SEM photographs clearly show the spherical shape for all esterified adducts. However, there are some changes on the surface of the support and size of adduct also vary from one esterified adduct to another. SEM images of Est-ME shows a particle size of 10-20 μm. An Est-MiP and Est-M2B show a particles size of 50 μm and 20 μm for Est-MiB.

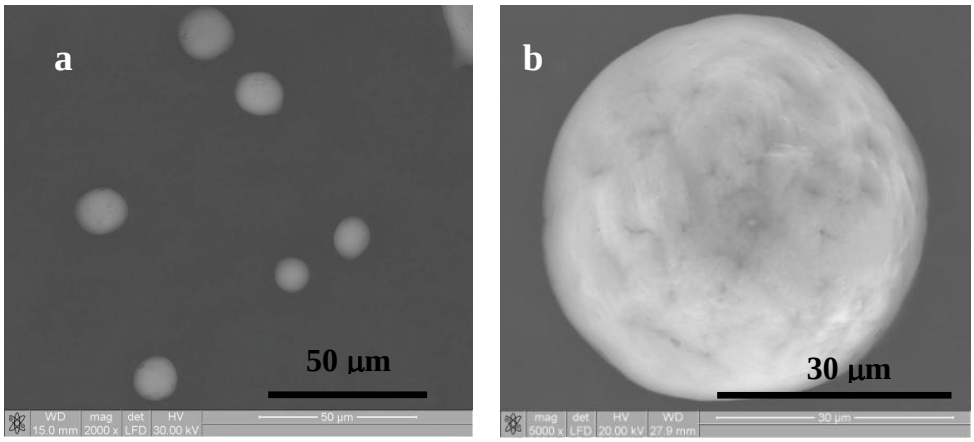

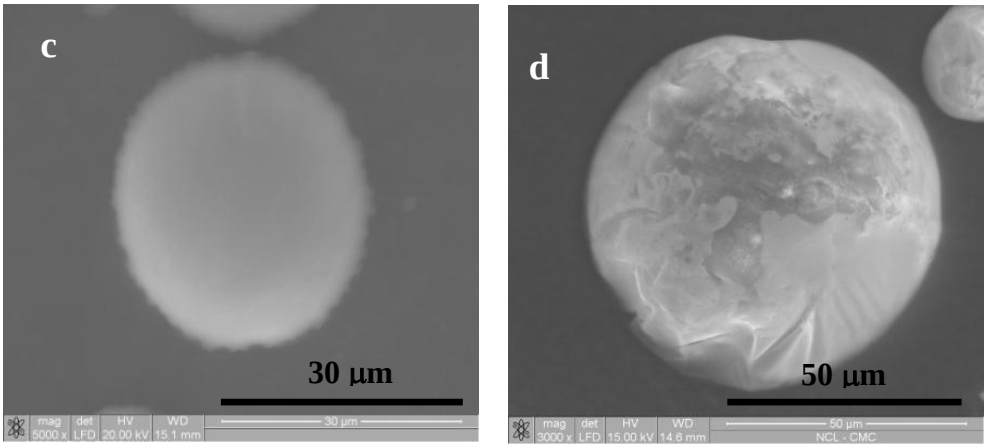

Figure 5.6: SEM images of esterified molecular adduct, (a) Est-ME and (b) Est-MiP (c) Est-MiB and (d) Est-M2B.

5.2.2. Characterization of titanated esterified adduct

In this section, the characterization details of Z-N catalyst supported on Est-ME and Est-MiP adduct and its activity study are discussed in detail. The main idea is to understand the role of ester in the catalytic system and its influence in olefin polymerization.

5.2.2.1. Powder X-ray diffraction

After treatment of these adducts with $TiCl_4$, characteristic peaks for the molecular adduct disappear in the catalyst, and it shows broad diffraction features between 15° and 23°, 29° and 34°, and 49 and 51° corresponding to structurally disordered δ-$MgCl_2$ (Figure 5.7). The low-angle peak observed below 10° for Est-ME and Est-MiP disappears, indicating a likely removal of EtOH molecules upon titanation; the same has been confirmed by solid state NMR, and it will be discussed later.

The diffraction feature at about 16° is due to the stacking of -Cl-Mg-Cl- triple layers ((003) plane) along the crystallographic direction. Signals at 29-34° (101/104) and 49-51° are also related to stacking faults in the triple layers [32]. The growth of $MgCl_2$ crystal was terminated by the surface incorporated $TiCl_4$ and the alkyl benzoate ester coordinated, leading to assemblies of fine $MgCl_2$ crystallites that could be identified by the characteristic broad peaks in XRD analysis. Furthermore, the incorporated $TiCl_4$ would be located on the

surface of $MgCl_2$ leading to effective formation of the active species.

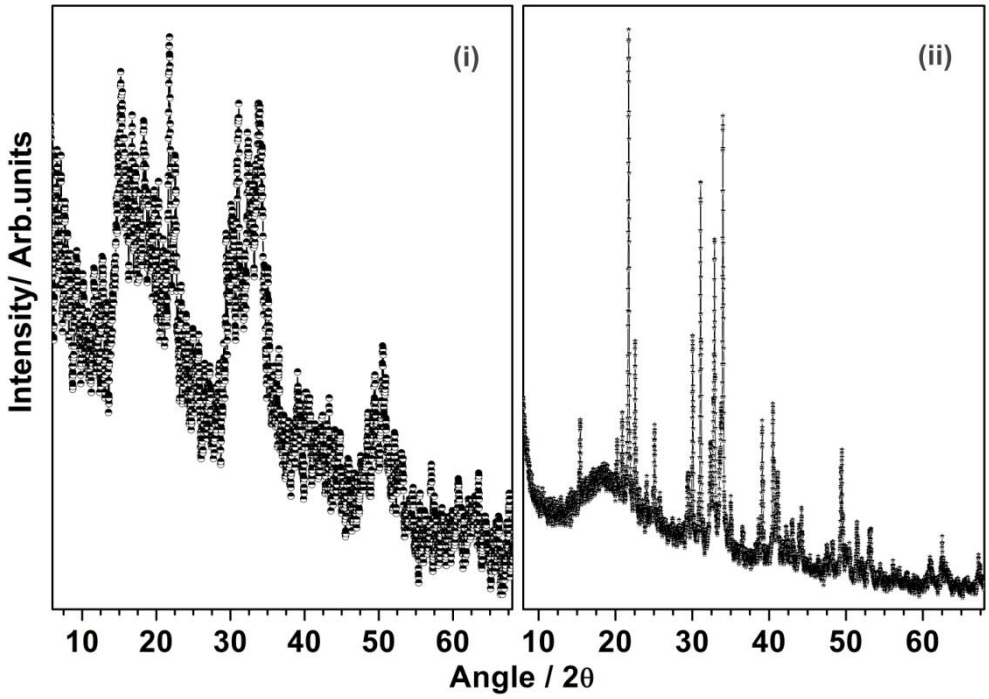

Figure 5.7: XRD patterns of Titanated catalyst (i) Ti/Est-ME and (ii) Ti/Est-MiP.

5.2.2.2. Thermal Analysis

Thermal analysis of titanated catalysts (Figure 5.8) also shows weight loss, and in particular DTA shows profound changes. There is no weight loss observed below 100 °C for both titanated catalysts indicating a substantial removal of alcohol from the above catalysts. The weight loss observed between 130 and 250 °C from Ti/Est-ME and Ti/Est-MiP might be due to desorption of various trapped components, like chlorinated ethers and solvent molecules. The presence of chlorinated ethers and solvent molecules has been supported by NMR data, which will be discussed later.

5.2.2.3. IR Spectroscopy

Figure 5.9 shows the IR spectra of titanated catalysts, (i) Ti/Est-ME and (ii) Ti/Est-MiP. The Ziegler-Natta catalyst supported on esterified adduct (Ti/Est-ME and Ti/Est-MiP) shows the presence of carbonyl group which indicate that the formed aromatic ester is strongly coordinated to $MgCl_2$ and not washed away during the catalyst preparation. However, the

$\nu_{C=O}$ of ester shifts from 1730 cm^{-1} on Et ME to 1680 cm^{-1}due to the changes in the electronic environment around the support material [27]. However, there is no shift on the $\nu_{C=O}$ frequency of ester in Ti/Est-MiP.

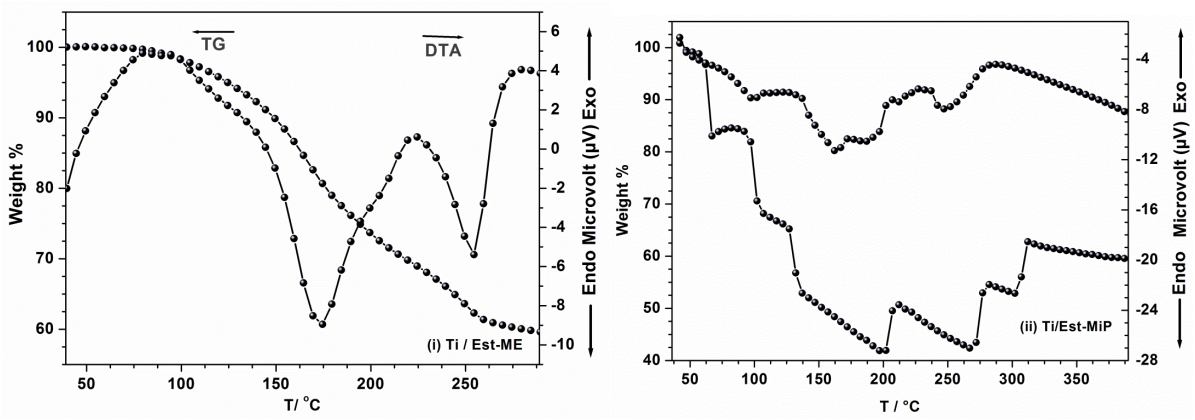

Figure 5.8: TG-DTA analysis of Titanated catalyst, (i) Ti/Est-ME and (ii) Ti/Est-MiP.

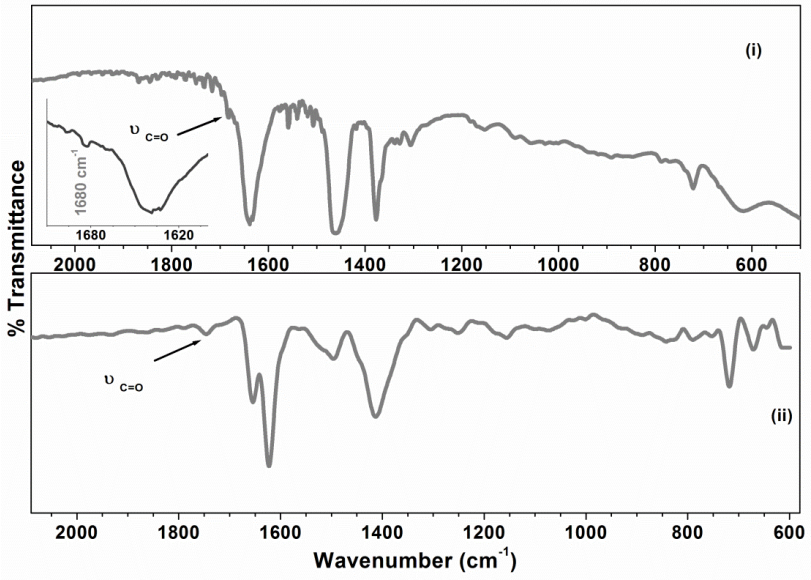

Figure 5.9: IR spectra of titanated catalysts, (i) Ti/Est-ME and (ii) Ti/Est-MiP.

5.2.2.4. Solid- state NMR Spectroscopy

The presence of the ester as IED in the final catalyst (Ti/Est-ME) was confirmed from the ^{13}C CP/MAS spectra shown in Figure 5.10 (i). As expected, various steps involved in the final catalyst preparation did not remove the ester group from the support, and the carbonyl carbon in the ester group appears at~170 ppm. ^{13}C CP/MAS spectra of Ti/Est-ME show an

additional peak at 94 and 87.6 ppm, respectively. This may be due to the formation of small amounts of chlorinated ether [27]. The reactions between esterified alcoholic adduct with $TiCl_4$ produces HCl, which in turn leads to the formation of chlorinated ethers. The latter remains trapped within the pores of the support and could be observed by ^{13}C CP/MAS NMR; weight loss in TG-DTA also corresponds to the loss of chlorinated ether molecules (see Figure 5.8). The ^{1}H MAS spectrum of Ti/Est-ME catalyst show very sharp peaks at 8 and 2.5-1.6 ppm (Figure 5.10 (ii)) corresponding to protons from aromatic and ethyl species and chlorinated ethers, respectively.

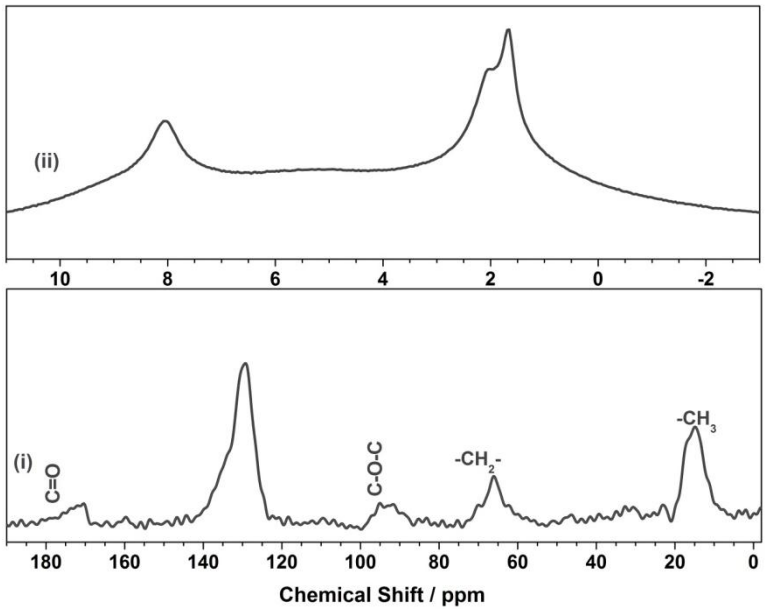

Figure 5.10: (i) ^{13}C CP-MAS and (ii) ^{1}H NMR spectra of titanated catalyst, Ti/Est-ME.

5.2.2.5. Scanning Electron Microscopy (SEM)

SEM analysis of titanated catalyst supported on esterified adduct shows entirely different morphology from the adduct system. First of all the particle size has reduced drastically from 20-50 μm on pure esterified adducts (Figures. 5.6 a and b) to less than 4 μm-10μm on titanated catalysts (Figures. 5.11 a and b). The porous structure of the titanated catalysts is attributed to the removal of alcohol molecules from pure adducts and this allows the creation of pores as well as the incorporation of $TiCl_3$ on the surface and pores.

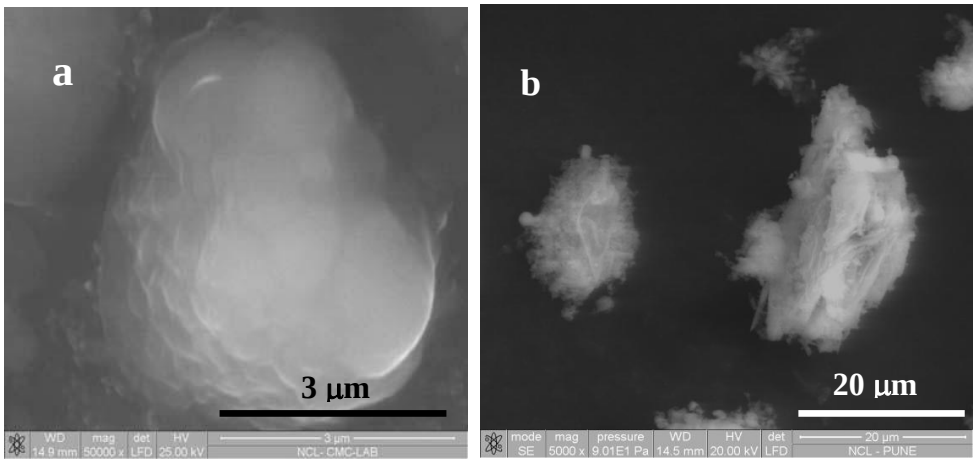

Figure 5.11: SEM images of (a) Ti/ Est-ME (b) Ti/Est-MiP.

5.2.2.6. Textural Characteristics

Table 5.1 shows the BET surface area and pore volume of titanated catalysts. It is to be mentioned here that the surface area of as-prepared molecular adducts shows a negligible value of 1-2 m^2/g. Apart from the much less porosity of molecular adducts, they could not be degassed (before surface area measurement) at temperatures higher than 40 °C as it would lead to loss of ethanol molecules. Surface area and pore size distribution measured through nitrogen adsorption isotherms on titanated catalysts are shown in Figure 5.12 and 5.13. As compared to Ti/Est-ME, Ti/Est-MiP show significantly high surface area (Table 5.1).

Table 5.1: Textural characteristics of titanated catalysts

Catalyst	Surface Area (m^2/g)	Pore Diameter (nm)	Pore Volume(cc/g)
Ti/Est-ME	22.2	4.06	0.046
Ti/Est-MiP	114.23	1.9	.336
Ti/ME	55.3	3.87	0.084
Ti/MiP	196.7	6	0.973

However, surface area of Ti/Est-ME and Ti/Est-MiP is low as compared to Ti/ME and Ti/MiP due to the presence of ester. Indeed high surface area of Ti/ME and Ti/MiP are due to the removal of all alcohol molecules and hence the creation of high porosity. Roughly, a third

of porosity is retained with Ti/Est-ME (compared to Ti/ME) indicating the presence of ester molecules in the final catalyst. A careful analysis of adsorption isotherms indicates type II adsorption isotherms for Ti/Est-ME and Ti/Est-MiP, respectively. An exponential increase in nitrogen adsorption observed for both catalysts at $P/P_0 = 0.8$ is to be noted. This is attributed to the presence of macropores in both the catalysts, particularly with slit-type pores. Indeed, the type II adsorption isotherm indicates an unrestricted monolayer-multilayer adsorption, which might be an important factor helping toward chain growth in polymerization.

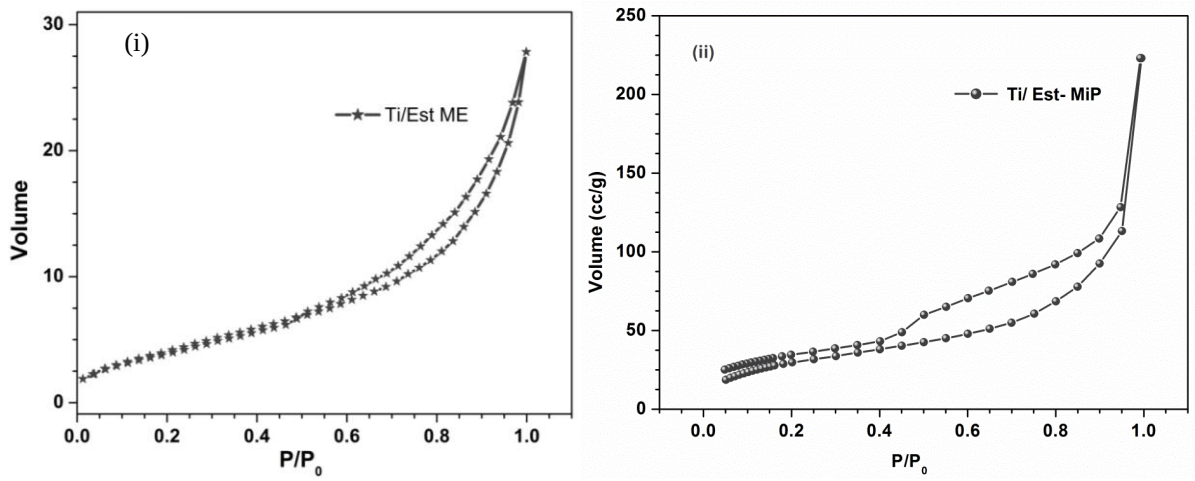

Figure 5.12: Adsorption Isotherm of (i) Ti/Est-ME and (ii) Ti/Est-MiP.

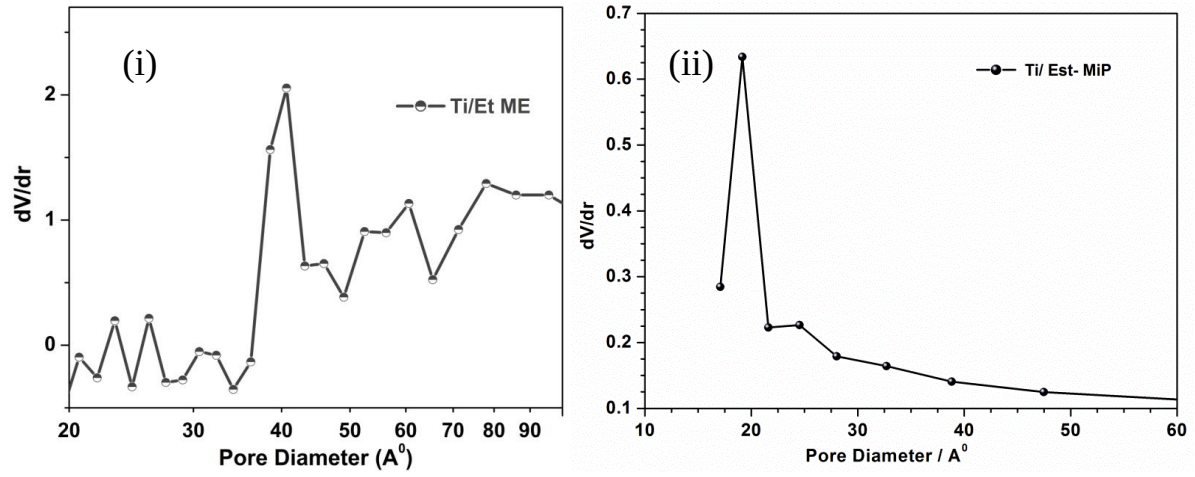

Figure 5.13: Pore-size distribution of titanated catalysts, (i) Ti/Est-ME and (ii) Ti/Est-MiP

5.2.3. Ethylene Polymerization

After the extensive characterization of molecular adduct and titanated catalyst, the activity of the catalyst was evaluated by ethylene polymerization (Table 5.2).Ethylene, rather

than propylene, polymerization was chosen as the benchmark for comparing the activities of Est-ME and Est-MiP derived catalysts so that potential differences in energetics arising out of different orientations of propylene could be ignored. Indeed, DFT calculations on a model catalyst had shown that the energy differences between transition states corresponding to different orientations of propylene in the presence of IED could be substantial [47]. Ethylene polymerization was carried out with Est-ME and Est-MiP molecular adducts supported catalyst, as mentioned earlier. By varying the support, the percentage of titanium loading also varied. 11 % titanium loading was present in Ti/Est-ME, but it decreased to 5.25 % in Ti/Est-MiP. Triethyl aluminium (TEAL) was used as the cocatalyst with Ti/Est-ME for ethylene polymerization. Higher yields (1400 g/g of catalyst) of polyethylene and productivity were obtained using Est-ME rather than the ME-supported catalyst (see Table 5.2).

Table 5.2: Titanation of $MgCl_2$-Based Adducts and Their Performance Evaluation for Ethylene Polymerization.

S. No	Support	Ti wt% (mmol)	Co-catalyst	Condition	PE Yield (g/g of catalyst)
1	Est-ME	11(0.225)	Et_3Al	75°C, 5atm	1400
2	Est-MiP	5.25(0.11)	Me_3Al	75°C, 5atm	3890
3	Est-MiP	5.25(0.11)	Et_3Al	75°C, 5atm	5794
4	Est-MiP	5.25(0.11)	iBu_3Al	75°C, 5atm	1950

Catalyst quantity = 0.1g; Al/Ti = 20 for Est-ME support; Al/Ti = 100 for Est-MiP. Dry hexane has been used as solvent.

The increase in activity is about 9 % and must be due to the presence of the coordinated ester moiety in the final Ti/Est-ME. Even though Ti/Est-ME exhibits lower surface area than that of Ti/ME, the higher activity must be attributed mainly to the presence of IED on the support. This also indicates that high surface area is not an absolute necessity for higher reactivity, and the right electronic environment of the final catalyst is an effective

way [48] of enhancing its productivity for ethylene polymerization. Activity of Ti/Est-MiP was high as compared to Ti/Est-ME but less compared to Ti/MiP. Ethylene polymerization activity of Ti/Est-MiP was tested with different cocatalyst such as Me_3Al, Et_3Al and iBu_3Al. A better catalyst activity of 5794 gm of polymer per gm of catalyst (Ti/Est-MiP) was obtained with Et_3Al. The reason may be due to the formation of different active site formation with different cocatalyst. Our study shows that among different cocatalyst, Et_3Al results in better activity.

5.2.3.1. Genesis of Higher Activity of Ti/Est-ME and Ti/Est-MiP

The detailed preparation, characterization by structural, spectroscopy, and microscopic analytical methods, and the evaluation of the titanated adducts for ethylene polymerization presented here provide some new information, especially on the molecular level properties and electronic structure of the molecular adducts and corresponding Ziegler-Natta catalysts. Although similar information has already been speculated in the literature, they are derived from the analysis of polymer product and hence in an indirect manner. The four pieces of direct evidence from our work in support of the idea that IED enhances the activity come from (a) IED's existence in the final catalysts by all the characterization methods employed, in spite of several steps involved in the preparation; (b) significant changes in vibrational features in IR and Raman studies of Ti/Est-ME and Ti/Est-MiP compared to the virgin adducts highlighting a stronger interaction between Ti^{3+}/Ti^{4+} in the adduct through the carbonyl group of IED; (c) higher polymerization activity observed with Ti/Est-ME and Ti/Est-MiP compared to Ti/ME; and (d) higher activity of Ti/Est-ME and Ti/Est-MiP at the cost of loss of surface area and pore volume compared to that of Ti/ME and Ti/MiP (Table 5.1). Although it is known that surface area generally increases the activity of catalysts, an increase in activity at the cost of textural properties underscores the origin of higher activity and is not due to textural properties or any preferred orientation of final catalysts. This is also

further supported by weak diffraction features of Ti/Est-ME and Ti/Est-MiP, as preferred orientation generally leads to higher intensity of XRD features. Nonetheless, some contribution from any of the particular crystallite facets cannot be ruled out at this stage, as studies such as high resolution TEM (HRTEM) might be necessary to confirm that. Our attempts to measure surface crystallanity by HRTEM studies were not successful due to the air-sensitive nature of Ti/Est-ME and Ti/Est-MiP and big particle sizes. It is unlikely that any preferred orientation of crystallites is present in Ti/Est-ME and Ti/Est-MiP. Titanation of Est-ME and Ti/Est-MiP introduces Ti on the surfaces of adduct and its coordination with the ester group, leading to broader peaks in XRD (Figure 5.7). Hence, from the above discussion and our earlier work on other catalytic systems, [26, 48] it is clear that the genesis of enhanced catalytic activity in the present case is best attributed to electronic interactions rather than other factors. Ti^{2+} is known to be inactive for polymerization, while partial reduction of $Ti^{4+/3+}$ to Ti^{2+} in a side reaction with TEAL is one of the main catalyst deactivation pathways. The coordination of IED to $Ti^{4+/3+}$ probably makes the active sites less susceptible to such deactivation than those in Ti/ME.

5.3. Conclusions

This chapter deals with the preparation of $MgCl_2$-based adducts, namely Est-ME, Est-MiP, Est-MiB, Est-M2B and their corresponding titanated Ziegler- Natta catalysts. In situ esterification of ME, MiP, MiB and M2B with BC leads to an adduct with a coordinative bound internal electron donor to $MgCl_2$. Structural, spectroscopic, textural, and microscopic studies of these adducts and final catalysts have been thoroughly investigated by many techniques. XRD studies indicate the structural changes due to ester formation and this adduct maintain the rhombohedral structure of $MgCl_2$. IR, Raman, and solid-state NMR show the characteristic signal for the ester moiety. SEM image shows that the morphology of adducts is perfectly spherical with a diameter between 10 and 50 μm. The XRD study of the

final titanated catalysts shows the presence of structurally disordered δ-$MgCl_2$. IR and ^{13}C CP/MAS NMR data of Ti/Est-ME and Ti/Est-MiP clearly indicate the existence of the ester moiety, even though the esterified support is titanated with $TiCl_4$. Significant changes observed in spectroscopic analysis of the ester moiety from a simple adduct to titanated catalysts highlight the changes in its electronic environment. Polymerization of ethylene using the Ziegler-Natta catalyst supported on the esterified $MgCl_2$ adduct shows more activity compared to the commercial Ti/ME adduct which is also high compared to the free $MgCl_2$ supported Ziegler-Natta catalyst. In spite of lower surface area, better polymerization activity associated with Ti/Est-ME and Ti/Est-MiP than Ti/ME highlights the significance of the right electronic environment rather than textural characteristics. The present study motivates the preparation of such novel catalysts with complex alcohols in the future.

5.4. References

1. E. Albizzati, U. Giannini, G. Collina, L. Noristi, L. Resconi, In *Polypropylene Handbook: Polymerization, Characterization, Properties, Applications*; E. P. Moore, Ed.; Hanser Publ., Jr.: NY, (1996) p 11.
2. L. Luciani, N. Kashiwa, P. C. Barb, A. Toyota, Ger. 2643143 , Montedison and Mitsui Petrochemical, invs: *Chem. Abstr*. **1977**, *87*, 68893v.
3. E. Albizzati, G. Cecchin, J.C. Chadwick, G. Collina, U. Giannini, G. Morini, L. Noristi, L. Resconi, *In: Pasquini N (ed) Polypropylene handbook*, 2nd edn. Carl Hanser Verlag, Munich, 2005, Ch. 2.
4. J.C. Chadwick, *Macromol. Symp*. **173** (2001) 21.
5. G. Cecchin, G. Morini, A. Pelliconi, *Macromol Symp.* **173** (2001) 195.
6. S.A. Sergeev, G.D. Bukatov, V. A. Zakharov, E. M. Moroz, *Makromol Chem*. **184** (1983) 2421.
7. M. Terano, T. Kataoka, T. Keii, In: Keii T, Soga, K. (eds) *Catalytic polymerization of*

olefins. Kodansha-Elsevier, Amsterdam, **1986**, p 407

8. P. Sormunen, T. Hjertberg, E. Iiskola, *Makromol. Chem.* **191** (1990) 2663.
9. M. Terano, M. Saito, T. Kataoka, *Makromol. Chem. Rapid. Commun.* **13** (1992) 103.
10. V. Busico, P. Corradini, L. D. Martino, A. Proto, V. Savino, E. Albizzati, *Makromol. Chem*. **186** (1985) 1279.
11. M.C. Sacchi, I. Tritto, C. Shan, R. Mendichi, L. Noristi, *Macromolecules* **24** (1990) 6823.
12. D. Ribour, V. Monteil, R. Spitz, *J. Polym. Sci. A: Polym. Chem*. **46** (2008) 5461.
13. A. Boulif, D. J. Lone¨r, *J. Appl. Cryst.* **24** (1991) 287.
14. G. Metz, X. Wu, O. S. Smith, *J. Magn. Reson. A*. **110** (1994) 219.
15. A. Andoni, J.C. Chadwick, J. W. Niemantsverdriet. P.C. Thüne, *J. Catal.* **257** (2008) 81.
16. K. Soga, T. Shiono, Y. Doi, *Makromol. Chem.* **189** (1988) 1531.
17. M.C. Sacchi, F. Forlini, I. Tritto, P. Locatelli, G. Morini, G. Baruzzi, E. Albizzati, *Macromol. Symp.* **89 (1995)** 91.
18. V. Busico, P. Corradini, L.D. Martino, A. Proto, E. Albizzati, *Makromol. Chem.* **187** (1986) 1115.
19. V. Busico, P. Corradini, L.D. Martino, A. Proto, V. Savino, E. Albizzati, *Makromol. Chem.* **186** (1985) 1279.
20. M.C. Sacchi, I.Tritto, P. Locatelli, *Prog. Polym. Sci.* **16** (1991) 331.
21. P.C. Barbe, G. Cecchin, L. Noristi, *Adv. Polym. Sci.* **81** (1987) 1.
22. L. Noristi, P. C. Barbe`, G. Baruzzi, *Macromol. Chem.* **192** (1995) 115.
23. N. Kashiwa, S. Kojoh, *Macromol. Symp*. **89** (1995) 27.
24. S. Bhaduri, V. K. Gupta, U.S. Patent 6841633, 2005.
25. K. S. Thushara, R. Mathew, T. G. Ajithkumar, P. R. Rajamohanan, S. Bhaduri, C. S. Gopinath, *J. Phys. Chem. C (Letters)* **113** (2009) 8556.
26. K. S. Thushara, E. S. Gnanakumar, R. Mathew, R. K. Jha, T. G. Ajithkumar, P. R.

Rajamohanan, K. Sarma, S. Padmanabhan, S. Bhaduri, C. S. Gopinath, *J. Phys.Chem. C*, **115** (2011) 1952.

27. K. S. Thushara, E. S. Gnanakumar, R. Mathew, T.G. Ajithkumar, P.R. Rajamohanan, S. Bhaduri, C. S. Gopinath, *Dalton Trans.* **41** (2012) 11311.
28. K.S. Thushara, T.G. Ajithkumar, P.R. Rajamohanan, C. S. Gopinath, (*submitted to Appl. Cata.A*).
29. C. R. Tewell, F. Malizia, J. W. Ager III, G. A. Somorjai, *J. Phys. Chem. B* **106** (2002) 2946.
30. K. Balasubrahmanyam, *J. Chem. Phys.* **44** (1966) 3270.
31. F. R. Dollish, W. G. Fateley, F. Bentley, *Characteristic Raman Frequencies of Organic Compounds*; John Wiley & Sons: New York, 1974.
32. P. Sobota, *Coord. Chem. Rev.* **248** (2004) 1047.

Chapter 6

6. Conclusions and Future Scope of the Work

6.1. Conclusions

Importance of Ziegler-Natta catalyst and different generation of the same to improve the activity and stereospecificity of the polymer, in case of polypropylene, also explained in chapter 1. It also gives an insight into the discovery of $MgCl_2$ supported Ziegler-Natta catalyst, role of electron donor as well. In the case of Z-N catalyst, the fundamental molecular level understanding of the $MgCl_2$ support is not explored sufficiently. To address this issue, a systematic study of molecular level properties of $MgCl_2$ based molecular adducts with different alkyl alcohols and their corresponding Ziegler-Natta catalyst was carried out in order to correlate structure activity relationship with olefin polymerization activity.

Simple Azeotropic Distillation has been employed to prepare $MgCl_2$.n ROH adduct where R= ethyl, isopropyl, isobutyl, 2-butyl and tertiary butyl. **Chapter 2** mainly addresses the detailed procedures involved in the preparation methods to synthesize molecular adduct and active Ziegler-Natta catalyst. Reaction conditions for ethylene polymerization process also explained briefly. Theory and experimental procedures involved in various physicochemical and spectroscopic characterization techniques were discussed.

Chapter 3 deals with studies of $MgCl_2$- primary alcohol molecular adducts which is divided into two parts - **Part A** and **Part B**. **Part A** deals with characterization and catalytic activity studies of $MgCl_2$.6EtOH (MgEtOH) and $MgCl_2$.4(*i*-BuOH) (Mg-*i*-BuOH) and corresponding titanated Z-N catalyst. PXRD studies of MgEtOH and Mg-*i*-BuOH demonstrate that the alcohol molecule are inserting in the Cl-Mg-Cl triple layer structure, which results the formation of characteristic diffraction feature $2\theta \leq 10°$. Raman mode at 684 cm^{-1} and 712 cm^{-1} underscores the formation of the Mg-O bond between Mg and alcoholic oxygen in MgEtOH and Mg-*i*-BuOH. Solid state NMR is used extensively for the structural elucidation of these molecular adducts. TG-DTA and SEM analysis shows that number of coordinating

alcohols and particle morphology varies by changing the alcohol from ethanol to isobutanol in $MgCl_2$.nROH. Changing the Lewis base affects the surface area, pore diameter, pore volume and % Ti loading etc and hence the activity of Z-N catalyst. It is observed that changing the alcohol from simple to bulky, there is an overall change in electronic property of the active $MgCl_2$. Polymerization of ethylene using titanated Mg-*i*-BuOH shows less activity compared to Ti/MgEtOH catalyst.

Part B brings out separate local field and variable Temperature NMR studies of Mg-*i*-BuOH adduct. The isobutanol adduct formation is very sensitive to conditions used for preparation, such as temperature and set to reflux time. Structural property of adducts prepared under different conditions have been characterized by, non ambient solid state NMR and XRD. Formation of two phases has been identified and one of which is found to be stable adduct containing four molecules of isobutanol. To study the temperature dependence, in-situ heating NMR has also been carried out. From the NMR study, with in-situ heating and cooling, it is seen that there is a phase transformation occurring from kinetically stable to thermodynamically stable state while heating the adduct from RT to 110 °C. SLF solid-state NMR experiments reveal that out of the four isobutanol molecules, two alcohol molecules exhibits high mobility as compared to the remaining alcohol alcohols.

Chapter 4 describes the structural, spectroscopic and catalytic activity studies of $MgCl_2$.4 (i-PrOH), $MgCl_2$. 4(2-BuOH) and $MgCl_2$.2 (tBuOH) and their titanated catalysts. The overall conclusion from the chapter 4 is summarized here: XRD pattern of MgiPrOH adduct shows a characteristic low angle peak at 9.95°. ^{13}C CP/MAS spectrum of the MgiPrOH adduct shows four equally intense methyl and two methine signals around 24-27 and 65-67 ppm, respectively. Characteristic feature of $MgCl_2 \cdot 4(CH_3)_2CHOH$, with a secondary alcohol showed two different sets of magnetically in equivalent isopropanol. Titanated catalyst shows the highest surface area among all other catalyst we prepared with different alcohols. With

triethyl aluminium as a cocatalyst, ultrahigh molecular weight polyethylene (UHMWPE) was obtained with high yield (14 kg/g catalyst or 5.75 kg/mmol of Ti) that shows that the productivity is comparable to or better than many commercial catalysts. ^{13}C CP/MAS spectrum of the UHMWPE sample clearly indicated the presence of highly crystalline domains compared to a commercial high density polyethylene (HDPE) sample.

Intense peak at 8.9° for Mg2-BuOH in the XRD pattern indicate the formation of molecular adduct with oriented crystallites along (00z) direction. Low intensity peak at 712 cm^{-1} in Raman spectrum exhibits the characteristic Mg-O vibration mode for molecular adduct. The 2-BuOH/$MgCl_2$ ratio was found to be four from TG-DTA analysis which is further supported by liquid NMR study. Analysis of ^{13}C CPMAS spectra of Mg2-BuOH adducts show five signals; $\underline{C}HOH$ peak appears at 69.7 ppm, $\underline{C}H_2$ carbon peak at 29.6 ppm. Out of two methyl groups, methyl group attached directly to carbon atom bearing hydroxyl group shows a chemical shift value of 20.6 ppm. The second methyl group which is three bonds away from hydroxyl group shows two signals appearing at 10.6 and 9.2 ppm. The single pulse MAS (HPDEC) spectrum of this adduct, collected with sufficient relaxation delay, showed that these two methyl signals possess same area and the chemical shifts are different from that of any non-coordinated (free) 2-butanol molecules. Formation of rod shaped with fibrous nature is the special feature of Mg2-BuOH. Activity of this catalyst for ethylene polymerization is comparable with the commercially available Z-N catalyst derived from $MgCl_2$.6EtOH (MgEtOH) adducts. The aforementioned Z-N catalyst exhibits a high surface area of 120 m^2/g.

MgtBuOH shows a high intense peak at $2\theta = 9.8°$ which is similar to 2θ of MgEtOH. The polymerization activity of Z-N catalyst supported on MgtBuOH exhibits much better performance in terms of activity and polymer property compared to commercial Z-N catalyst. To study the effect of cocatalyst, ethylene polymerization was tested with three different

types of trialkyl aluminium compounds. The best activity was observed with triethylaluminium with a polymer yield of 8120 g /g of catalyst.

Chapter 5 addresses the characterization of esterified $MgCl_2$. nROH (R= ethyl, isopropyl, isobutyl and 2-butyl) with benzoyl chloride and their catalytic activity studies for ethylene polymerization. Insitu esterification of $MgCl_2$.nROH with BC leads to an adduct with a coordinatively bound internal electron donor to $MgCl_2$. Different physico-chemical techniques are used for structural, spectroscopic, textural, and microscopic studies of these adducts and final catalysts. XRD pattern shows the structural changes due to ester formation in esterified alcoholic adduct. IR, Raman, and solid-state NMR show the characteristic signal for the ester moiety. An optical microscopy image shows that the morphology of esterified adducts are perfectly spherical with a diameter between 10 and 50 μm. The XRD study of the final titanated catalysts (Ti/Est-ME and Ti/Est-MiP) shows the presence of structurally disordered δ-$MgCl_2$. IR and ^{13}C CP/MAS NMR data of Ti/Est-ME clearly indicate the existence of the ester moiety, even though the Est-ME and Est-MiP supports are titanated with $TiCl_4$. Significant changes observed in spectroscopic analysis of the ester moiety from a simple adduct to titanated catalysts highlight the changes in its electronic environment. The Ziegler-Natta catalysts supported on the esterified $MgCl_2$ adduct shows better activity compared to the Ti/ME adduct. Even though Ti/Est-ME and Ti/Est-MiP exhibits lower surface area, better polymerization activity associated with Ti/Est-ME and Ti/Est-MiP than Ti/ME which highlights the significance of the right electronic environment rather than textural characteristics.

6.2. Future scope of the work

Based on the observation of the present studies, in addition to olefin polymerization this heterogeneous Z-N catalyst can be explored for some important industrial application. In this dissertation, role of Lewis bases such as alcohols and esters and its influence in

modifying Z-N catalysts for ethylene polymerization has been explored. Future study should also focus more on effect of diether, phthalate, silane etc on activity of Z-N catalyst, propylene polymerization and oligomerization reaction using the Z-N catalyst supported on $MgCl_2$.nROH.

6.2.1. Study the effect of Lewis bases such as Diether, Phthalate, and Silane

In Z-N catalyst system, not only alcohols and alkyl and aryl esters but other Lewis bases such as diether, phthalate etc are used as internal electron donor (IED). Even though a drastic improvement in the activity was observed with this IED's, fundamental molecular level understanding is still lagging. A systematic study of the $MgCl_2$.n IED and the active $TiCl_x$ supported on $MgCl_2$.n IED will give an idea of interaction of IED with $MgCl_2$ and $TiCl_x$ and its influence in polymerization activity. Finally, DFT calculation is also necessary to support the experimental evidence.

6.2.2. Effect of mixed alcohols in tuning the textural properties of $TiCl_x$/ $MgCl_2$ catalyst

Present study shows that even though alcohol is not an integral part of the active Z-N catalyst, it indirectly tunes the textural properties such as surface area, pore volume, pore size distribution and even % Ti loading. Introduction of bulky alcohols in the $MgCl_2$ molecular adduct results in an increase in surface area of Z-N catalyst which in turn enhances the ethylene polymerization activity. Different alcohols generate different textural characteristics, which in turn affect Ti- loading and its oxidation state and hence the final polymerization activity. By introducing mixed alcohols in the molecular adduct, above textural characteristics can be modified to enhance the polymerization activity. Indeed the same may be explored for oligomerization of olefins towards petrochemicals.

6.2.3. Propylene Polymerization

We discussed much about role of Lewis bases such as alcohol and alkyl benzoate in ethylene polymerization in the dissertation. Our study shows that the presence of ester moiety

in the final Z-N catalyst enhances the polyethylene yield, so this should be extended to polypropylene polymerization with and without IED's.

6.2.4. Oligomerization of 1-decene and ethylene using M/$MgCl_2$.nROH where M= Ti, V

Oligomers are base fluids of higher α-olefins used for preparing lubricants, hydraulic fluids, transmission fluids etc. This material consists of a mixture of dimer to pentamer associated with minute amounts of higher oligomers in some cases. The most widely used catalyst for the production of poly (α-o1efin) is BF catalyst via cationic polymerization. Few Ziegler catalysts are available for oligomerization with a combination of alkylaluminum or an alkylaluminum halide. Oligomerization of 1-decene using M/$MgCl_2$.nROH catalyst where M= Ti or V could be extended and there is a scope for that.

List of Publications

1. *"$MgCl_2$ · $4(CH_3)_2CHOH$: A New Molecular Adduct and Super Active Polymerization Catalyst Support"* **K. S. Thushara**, Renny Mathew, T. G. Ajithkumar,P. R. Rajamohanan, Sumit Bhaduri, Chinnakonda S. Gopinath, *J.Phys.Chem.C*, **2009**, *113*, 8556–8559.
2. *"Electronic Structure and Catalytic Study of Solid Solution of GaN in ZnO"* Maitri Mapa, **K. S. Thushara**, Biswajit Saha, Purushottam Chakraborty, C. M. Janet,R. P. Viswanath, C. Madhavan Nair, K. V. G. K. Murty, Chinnakonda S. Gopinath, *Chem. Mater.* **2009**, *21*, 2973–2979.
3. *"Fabrication of homogeneous nanoparticle/nanoneedle $BaTiO_3$ and $Ba_{0.8}Sr_{0.2}TiO_3$ smooth thin films by simple dip coating"* Mamta Saini, K. Vivekanand, Pankaj Poddar, K.V.G.K. Murty, **K.S. Thushara**, Chinnakonda S. Gopinath, *Int. J. Nanotechnol.*, **2010**,*7*,919-931.
4. *"Toward an Understanding of the Molecular Level Properties of Ziegler-Natta Catalyst Support with and without the Internal Electron Donor"* **K. S. Thushara**, Edwin S. Gnanakumar, Renny Mathew, Ratnesh K. Jha, T. G. Ajithkumar, P. R. Rajamohanan,Krishna

5. Sarma, Sudhakar Padmanabhan, Sumit Bhaduri, Chinnakonda S. Gopinath, *J. Phys. Chem. C*, **2011**, *115*, 1952–1960.
6. *"$MgCl_2$.6$PhCH_2OH$ – A new molecular adduct as support material for Ziegler–Natta catalyst: synthesis, characterization and catalytic activity"* Edwin S. Gnanakumar, **K. S. Thushara**, Deu S. Bhange, Renny Mathew, T. G. Ajithkumar, P. R. Rajamohanan, Sumit Bhaduri and Chinnakonda S. Gopinath, *Dalton Trans.*, **2011**,*40*, 10936-10944.
7. *"$MgCl_2$.4($(CH_3)_2CHCH_2OH$): A New Molecular Adduct for the preparation of $TiCl_x/MgCl_2$ Catalyst for Olefin Polymerization"* **K. S. Thushara**, Edwin S. Gnanakumar, Renny Mathew, T. G. Ajithkumar, P. R. Rajamohanan, Sumit Bhaduri, Chinnakonda S. Gopinath, *Dalton Trans.*, **2012**,*41*, 11311-11318.
8. *"$MgCl_2$.6$C_6H_{11}OH$: A High Mileage Porous Support for Ziegler-Natta Catalyst"* Edwin S Gnanakumar, **K. S. Thushara**, Ravikumar K Gowda, Sumesh K Raman, Thalasseril G. Ajithkumar, Pattuparambil Ramanpillai Rajamohanan, Debashis Chakraborty, and Chinnakonda Subramanian Gopinath, *J. Phys. Chem. C*, **2012**, *116*, 24115−24122.
9. *"Structural Investigations of porous and rod shaped $MgCl_2$-2-Butanol molecular adduct as a supporting material for Ziegler-Natta Olefin Polymerization"* **K. S. Thushara**, T. G. Ajithkumar, P. R. Rajamohanan, C. S. Gopinath (submitted to *Appl. Cata. A*).
10. *"An investigation of Magnesium Chloride Isobutanol adduct for supported Ziegler-Natta Catalysis using Variable Temperature Solid-state NMR"* **K. S. Thushara**, T. G. Ajithkumar, P. R. Rajamohanan, C. S. Gopinath. (*Submitted to RSC Advances*).

Presentations in National/International Conferences/Symposia

1. ***"Separate Local Field and Variable Temperature NMR study of Magnesium Chloride-Isobutanol adduct for supported Ziegler-Natta Catalysis",*** National Science Day, NCL, Pune February 27-28, 2013.

2. ***"Role of support in Heterogeneous Ziegler-Natta Olefin Polymerization",*** National Science Day, NCL, Pune February 27-28, 2012.

3. ***"Solid state NMR: Theory and applications"*** Indo-French workshop, NCL, Pune July 28-29, 2011.

4. ***"Influence of Ethanol and Its Esterified $MgCl_2$ Adducts towards Zeigler Natta Polymerization of Ethylene: A comparative study"*** National Science Day, NCL, Pune February 27-28, 2010.

5. ***"Reversible nature of a novel Zeigler-Natta catalyst support material using In-situ NMR study"***.20th National Symposium on Catalysis, NCCR, IITM, Chennai. Dec 19-22, 2010.

6. ***"Synthesis and characterization of new catalyst Support Material for Alkene Polymerization"***19th National Symposium on Catalysis, Jan 18-21, 2009 NCL, Pune, India.

7. "***Combustion synthesis and characterization of Ga and N incorporated ZnO"***, International Conference on Advanced Material (ICAM-2008), School of Chemical Sciences, Mahatma Gandhi University, Kottayam, India Feb 18-21, 2008.

Awards and Fellowships

1. **Best Research Scholar** in **Catalysis** (February -2013).
2. Awarded **Senior Research Fellowship** by Council of Scientific and Industrial Research (CSIR), India.
3. First rank in M.Sc (Inorganic) Chemistry from Mahatma Gandhi University, Kottayam, Kerala (2005-2007).